

Addis Ababa University

Addis Ababa Institute of Technology

School of Electrical and Computer Engineering

Self-Tuning Fuzzy PID Based Position Control of Stack Piezoelectric Actuator for High Precision Applications

A Thesis Submitted to the School of Graduate Studies, Addis Ababa Institute of Technology, Addis Ababa University, in Partial Fulfillment of the Requirements for the Degree of Master of Science in Electrical Engineering (Control Engineering)

By: Tesfahun Desale

Advisor: Dr. Dereje Shiferaw

October 2019

Addis Ababa, Ethiopia

Addis Ababa University
Addis Ababa Institute of Technology
School of Electrical and Computer Engineering

Self-Tuning Fuzzy PID Based Position Control of Stack Piezoelectric Actuator for High Precision Applications

A Thesis Submitted to the School of Graduate Studies, Addis Ababa Institute of Technology, Addis Ababa University, in Partial Fulfillment of the Requirements for the Degree of Master of Science in Electrical Engineering (Control Engineering)

By: Tesfahun Desale

Approved by Board of Examiners

_____	_____	_____
Chairman, Department of Graduate committee	Signature	Date
Dr. Dereje Shiferaw Advisor	_____ Signature	_____ Date
Dr.Lebsework Negash Internal Examiner	_____ Signature	_____ Date
Mr. Teshome Hambissa External Examiner	_____ Signature	_____ Date

DECLARATION

I, the undersigned, declared that this MSc thesis is my original work, has not been presented for fulfillment of a degree in this or any other University, and all sources of materials used for the thesis have been fully acknowledged.

Tesfahun Desale
Name

_____
Signature

Addis Ababa, Ethiopia
Place

October 2019
Date of submission

This thesis has been submitted with my approval as a university advisor.

Dr. Dereje Shiferaw
Advisor

_____
Signature

ACKNOWLEDGMENTS

First of all, I am highly grateful to my advisor, Dr. Dereje Shiferaw for his encouragement, insight guidance, and professional expertise. My special thanks go to all instructors who thought me during my graduate study. I take this opportunity to thank Woldia University for giving me the chance to continue my graduate study in Electrical Engineering. No words of thanks are enough for my family for their unwavering support and love offered throughout the thesis work and my graduate study specially my beloved wife, Betelhem Ambachew.

TABLES OF CONTENT

Table of Contents page

DECLARATION ii

ACKNOWLEDGMENTS iii

LIST OF ABBREVIATIONS vii

LIST OF FIGURES viii

LIST OF TABLES x

ABSTRACT xi

1. CHAPTER ONE 1

INTRODUCTION 1

1.1 Introduction 1

1.2 Statement of the Problem 3

1.3 Relevance and Scope of the Thesis 3

1.4 Objectives 3

1.4.1 General Objective 3

1.4.2 Specific Objectives 3

1.5 Outline of the Thesis 4

2. CHAPTER TWO 5

BACKGROUND AND LITERATURE REVIEW 5

2.1 Background 5

2.2 Common Types of Piezoelectric Ceramics 6

2.3 Working Principles of PEAs 7

2.4 Behavior of PEAs 8

2.5 Types of PEA Configuration 8

2.5.1 Stack Design 8
2.5.2 Laminar Design 9
2.5.3 Monolithic Ceramic Tube 9
2.5.4 Partial-Rotation Design 10
2.6 Force Generation 11
2.7 Resonant Frequency 12
2.8 Response of PEA 12
2.9 Creep 13
2.10 Electrical Requirements for Piezo Operation 13
2.10.1 Static Operation 14
2.10.2 Dynamic Operation 14
2.11 Applications of Precision Motion Control Systems 15
2.11.1 Semiconductor 15
2.11.2 Magnetic and Optical Memory Manufacturing 16
2.11.3 Optical Manufacturing 16
2.11.4 High Resolution Imaging 16
2.11.5 Precision Metrology 16
2.12 PID Controller 16
2.12.1 Algorithm of PID Controller 17
2.12.2 Limitations of PID Control 19
2.13 Fuzzy Logic Controller 20
2.13.1 Fuzzy Sets 21
2.13.2 Fuzzy Logic Control Components 23
2.14 Related Works 30
3. CHAPTER THREE 34
MATERIALS AND METHODS 34

3.1 Modeling of Stack PEA 34
3.1.1 Electromechanical Model of Stack PEA 34
3.1.2 Hysteresis Modeling of Stack PEA 37
3.1.2.1 Bouc-Wen Hysteresis Model 38
3.1.3 Gaussian Stochastic Linearization 40
3.2 Design and Analysis of Stack PEA Control System 45
3.2.1 Design and Analysis of PID 45
3.2.1.1 Loop Tuning Mechanism 46
3.2.2 Simulink Model for PID Controller 49
3.2.3 Modeling and Analysis of FPID Controller 49
3.2.3.1 Fuzzy Inference System 51
3.2.3.2 Fuzzier Design 54
3.2.3.3 Rule Base Construction 55
3.2.3.4 Defuzzification Design 57
3.2.4 Simulink Model of Overall System 60
4. CHAPTER FOUR 62
SIMULATION RESULTS AND DISCUSSIONS 62
4.1 Comparison of PID and FPID Controller Mechanisms 62
4.1.1 Comparison of PID and FPID Controller in Parameter Variations 63
4.1.2 Comparison of PID and FPID Controllers in Disturbance Rejection and Delay Time 72
5. CHAPTER FIVE 75
CONCLUSIONS AND RECOMMENDATIONS 75
5.1 Conclusions 75
5.2 Recommendations 76
REFERENCES 77
APPENDIXES 82

LIST OF ABBREVIATIONS

AFM	Atomic Force Microscopy
ce	rate of change of error
e	Error
FL	Fuzzy Logic
FLC	Fuzzy Logic controller
FPID	Fuzzy Proportional, Integral and Derivative
NB	Negative Big
NM	Negative Medium
NS	Negative Small
PB	positive Big
PEA	Piezoelectric Actuator
PID	Proportional Integral and Derivative
PI-FLC	Proportional Integral Fuzzy Logic Controller
PM	Positive Medium
PMB	Positive Medium Big
PMS	Positive Medium Small
PS	Positive small
PVB	Positive Very Big
PVS	Positive Very Small
STM	Scanning Tunnel Microscopy
Z	Zero

LIST OF FIGURES

Figure 2.1: Schemes of various actuators 5
Figure 2.2: Construction of a stack actuator 8
Figure 2.3: Laminar design 9
Figure 2.4: Tube design 10
Figure 2.5: Construction of partially rotating actuator 11
Figure 2.6: General block diagram of PID controller 19
Figure 2.7: Fuzzy logic system chart showing both input and output grades 23
Figure 2.8: FLC operation 24
Figure 2.9: Membership function chart 25
Figure 2.10: Membership function shapes: (a) S, (b) Z, (c) Λ, and (d) Π 25
Figure 2.11: Asymmetrical membership functions 25
Figure 2.12: Incorrect membership function shapes 25
Figure 2.13: Fuzzy logic input using seven membership function labels 26
Figure 2.14: Fuzzy set with five membership functions 26
Figure 2.15: Fuzzy logic rule matrix 27
Figure 2.16: (a) Fuzzy input grades and (b) the resulting output grades 28
Figure 2.17: Fuzzy inference using Mamdani's max-min compositional operation 29
Figure 3.1: General block diagram of FPID based position control for stack PEA 34
Figure 3.2: Illustration of a PZT stack actuator 35
Figure 3.3: Electromechanical model 36
Figure 3.4: Force versus displacement for a hysteresis functional 38
Figure 3.5: Schematic of mechanical system 41
Figure 3.6: Generic experimental hysteretic loop 41
Figure 3.7: Simulink model of PID controller 49
Figure 3.8: Fuzzy logic process 51
Figure 3.9: Fuzzy Inference System of the proposed system 52
Figure 3.10: Surface viewers of Kpf, Kif and Kdf 53
Figure 3.11: Membership function for position error and rate of position error (e,ce) 54
Figure 3.12: Typical step response of the system 55
Figure 3.13: Membership function fuzzy output for proportional gain Kpf 57

Figure 3.14: Membership function fuzzy output for proportional gain Kif 58
Figure 3.15: Membership function fuzzy output for proportional gain Kdf 58
Figure 3.16: Over all simulink model of FPID and PID controller 60
Figure 3.17: Model components under FPID block 61
Figure 3.18: PID controller block model components under FPID block 61
Figure 4.1: Unity step response of the system 62
Figure 4.2: Simulation results of FPID and PID controller 63
Figure 4.3: Simulation results of FPID and PID controllers with 50% decrease damping factor 64
Figure 4.4: Simulation results of FPID and PID controllers with 75% increase damping factor. 65
Figure 4.5: Simulation results of PID and FPID controller with 50% decrease mass 66
Figure 4.6: Simulation results of FPID and PID controllers with 75% increase mass 67
Figure 4.7: Simulation results of PID and FPID controller for 50% decrease stiffness 68
Figure 4.8: Simulation results of PID and FPID controller with 75% increase stiffness 69
Figure 4.9: Simulation results of PID and FPID controller with ±15% Dc gain 70
Figure 4.10: Simulation results of PID and FPID controller with ±25% Dc gain 71
Figure 4.11: Simulation results of PID and FPID controller with 50% increase Dc gain 72
Figure 4.12: Disturbance signal added to the system after settling time 73
Figure 4.13: The simulation result of disturbance rejections of PID and FPID controller 73
Figure 4.14: Response of the stack PEA with time delay 74

LIST OF TABLES

Table 3.1: Effects of independent P, I and D tuning on closed-loop response 48
Table 3.2: Membership function universe of discourse of error and change of error in position 54
Table 3.3: Rule table for Kpf 56
Table 3.4: Rule table for Kif 56
Table 3.5: Rule table for Kdf 57
Table 3.6: Membership function universe of discourse for Kpf 58
Table 3.7: Membership function universe of discourse for Kif 59
Table 3.8: Membership function universe of discourse for Kdf 59
Table 4.1: The comparison of PID and FPID controller 63
Table 4.2: The comparison of PID and FPID controller with 50% decrease damping factor 64
Table 4.3: The comparison of PID and FPID controller with 75% increase damping factor 65
Table 4.4: The comparison of PID and FPID controller with 50% decrease mass 66
Table 4.5: The comparison of PID and FPID controller with 75% increase mass 67
Table 4.6: The comparison of PID and FPID controller with 50% decrease stiffness 68
Table 4.7: The comparison of PID and FPID controller with 75% increase stiffness 69
Table 4.8: The comparison of PID and FPID controller with ±15% Dc gain 70
Table 4.9: The comparison of PID and FPID controller with ±25% Dc gain 71
Table 4.10: The comparison of PID and FPID controller with 50% increase Dc gain 72

ABSTRACT

In the area of micro and nano-scale systems, the piezoelectric actuator (PEA) has become an increasingly popular candidate as a precise actuator. But control problems associated with system uncertainties and system inherent nonlinearities remain big challenges for control engineers. In this paper stack PEA is modeled with hysteresis effect using rate independent hysteresis in order to increase precision. The hysteresis is linearized using Gaussian stochastic linearization technique and self-tuning fuzzy PID controller is designed in this paper. The system response of the system is compared with traditional PID controller. The self-tuning fuzzy PID controller perform better than the traditional PID controller with different conditions. The comparison included parameter variations, external disturbance rejection and delay time.

Key words: Stack PEA, hysteresis, linearization, PID controller, self-tuning FPID controller

CHAPTER ONE

INTRODUCTION

1.1 Introduction

In the area of micro and nano-scale systems, the piezoelectric actuator (PAE) has become an increasingly popular candidate as a precise actuator, due to its ability to achieve high precision and its versatility to be implemented in a wide range of applications. More specifically, the PAE can provide very precise positioning (of the order of nanometers) and generate high forces (up to few thousands newton) [1] [2].

Actuators (be it electromechanical, pneumatic or hydraulic) provide the necessary energy to accomplish most tasks that involve any motion in any machine tool. Hence the need for faster and better machine tools would also imply better actuators or using the existing actuators in a manner to derive better performance from them. Piezoelectric actuators belong to the type of direct drive actuators that rely on the (inverse) piezoelectric effect to produce a force or motion. The piezoelectric effect is a phenomenon in which a charge is produced on the surface of the material exhibiting that phenomenon upon application of an external pressure.

The converse effect (production of a force upon application of charge) is the inverse-piezoelectric effect which is exploited in piezoelectric actuators. Due to the solid-state nature of this effect, they do not rely on gearing mechanisms or any sliding motion to support the moving parts. This offers them an enormous advantage in attaining high bandwidth (due to the reduced inertia eliminated in the gears) and accuracy (due to the absence of friction, backlash play and due to the infinitesimal nature of this effect itself [2].

The increasingly widespread industrial applications of the PEA in various optical fiber alignment, mask alignment, and medical micromanipulation systems. These are self-evident testimonies of the effectiveness of the PEA in these application domains inspire of the benefits of a PEA. And in these application domains, there are challenges in the design and control of these devices are the crystals can withstand very little tensile stresses and the materials are inherently nonlinear. The main disadvantages of piezoelectric actuators are hysteresis phenomena. The hysteresis phenomena arise from materials polarization and molecule friction. As the input voltage alternates

between increasing and decreasing, and its displacement amount have inconsistent phenomenon [1] [2].

Fuzzy logic is a superset of conventional logic that has been extended to handle the concepts of 'completely true' and 'false' values. As its name suggests, it is the logic underlying modes of reasoning which are approximate rather than exact. The importance of fuzzy logic derives from the fact that most modes of human reasoning and especially common-sense reasoning are appropriate in nature. Fuzzy logic is having many values. Here these appropriate values are not fixed time binary sets. So, it is having a truth value that ranges in degree between 0 and 1 [3].

Various control strategies and methodologies are available for position control of PEA such as, a charge controller for linear operation of a piezoelectric stack actuator [4] , adaptive PI-based sliding mode control for nano-positioning of piezoelectric actuators [5] , sliding mode-based robust control for piezoelectric actuators with inverse dynamics estimation [6] , discrete sliding mode control of piezo actuator in nano-scale range [7], nano-positioning fuzzy control for piezoelectric actuators [8] and adaptive PI control of piezoelectric systems using Takagi-Sugeno fuzzy logic [9]. These approaches improve the control performance of the motor from different aspects. Nevertheless, all the above controller techniques depend on the exact mathematical model of the drive system, which is difficult to achieve practically except the fuzzy logic-based controllers.

FL controllers based on fuzzy set theory are used to represent the experience and knowledge of a human operator in terms of linguistic variables that are called fuzzy rules. Since an experienced human operator adjusts the system inputs to get a desired output by just looking at the system output without any knowledge on the system's dynamics and interior parameter variations, the implementation of linguistic fuzzy rules based on the procedures done by human operators does not also require a mathematical model of the system.

Therefore a FLC becomes nonlinear and adaptive in nature having a robust performance under parameter variations with the ability to get desired control actions for complex, uncertain, and nonlinear systems without the requirement of their mathematical models and parameter estimation [10]. In this thesis self-tuning scheme using fuzzy logic PID controller is proposed to improve the performance of PEA.

1.2 Statement of the Problem

Fast response with no or very little overshoot and extremely high precision are some of the desired characteristics of any nano positioning system. There are three major issues: hysteresis, creep and vibration. As a result of the hysteresis characteristic, the piezoelectric actuator will produce a 10-15% error of the full range under an open-loop control system. With the increase of the input signal frequency, the error will even reach 35% [11] [12] [13]. The major problems in applying a conventional control algorithm (PI, PD and PID) and the sliding mode control controller to control piezoelectric actuator are the piezoelectric actuators have the disadvantage of hysteresis, resonant frequency and creep behaviors, which severely limit system performance such as giving rise to undesirable inaccuracy or oscillations, even leading to instability. Since these errors are very high for high precision like diesel fuel injector, optic alignments, stent and microscopy systems. Conventional and sliding mode controllers are not effective so much. Fuzzy logic controller which introduces steady state error also not appropriate for high precision application PEAs. Therefore, it is necessary that developing an intelligent control technique to enhance the performance of PEAs.

1.3 Relevance and Scope of the Thesis

To have good understanding the use of FPID controllers in controlling nonlinear activities like PEAs and to study and design linearized stack PEA with implementable design for the future in order to produce high precision.

1.4 Objectives

1.4.1 General Objective

The general objective of this thesis is to design and simulate FPID based position control of stack PEA for high precision applications using MATLAB /Simulink software application

1.4.2 Specific Objectives

The specific objectives of this thesis are:

- ✓ To model a stack PEA including hysteresis effect.
- ✓ To linearize stack PEA hysteresis.
- ✓ To design PID controller for stack PEA.
- ✓ To design self-tuning FPID controller for stack PEA.

- ✓ To simulate self-tuning FPID controller for stack PEA using MATLAB simulink.
- ✓ To analyze and compare the performance of self-tuning FPID for PEA with conventional PID controller.

1.5 Outline of the Thesis

This thesis is organized in to five chapters. The first chapter present the overview of PEAs control mechanism, statement of the problem, relevance and objectives of the study. Chapter two presents a review of the main theoretical backgrounds about PEA, different literatures related to PEA systems and their position control system, are reviewed. The other topics included in this chapter are on the study of fuzzy inference systems and PID controllers. Chapter three focuses on electromechanical modeling of stack PEA, hysteresis and its modeling, design and analysis of PEA and Simulink model of overall system. Simulation and experimental results are presented and discussed in chapter four. Finally, chapter five presents conclusions and recommendations.

CHAPTER TWO

BACKGROUND AND LITERATURE REVIEW

2.1 Background

An actuator is the generic name referring to devices that convert input energy into mechanical energy, and various actuators have been developed and put to practical use according to various types of input energy (Figure 2.1). The electromagnetic, hydraulic and pneumatic actuators achieve displacement indirectly by moving a piston by electromagnetic force or pressure. On the other hand, the piezoelectric actuator achieves displacement by directly applying deformation of a solid, and thus features a higher displacement accuracy, larger generation force and higher response speed than other types of actuators. These advantages have resulted in the piezoelectric actuator being applied mainly in industrial equipment requiring precision position control, such as the ultrafine-movement stage of semiconductor exposure systems, precision positioning probes and probes for STM and AFM. In addition, other advantages including the no necessity of a driving coil, ease of implementation of small devices, high energy conversion efficiency and low power consumption have recently led to application in consumer equipment such as digital cameras and cellular phone terminals [14].

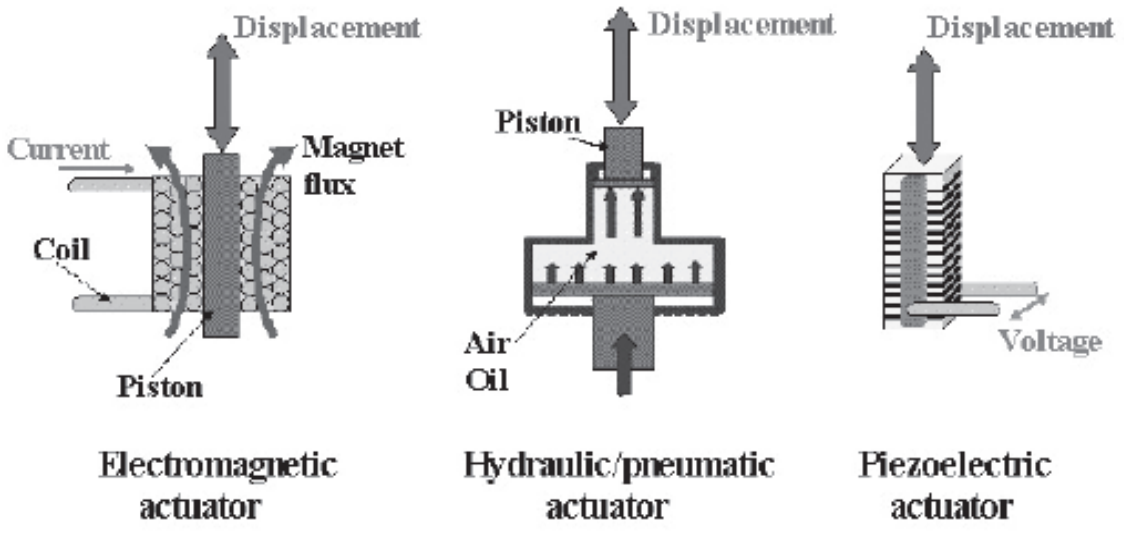


Figure 2.1: Schemes of various actuators [14]

2.2 Common Types of Piezoelectric Ceramics

Piezoelectric ceramics (piezoelectric ceramics): A piezoelectric effect of the ceramic is known as piezoelectric ceramics due to the polarization treatment of ferroelectric ceramics spontaneous polarization random orientation, so there is no piezoelectricity. Polarization is carried out by spontaneous polarization in the direction of polarization. After the removal of the electric field, ceramic body still retains a certain total residual polarization, so the ceramic body with piezoelectricity as a piezoelectric ceramic. In the high temperature gradient field of high temperature orientation of the crystallization of non-ferroelectric glass ceramic also has piezoelectricity. Common types are [15]:

Barium titanate ceramics

Barium titanate ceramics is a typical perovskite structure of ferroelectric ceramics. It is usually barium carbonate and titanium dioxide as the main raw material, pre-synthesized and then sintered at high temperatures [15].

Lead titanate ceramics

Lead titanate ceramics are ferroelectric ceramics with perovskite structures. It is usually made of lead tetrachloride (or lead oxide) and titanium dioxide and a small amount of additives in advance and then sintered at high temperatures [15].

Binary system ceramic (binary system ceramics)

The binary ceramic is a solid solution formed by two kinds of chemicals of the general chemical type ABO_3, wherein A represents a divalent cation ion Pb^{2+},Ba^{2+}, Mg^{2+}, Ca^{2+}, Sr^{2+}, or a monovalent cation $K^{+}$and Na^{+}. B represents tetravalent positive ions Zr^{4+}, Ti^{4+} or pentavalent Nb^{5+}. The most common binary piezoelectric ceramic is PbZrXTi1-XO3. By adjusting the molar ratio of the two ABO_3-type structures, and by modifying the elements and additives, a variety of different materials can be obtained [15].

Lead zirconate ceramic

Lead zirconium titanate ceramics are commonly referred to as PZT ceramics, which are currently widely used. It is PbZrO3 and PbTiO3 solid solution with perovskite type structure, when the zirconium and titanium ratio of 53/47 or so (that is, near the eutectic phase boundary) with the strongest piezoelectric properties.

2.3 Working Principles of PEAs

PEAs utilize the converse piezoelectric effect of PEA materials to generate displacement and force, i.e. a piece of piezoelectric material will be mechanically strained if subject to an electric field (by placing it into the electric field or applying voltages to its surfaces) .This property is resulted from the microscopic structure of piezoelectric materials as explained in the following. Most piezoelectric materials used in PEAs, e.g. lead zirconate titanate, undergo a structural phase transition as its temperature drops through the so-called curie temperature, during which their structurally and electrically symmetric cubic unit cells deform into structurally and electrically asymmetric tetragonal unit cells, resulting in spontaneous strain and polarization groups of adjoining unit cells with uniformly oriented spontaneous polarization are called Weiss or ferroelectric domains [11].

The directions of spontaneous polarization of different domains thus developed are random, so in this state the piezoelectric materials exhibit no overall piezoelectric behavior. To fabricate PEAs from such piezoelectric materials, they are further exposed to a strong electric field (106 to 107 V/m) at a temperature just below the Curie temperature, forcing the directions of spontaneous polarization of the domains to align with the electric field. Such alignment can be approximately preserved after the removal of the electric field. This process is referred to as poling [11] .

After poling, due to the approximate alignment of the spontaneous polarization of the domains, the deformations of the domains in the direction of their respective spontaneous polarization resulting from the application of a voltage to the piece of piezoelectric material (which generates an electric field that either enhance or suppress the spontaneous polarization of the domains, causing their dimension to change in the direction of the spontaneous polarization) can accumulate and causes an overall deformation or displacement. Thus, the piece of piezoelectric material now possesses overall piezoelectric property including the converse piezoelectric effect and can be used as a PEA [11].

2.4 Behavior of PEAs

In micro and nano-positioning applications, typical behavior of PEA concerned include hysteresis, creep, and vibration dynamics. Hysteresis is the nonlinear dependence of a system not only on its current input but also on its past input. In PEAs, hysteresis exists in both the electric field (voltage)-polarization relationship and the electric field (voltage)-strain (deformation or displacement) relationship, with the latter being mostly concerned in micro and nano-positioning, and it is caused by the nonlinearities in the converse piezoelectric effect of the unit cells and the switching and movement of domain walls .The relationship between the actuating force exerted on the PEA and the resulting displacement of the PEA is linear, as such the electric field (voltage)-strain (displacement) hysteresis can also be treated as the result of the voltage-internal actuating force hysteresis [11].

2.5 Types of PEA Configuration

The PEA offers unique and compelling advantages in nanometer resolution and high-speed applications. To derive maximum performance from PAEs, a variety of configuration can be designed to adapt to various requirements [1].

2.5.1 Stack Design

The most common design for PAs is a stack of ceramic layers (see Figure 2.2). Such devices can achieve high displacements and holding forces. Standard designs which can withstand pressures of up to 100kN are available in commercial products (e.g., products from Physik Instrument), and preloaded actuators can also be operated in a push-pull mode [1].

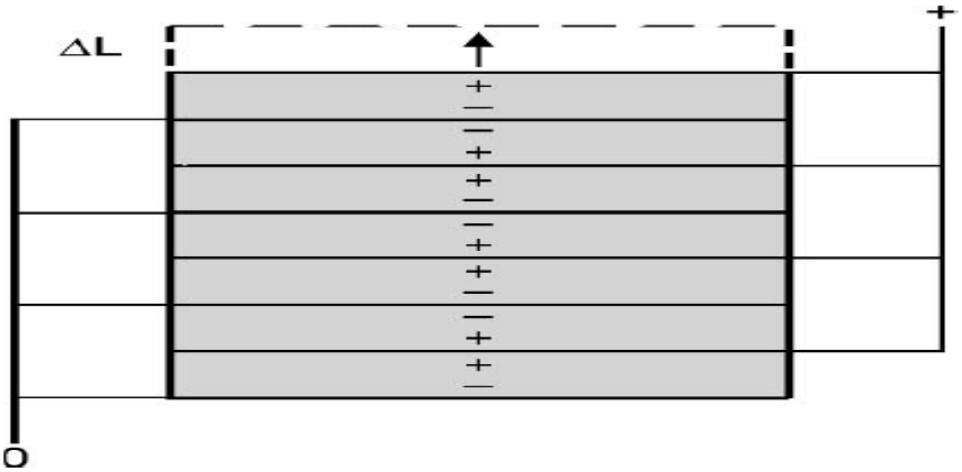


Figure 2.2: Construction of a stack actuator [1]

2.5.2 Laminar Design

This design uses thin laminated ceramic sheets (see Figure 2.3). When a voltage is applied to the device, the actuator sheet contracts. The displacement in the device is caused by the contraction in the material being perpendicular to the direction of polarization and electric field application. The maximum travel of the laminar actuators is a function of the length of the sheets, while the number of sheets arranged in parallel will determine the stiffness and force generation of the ceramic element. Laminar actuators are easily integrated in conventional composite layers [1].

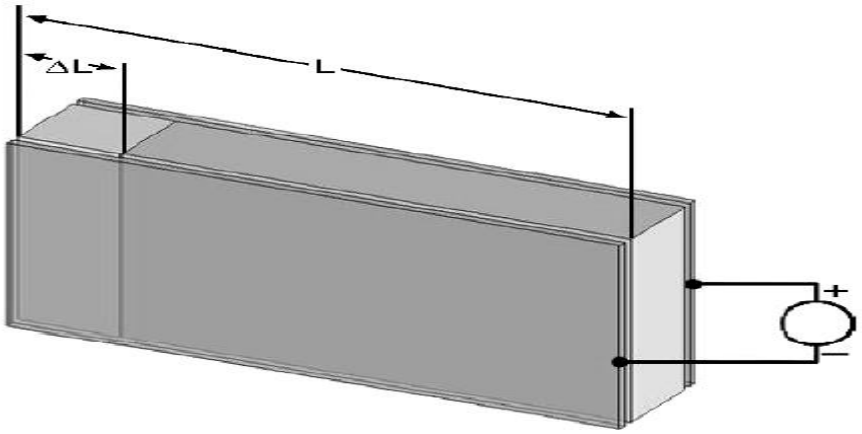


Figure 2.3: Laminar design [1]

2.5.3 Monolithic Ceramic Tube

The monolithic ceramic tube is yet another form of piezo actuator. Figure 2.4 shows a design structure. The surface of a tube is partitioned into four regions and they are connected along with one end of the tube to electrodes. Thus, it becomes possible to apply voltages to the tube to initiate motion in various directions. For example, when an electric voltage is applied between the outer and inner diameter of a thin-walled tube, the tube contracts axially and radially. A variety of chemical and materials processing applications use ceramic tubes. Ceramic tubes are also used to fabricate electrical parts for high voltage or power applications such as insulators, igniters or heating elements [1].

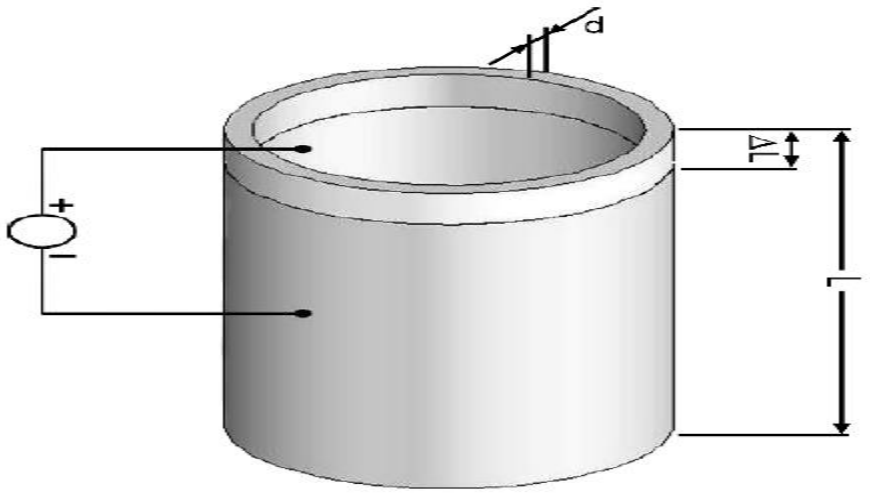


Figure 2.4: Tube design [1]

2.5.4 Partial-Rotation Design

The design employs a piezoelectric cylinder from LPZT (lithium-lead-zirconium titanite) ceramic with radial polarization. The sketch of the design is presented in Figure 2.5, in which a piezoelectric cylinder (2) is mounted on a rigid base (1). The movement at the free end of the piezoelectric cylinder is transmitted to a friction pad (3). A spring (4) provides a normal force against the friction pad to generate friction force. A stopper (5) and a rod (6) serve to act as the axis of rotation. The actuator is designed based on the indirect mode of actuation, therefore reducing the effect of hysteresis in the actuator output. The outer surface of the piezoelectric cylinder is divided into several sections. In the design, four sections are used, although the number of sections can be increased if a finer resolution is desired. The inner surface is a common electrical contact point. With this construction, the cylinder will expand unevenly when a voltage is applied across a section. By applying a voltage orderly across adjacent sections in a controlled manner, an incomplete rotating wave can be produced at the end of the piezoelectric cylinder, ready to be transmitted to the friction disc mounted on top of the cylinder. To reverse the direction of the rotation, a negative voltage can be applied across the sections. By controlling the duration of the positive and negative voltage applied, the sweeping angle of the motor can be controlled [1].

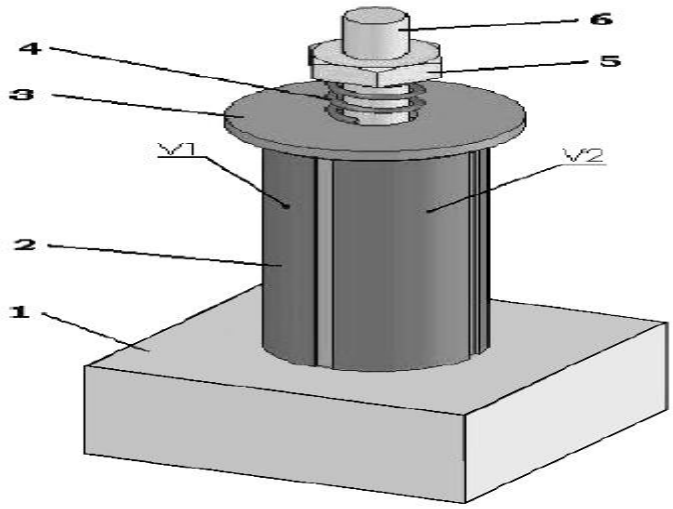


Figure 2.5: Construction of partially rotating actuator [1]

2.6 Force Generation

In most applications, piezo actuators are used to produce displacement. If used in a restraint, they can be used to generate forces, e.g. for stamping. Force generation is always coupled with a reduction in displacement. The maximum force (blocked force) a piezo actuator can generate depends on its stiffness and maximum displacement. At maximum force generation, displacement drops to zero [16].

$$F_{max} \approx K_T \Delta L_o \quad (2.1)$$

Maximum force that can be generated in an infinitely rigid restraint (infinite spring constant).

Where:

- ✓ ΔL_o is max. nominal displacement without external force or restraint [m]
- ✓ K_T is piezo actuator stiffness $[N/m]$

In actual applications the spring constant of the load can be larger or smaller than the piezo spring constant. The force generated by the piezo actuator is [16]:

$$F_{maxeff} \approx K_T \Delta L_o \left(1 - \frac{K_T}{K_T + K_s}\right) \quad (2.2)$$

Effective force a piezo actuator can generate in a yielding restraint

Where:

- ✓ ΔL_o is max. nominal displacement without external force or restraint [m]
- ✓ K_T is piezo actuator stiffness $[N/m]$

- ✓ K_s is stiffness of external spring [N/m]

2.7 Resonant Frequency

In general, the resonant frequency of any spring/mass system is a function of its stiffness and effective mass. Unless otherwise stated, the resonant frequency given in the technical data tables for actuators always refer to the unloaded actuator with one end rigidly attached. For piezo positioning systems, the data refers to the unloaded system firmly attached to a significantly larger mass [16].

$$f_o = \left(\frac{1}{2\pi}\right)\sqrt{\frac{K_T}{m_{eff}}} \tag{2.3}$$

Resonant frequency of an ideal spring/mass system.

Where:

- ✓ f_o is resonant frequency of unloaded actuator [Hz]
- ✓ K_T is piezo actuator stiffness $[N/m]$
- ✓ m_{eff} is effective mass (about $\frac{1}{3}$ of the mass of the ceramic stack plus any installed end pieces) [kg]

2.8 Response of PEA

Fast response is one of the characteristic features of piezo actuators. A rapid drive voltage change results in a rapid position change. This property is especially welcome in dynamic applications such as scanning microscopy, image stabilization, switching of valves/shutters, shock-wave generation, vibration cancellation systems, etc. [16].

$$T_{min} \approx \frac{1}{3f_o} \tag{2.4}$$

Minimum rise time of a piezo actuator (requires an amplifier with enough output current and slew rate).

Where:

- ✓ T_{min} is minimum time [s]
- ✓ f_o is resonant frequency [Hz]

2.9 Creep

Creep is the phenomenon that the output displacement of the PEA changes (slowly increases or decreases) over a long time period as the input voltage to the PEA is kept constant. It is usually treated as a mechanical property rather than an electro-mechanical property of the piezoelectric material and the distributive vibration dynamics is due to the distributive nature of the piezoelectric material [11].The creep response in a PEA has a logarithmic shape over time, so it is sometimes referred to as the log (t) type creep, and the nonlinear creep model given by equation (2.5) has been used to represent such creep behavior.

$$y(t) = y_o \left[1 + \gamma log_{10}\left(\frac{t}{t_o}\right)\right] \tag{2.5}$$

Where

- ✓ $y(t)$ is the creep model output.
- ✓ y_o is the creep output at t_o after the static input voltage is applied.
- ✓ γ is a coefficient depending on the input voltage.

The dependence of γ on the input voltage and the un-boundness of such a nonlinear creep model as $t \to 0$ and $t \to +\infty$ pose difficulties in its implementation.

2.10 Electrical Requirements for Piezo Operation

When operated well below the resonant frequency, a piezo actuator behaves as a capacitor: The actuator displacement is proportional to stored charge (first order estimate). The capacitance of the actuator depends on the area and thickness of the ceramic, as well as on its material properties. For piezo stack actuators, which are assembled with thin, laminar wafers of electroactive ceramic material electrically connected in parallel, the capacitance also depends on the number of layers. The small-signal capacitance of a stack actuator can be estimated by [16]:

$$C \approx n\mathcal{E}_{33}T\, {}^{A}/_{d_s} \tag{2.6}$$

Where:

- ✓ C is capacitance [F (As/V)]
- ✓ n is number of layers $= \frac{l_o}{d_s}$
- ✓ $\mathcal{E}_{33}T$ is dielectric constant $[As/Vm]$
- ✓ A is electrode surface area of a single layer $[m^2]$

- ✓ d_s is distance between the individual electrodes (layer-thickness) [m]
- ✓ l_o is actuator length

2.10.1 Static Operation

When electrically charged, the amount of energy stored in the piezo actuator is $E = (\frac{1}{2})CU^2$ Every change in the charge (and therefore in displacement) of the PZT ceramics requires a current i:

$$i = \frac{dQ}{dt} = C\frac{dU}{dt} \tag{2.7}$$

Relationship of current and voltage for the piezo actuator

Where:

- ✓ i is current [A]
- ✓ Q is charge [coulomb (As)]
- ✓ C is capacitance [F]
- ✓ U is voltage [V]
- ✓ t is time [s]

2.10.2 Dynamic Operation

The following equations describe the relationship between amplifier output current, voltage and operating frequency. They help to determine the minimum specifications of a piezo amplifier for dynamic operation [16].

Long-term average current required for sinusoidal operation is given by

$$i_a \approx fCU \tag{2.8}$$

Peak current required for sinusoidal operation

$$i_{max} \approx f\pi CU_{p-p} \tag{2.9}$$

Maximum operating frequency with triangular waveform, as a function of the amplifier output current limit is given by

$$f_{max} = \frac{i_{max}}{2CU_{p-p}} \tag{2.10}$$

Where:

- ✓ i_a is average amplifier source/sink current [A]
- ✓ i_{max} is peak amplifier source/sink current [A]
- ✓ f_{max} is maximum operating frequency [Hz]
- ✓ C is piezo actuator capacitance [Farad (As/V)]
- ✓ U_{p-p} is peak-to-peak drive voltage [V]
- ✓ f is operating frequency [Hz]

The average power a piezo driver has to be able to provide for sinusoidal operation is given by [16]:

$$P_a = CU_{max}U_{p-p}f \tag{2.11}$$

Peak power for sinusoidal operation is:

$$P_{max} \approx \pi CU_{max}U_{p-p}f \tag{2.12}$$

Where:

- ✓ P_a is average power [W]
- ✓ P_{max} is peak power [W]
- ✓ C is piezo actuator capacitance [F]
- ✓ f is operating frequency [Hz]
- ✓ U_{p-p} is peak-to-peak drive voltage [V]
- ✓ U_{max} is nominal voltage of the amplifier [V]

2.11 Applications of Precision Motion Control Systems

A summary of the relevant industries and applications of precision motion control systems are briefly summarized and outlined in the following subsections [1] [14] .

2.11.1 Semiconductor

- ✓ Microlithography
- ✓ Substrate coating
- ✓ Memory repair
- ✓ Laser direct writing
- ✓ Microscope XY inspection

- ✓ Wafer probing
- ✓ Wire bonding

2.11.2 Magnetic and Optical Memory Manufacturing

- ✓ Disk drive read/write head machining
- ✓ Disk and head inspection
- ✓ Air bearing spin stands
- ✓ Optical disk mastering
- ✓ Precision grinding, dicing, and slicing
- ✓ Tape head machining
- ✓ Flying height testing

2.11.3 Optical Manufacturing

- ✓ Lens and mirror diamond turning machines
- ✓ Optical grinding machines
- ✓ Precision rotary scanning
- ✓ Diamond fly cutting machines
- ✓ Contact lens lathes
- ✓ Encoder and grating ruling engines

2.11.4 High Resolution Imaging

- ✓ Flat panel displays
- ✓ Internal and external drum plotters
- ✓ Constant velocity motion

2.11.5 Precision Metrology

- ✓ Sub-micron coordinate measuring machines
- ✓ Flatness and roundness measuring systems
- ✓ Vision and optical inspection
- ✓ Automotive, medical, electronics, optical components

2.12 PID Controller

The PID controller is the most common form of feedback. It was an essential element of early governors and it became the standard tool when process control emerged in the 1940s [17] [18] [19] [20]. In process control today, more than 95% of the control loops are of PID type, most loops

are PI control. PID controllers are today found in all areas where control is used. The controllers come in many different forms. There are standalone systems in boxes for one or a few loops, which are manufactured by hundred thousand every year. PID control is an important ingredient of a distributed control system. The controllers are also embedded in many special purpose control systems. PID control is often combined with logic, sequential functions, selectors, and simple function blocks to build the complicated automation systems used for energy production, transportation, and manufacturing. Many sophisticated control strategies, such as model predictive control, are also organized hierarchically. PID control is used at the lowest level; the multivariable controller gives the set points to the controllers at the lower level [21] PID controllers have survived many changes in technology, from mechanics and pneumatics to microprocessors via electronic tubes, transistors, integrated circuits. The microprocessor has had a dramatic influence on the PID controller. Practically all PID controllers made today are based on microprocessors. This has given opportunities to provide additional features like automatic tuning, gain scheduling, and continuous adaptation [17].

2.12.1 Algorithm of PID Controller

A PID controller continuously calculates an error value as the difference between a desired set point and a measured process variable. The controller attempts to minimize the error over time by adjustment of a control variable, such as the position of a control valve, a damper, or the power supplied to a heating element, to a new value determined by a weighted sum [17] [18] [22].

$$U(t) = K_p e(t) + K_i \int_0^\tau e(\tau)d\tau + K_d \frac{de(t)}{dt} \tag{2.13}$$

Where, K_p, K_i and K_d all non-negative, denote the coefficients for the proportional, integral and derivative terms, respectively (sometimes denoted *P*, *I*, and *D*).

Proportional term: accounts for present values of the error. Because a non-zero error is required to drive it, a proportional controller generally operates with a so-called steady-state error. Steady-state error (SSE) is proportional to the process gain and inversely proportional to proportional gain. SSE may be mitigated by adding a compensating bias term to the set point or output, or corrected dynamically by adding an integral term [22].The proportion gain is given by

$$P_{out} = K_p \tag{2.14}$$

Integral term: accounts for past values of the error. The contribution from the integral term is proportional to both the magnitude of the error and the duration of the error. The integral in a PID controller is the sum of the instantaneous error over time and gives the accumulated offset that should have been corrected previously. The accumulated error is then multiplied by the integral gain and added to the controller output. The integral term is given by:

$$I_{out} = K_i \int_0^{\tau} e(\tau) d\tau \tag{2.15}$$

The integral term accelerates the movement of the process towards set point and eliminates the residual steady-state error that occurs with a pure proportional controller. However, since the integral term responds to accumulated errors from the past, it can cause the present value to overshoot the set point value [22].

Derivative term: accounts for possible future values of the error, based on its current rate of change. The derivative of the process error is calculated by determining the slope of the error over time and multiplying this rate of change by the derivative gain. The magnitude of the contribution of the derivative term to the overall control action is termed the derivative gain, K_d [22]

The derivative term is given by:

$$D_{out} = K_d \frac{de(t)}{dt} \tag{2.16}$$

Derivative action predicts system behavior and thus improves settling time of the system. An ideal derivative is not causal, so that implementations of PID controllers include an additional low pass filtering for the derivative term, to limit the high Temperature gain and noise [22].

As a PID controller relies only on the measured process variable, not on knowledge of the underlying process, it is broadly applicable. By tuning the three parameters of the model, a PID controller can deal with specific process requirements. The response of the controller can be described in terms of its responsiveness to an error, the degree to which the system overshoot set point, and the degree of any system oscillation. The use of the PID algorithm does not guarantee optimal control of the system or even its stability [17].

Some applications may require using only one or two terms to provide the appropriate system control. This is achieved by setting the other parameters to zero. A PID controller will be called a PI, PD, P or I controller in the absence of the respective control actions. PI controllers are fairly common, since derivative action is sensitive to measurement noise, whereas the absence of an

integral term may prevent the system from reaching its target value [20] [21]. The PID controller algorithm that operates as a position algorithm is shown in the following Figure 2.6.

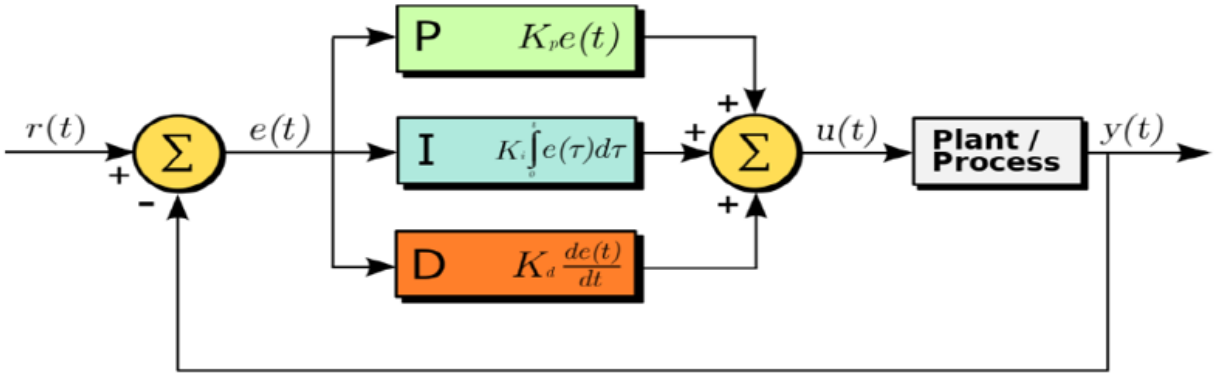


Figure 2.6: General block diagram of PID controller [22]

Where, $u(t)$ and $e(t)$ denotes the control and error signals of the system. K_p, K_i and K_d are the proportion, integral and derivative gain values respectively. The corresponding PID controller transfer function $G_c(s)$ is given as:

$$G_c(s) = K_p + \frac{K_i}{s} + K_d s \tag{2.17}$$

2.12.2 Limitations of PID Control

Although PID controllers can be used in many control situations with satisfactory performance, their performance in other applications may be relatively poor with no optimal performance. PID controllers, when used in cases that are non-linear may be unable to respond to the fluctuations in process behavior and may ultimately lag in their response to large disturbances. To solve such discrepancies, a knowledge of the control system can help include a feedforward control allowing the PID controller to only deal with the steady state error. Another serious challenge with the use of PID controllers is that they are linear and symmetric. Their performance in non-linear systems is unpredictable. This means that overshoot cannot easily be corrected like in linear systems. In trying to reduce overshoot in non-linear systems, the performance of the system may be compromised. Another issue with PID systems is that the derivative term can amplify high frequencies in a system and for non-linear systems, any large frequencies may be amplified to cause large discrepancies in the output of the system [22] [23].

2.13 Fuzzy Logic Controller

Fuzzy logic is a branch of artificial intelligence that deals with reasoning algorithms used to emulate human thinking and decision making in machines. These algorithms are used in applications where process data cannot be represented in binary form. For example, the statements "the air feels cool" and "he is young" are not discrete statements. Fuzzy logic interprets vague statements like these so that they make logical sense. In the case of the cool air, a PLC with fuzzy logic capabilities would interpret both the level of coolness and its relationship to warmth to ascertain that "cool" means somewhere between hot and cold. In straight binary logic, hot would be one discrete value (e.g., logic 1) and cold would be the other (e.g., logic 0), leaving no value to represent a cool temperature [24]. In contrast to binary logic, fuzzy logic can be thought of as gray logic, which creates a way to express in between data values. Fuzzy logic associates a grade, or level, with a data range, giving it a value of 1 at its maximum and 0 at its minimum [24].

Fuzzy logic requires knowledge in order to reason. This knowledge is provided by a person who knows the process or machine (the expert), is stored in the fuzzy system. For example, if the temperature rises in a temperature regulated batch system, the expert may say that the steam valve needs to be turned clockwise a "little bit." A fuzzy system may interpret this expression as a 10-degree clockwise rotation that closes the current valve opening by 5%. As the name implies, a description such as a "little bit" is a fuzzy description, meaning that it does not have a definite value [24].

Fuzzy logic has existed since the ancient times, when Aristotle developed the law of the excluded middle. In this law, Aristotle pointed out that the middle ground is lost in the art of logical reasoning; statements are either true or false. When PLCs were developed, their discrete logic was based on the ancient reasoning techniques. Thus, inputs and outputs could belong to only one set (i.e., ON or OFF); all other values were excluded. Fuzzy logic breaks the law of the excluded middle in PLCs by allowing elements to belong to more than just one set.

Around the 1920s, independent of Bertrand Russell, a Polish logician named Jan Lukasiewicz started working on multivalued logic, which created fractional binary values between logic 1 and logic 0. In a 1937 article in Philosophy of Science, Max Black, a quantum philosopher, applied this multivalued logic to lists (or sets) and drew the first set of fuzzy curves, calling them vague sets. Twenty-eight years later, Dr. Lofti Zadeh, the Electrical Engineering Department Chair at the

University of California at Berkeley, published a landmark paper entitled "Fuzzy Sets," which gave the name to the field of fuzzy logic. In this paper, Dr. Zadeh applied Lukasiewicz's logic to all objects in a set and worked out a complete algebra for fuzzy sets. Due to this groundbreaking work, Dr. Zadeh is considered to be the father of modern fuzzy logic [24] [25] [26].

2.13.1 Fuzzy Sets

Define a universe of discourse, X, as a collection of objects all having the same characteristics. The individual elements in the universe X will be denoted as x. In classical, or crisp, sets the transition for an element in the universe between membership and non-membership in a given set is abrupt and well-defined (said to be ''crisp''). For an element in a universe that contains fuzzy sets, this transition can be gradual. This transition among various degrees of membership can be led to the fact that the boundaries of the fuzzy sets are vague and ambiguous [24], [26]. Hence, membership of an element from the universe in this set is measured by a function that attempts to describe vagueness and ambiguity. Elements of a fuzzy set are mapped to a universe of membership values (degree to which a quality is possessed) using a function-theoretic form in the range of [0, 1]. If an element in the universe, say x, is a member of fuzzy set A, then this mapping is given by $\mu(x) \in [0, 1]$ [24].

Fuzzy Set Operations

Define three fuzzy sets A, B, and C on the universe X. For a given element x of the universe, the following function-theoretic operations for the set theoretic operations of union, intersection, and complement are defined for A, B, and C on X [26].

Union

$$\mu_{A\cup B}(x) = \mu_A(x) \vee \mu_B(x) = Max(\mu_A(x), \mu_B(x)) \tag{2.18}$$

Intersection

$$\mu_{A\cap B}(x) = \mu_A(x) \wedge \mu_B(x) = Min(\mu_A(x), \mu_B(x)) \tag{2.19}$$

Complement

$$\mu_{\hat{A}}(x) = 1 - \mu_A(x) \tag{2.20}$$

Excluded middle axioms, extended for fuzzy sets, are expressed by A∪A≠ X (axiom of excluded middle) and A∩A≠ ∅ (axiom of contradiction).

Fuzzy logic operation

The input to the fuzzy system is the output of the process, which is entered into the system via input interfaces. For example, in a temperature control application, the input data would be entered using an analog input module [24] [25] .This input information would then go through the fuzzy logic process, where the processor would analyze a database to obtain an output. Fuzzy processing involves the execution of IF...THEN rules, which are based on the input conditions. An input's grade specifies how well it fits into a particular graphic set (e.g., too little, normal, too much). Note that input data may also be represented as a count value ranging or as a percentage of error deviation. If the fuzzy logic system utilizes an analog input that has a count range from 0 to 4095, the graphs representing the input will cover the span from 0 to 4095 counts. Furthermore, the analog input information (0–4095 counts) may represent an error range, from –50% to +50%, of a process [24].The output of a fuzzy controller is also defined by grades, with the grade determining the appropriate output value for the control element.

Figure 2.7 illustrates a fuzzy logic cooling system chart with both input and output grades, where the horizontal axis is the input condition (temperature) and the vertical axis is the output (air-conditioner motor speed). In this chart, a single input can trigger more than one output condition. For example, if the input temperature is 137.5°F, then the temperature is part of two input curves it is 50% too cool and 50% normal. Consequently, the input will trigger two outputs the too cool input condition will trigger a less speed output, while the normal input will trigger a normal speed output condition. Since the fuzzy logic controller can have only one output, it completes a process called defuzzification to determine the actual final output value [24].

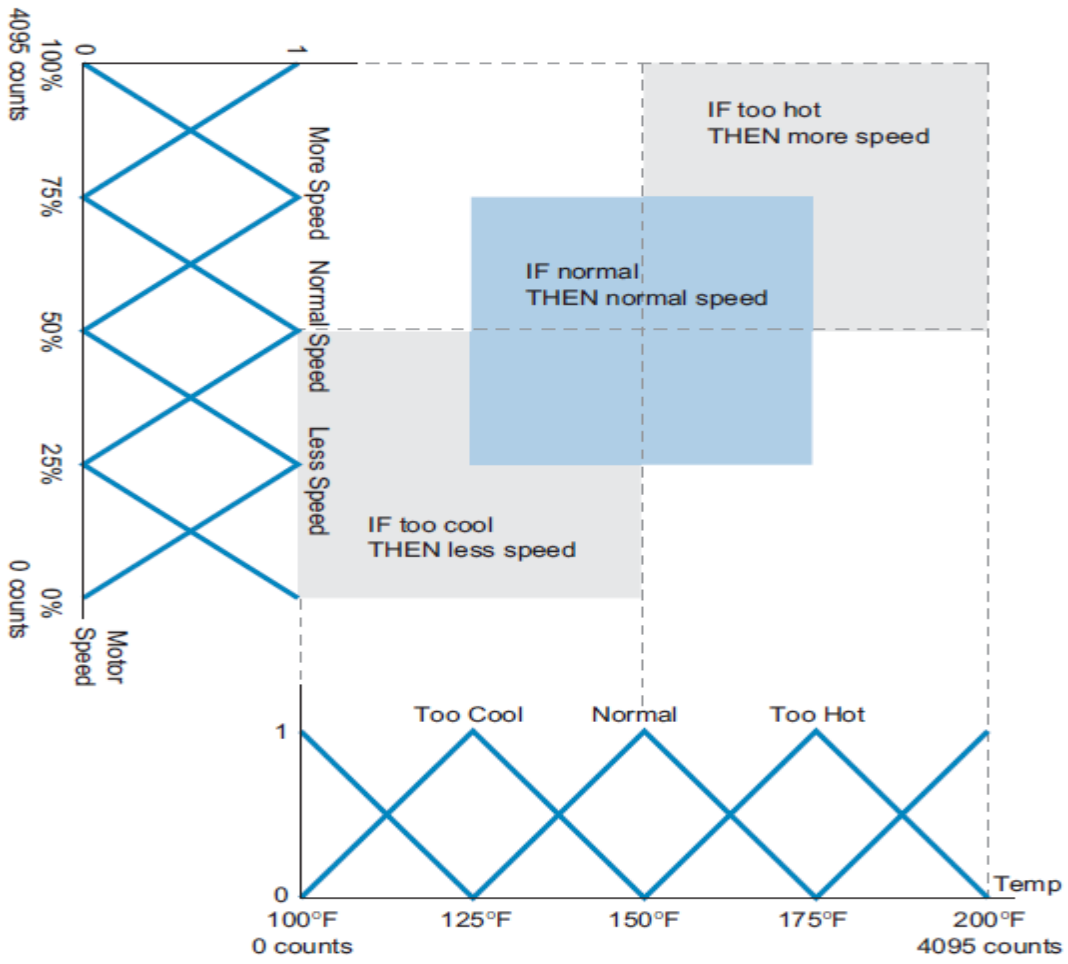


Figure 2.7: Fuzzy logic system chart showing both input and output grades [24]

2.13.2 Fuzzy Logic Control Components

The three main actions performed by a FLC are:

- Fuzzification
- Fuzzy Processing
- Defuzzification

As shown in Figure 2.8, when the fuzzy controller receives the input data, it translates it into a fuzzy form. This process is called fuzzification. The controller then performs fuzzy processing, which involves the evaluation of the input information according to IF…THEN rules created by the user during the fuzzy control system's programming and design stages. Once the fuzzy controller finishes the rule-processing stage and arrives at an outcome conclusion, it begins the

defuzzification process. In this final step, the fuzzy controller converts the output conclusions into "real" output data (e.g., analog counts) and sends this data to the process via an output module interface. If the FLC is located in the PLC rack and does not have a direct or built-in I/O interface with the process, then it will send the defuzzification output to the PLC memory location that maps the process's output interface module [24].

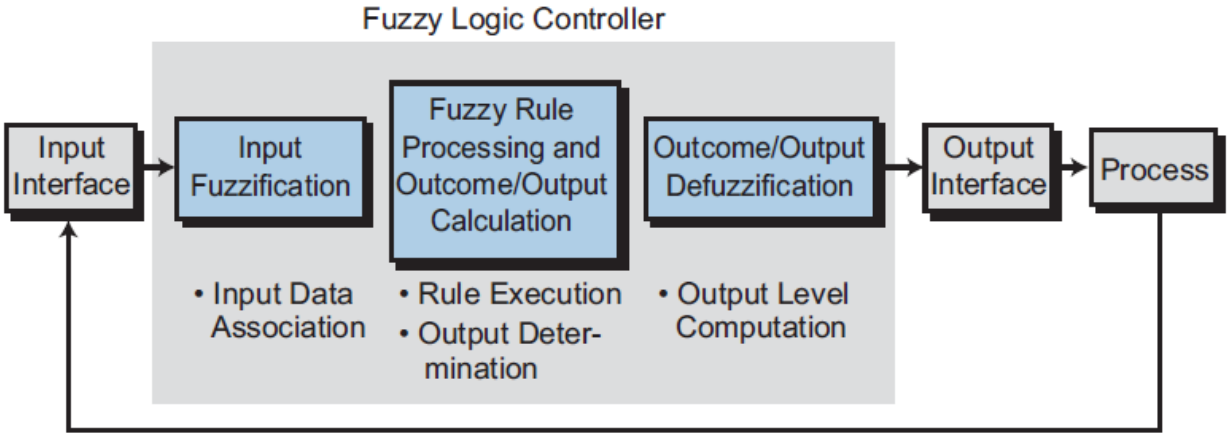


Figure 2.8: FLC operation [24]

Fuzzification Components

The fuzzification process is the interpretation of input data by the fuzzy controller. Fuzzification consists of two main components:

A) **Membership Functions**. During fuzzification, a fuzzy logic controller receives input data, also known as the fuzzy variable, and analyzes it according to user-defined charts called membership functions (see Figure 2.9). Membership functions group input data into sets, such as temperatures that are too cold, motor speeds that are acceptable, etc. The controller assigns the input data a grade from 0 to 1 based on how well it fits into each membership function (e.g., 0.45 too cold, 0.7 acceptable speed). Membership functions can have many shapes, depending on the data set, but the most common are the S, Z, Λ, and Π shapes shown in Figure 2.10. Note that these membership functions are made up of connecting line segments defined by the lines' end points. Each membership function can have up to three-line segments with a maximum of four end points. The grade at each end point must have a value of 0 or 1. As shown in Figure 2.11, a membership function's shape does not have to be symmetrical; however, it must comply with the previously discussed specifications. Figure 2.12 illustrates some incorrect membership function shapes [24].

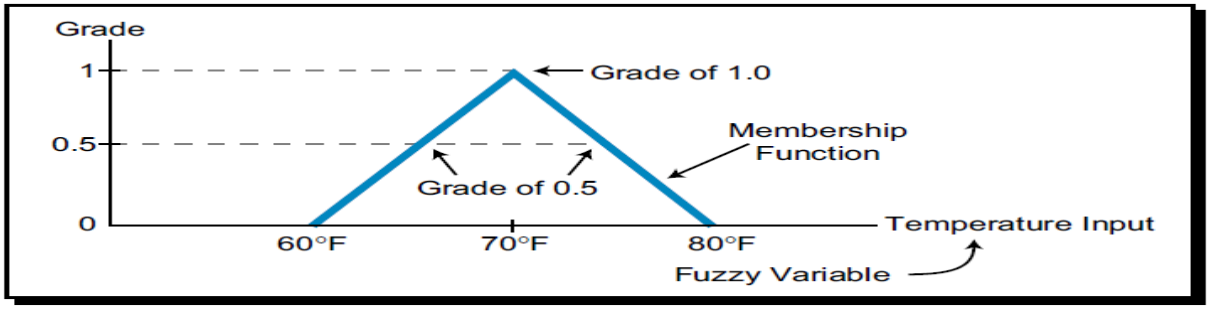


Figure 2.9: Membership function chart [24]

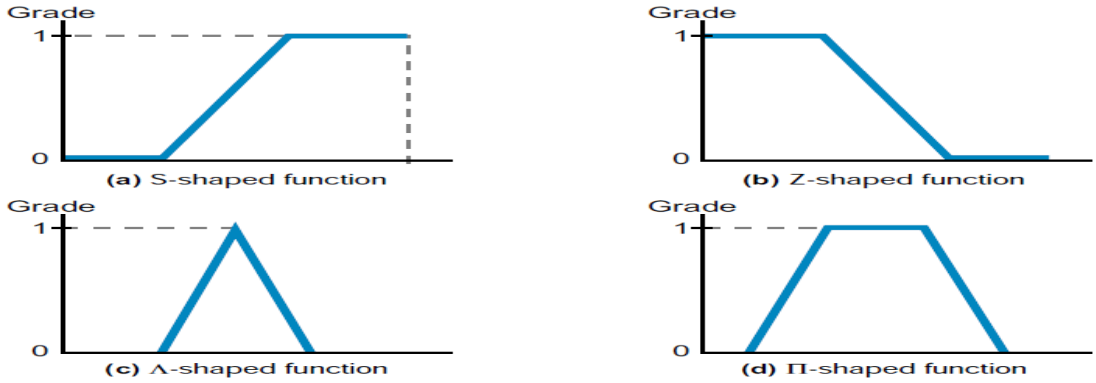


Figure 2.10: Membership function shapes: (a) S, (b) Z, (c) Λ, and (d) Π [24]

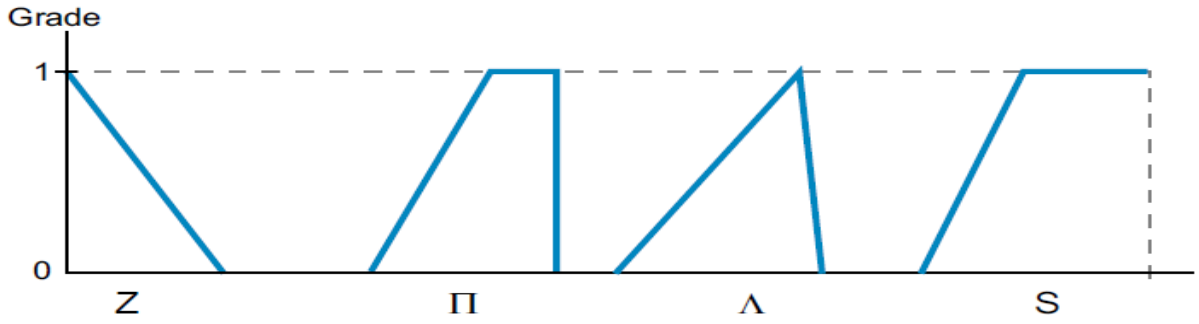


Figure 2.11: Asymmetrical membership functions [24]

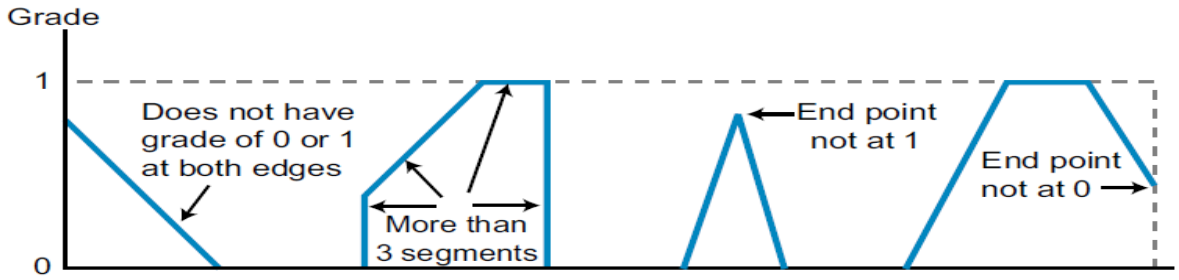


Figure 2.12: Incorrect membership function shapes [24]

Labels: Each fuzzy controller input can have several membership functions, with seven being the maximum and the norm, that define its conditions. Each membership function is defined by a name called a **label**. For example, an input variable such as temperature might have five membership functions labeled as cold, cool, normal, warm, and hot. Generically, the seven membership functions have the following labels, which span from the data range's minimum point (negative large) to its maximum point (positive large): NL (negative large), NM (negative medium), NS (negative small), ZR (zero), PS (positive small), PM (positive medium) and PL (positive large). Figure 2.13 illustrates an example of an input variable with seven Λ-shaped membership functions using all of the possible labels. A group of membership functions forms a **fuzzy set**. Figure 2.14 shows a fuzzy set with five membership functions. Although most fuzzy sets have an odd number of labels, a set can also have an even number of labels. For example, a fuzzy set may have four or six labels in any shape, depending on how the inputs are defined in relationship to the membership function [24].

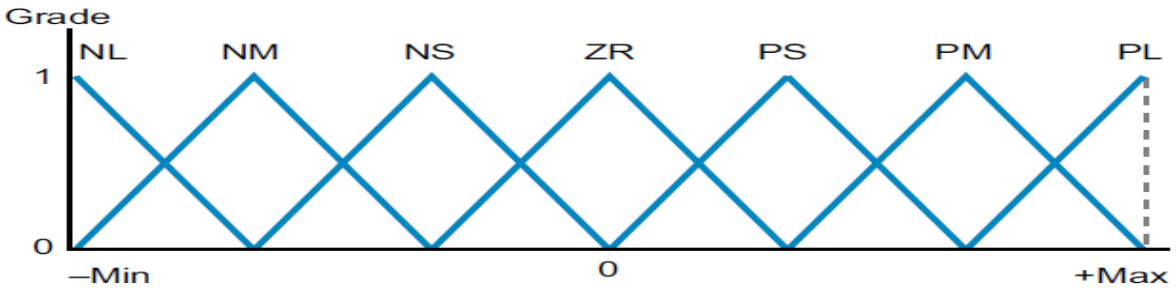


Figure 2.13: Fuzzy logic input using seven membership function labels [24]

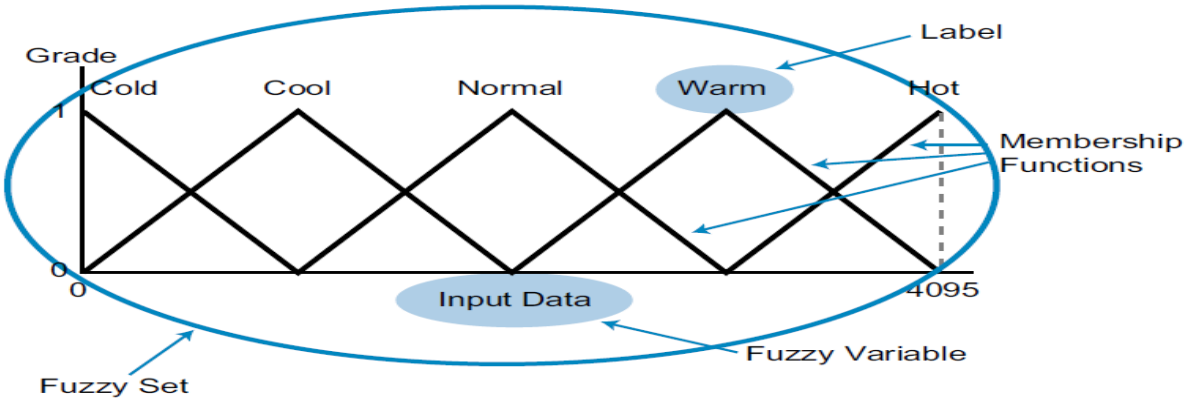


Figure 2.14: Fuzzy set with five membership functions [24]

Fuzzy Processing Components

During fuzzy processing, the controller analyzes the input data, as defined by the membership functions, to arrive at a control output. During this stage, the processor performs two actions:

Rule Evaluation: Fuzzy logic is based on the concept that most complicated problems are formed by a collection of simple problems and can, therefore, be easily solved. Fuzzy logic uses a reasoning process composed of IF...THEN rules, each providing a response or outcome. Basically, a rule is activated, or triggered, if an input condition satisfies the IF part of the rule statement. This results in a control output based on the THEN part of the rule statement. Sometimes, more than one rule is triggered at a time in a fuzzy control process. In this case, the controller evaluates all the rules to arrive at a single outcome value and then proceeds to the defuzzification process. Fuzzy logic rules with two inputs are often represented in matrix form to represent AND conditions. For example, Figure 2.15 illustrates a 3×3 matrix (9 rules) that uses two inputs, x_1 and x_2, and one output y_1. One advantage of this matrix representation is that it makes it easy to represent all the rules for a system. A five-label system translates into a 5×5 matrix with 25 rules, while a seven-label system produces a 7×7 matrix with 49 rules. An even membership function combination (e.g., a system with 6 labels for one input and 4 labels for another) will have a 24 rule matrix [24].

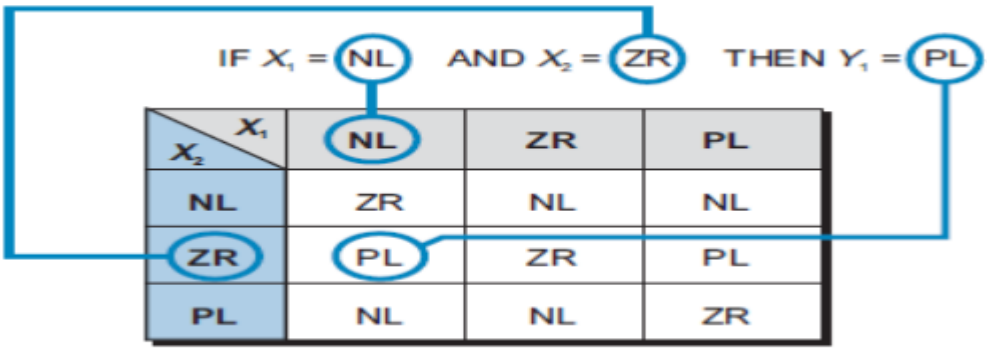


Figure 2.15: Fuzzy logic rule matrix [24]

2. Fuzzy Outcome Calculations: Once a rule is triggered, meaning that the input data belongs to a membership function that satisfies the rule's IF statement, the rule will generate an output outcome. This fuzzy output is composed of one or more membership functions (with labels), which have grades associated with them. The outcome's membership function grade is affected by the

grade level of the input data in its input membership function. In Figure 2.16a, the fuzzy input FI of 60% belongs to two membership functions, ZR and PS, corresponding to the grades of 0.6 and 0.4, respectively. These two grades will have an impact on the amount of the output (see Figure 2.16b) by intersecting the output membership functions at the same grade levels (0.6 and 0.4). However, the output membership function that is selected for the final output value depends on the user's programming of the IF...THEN rules [24] [25].

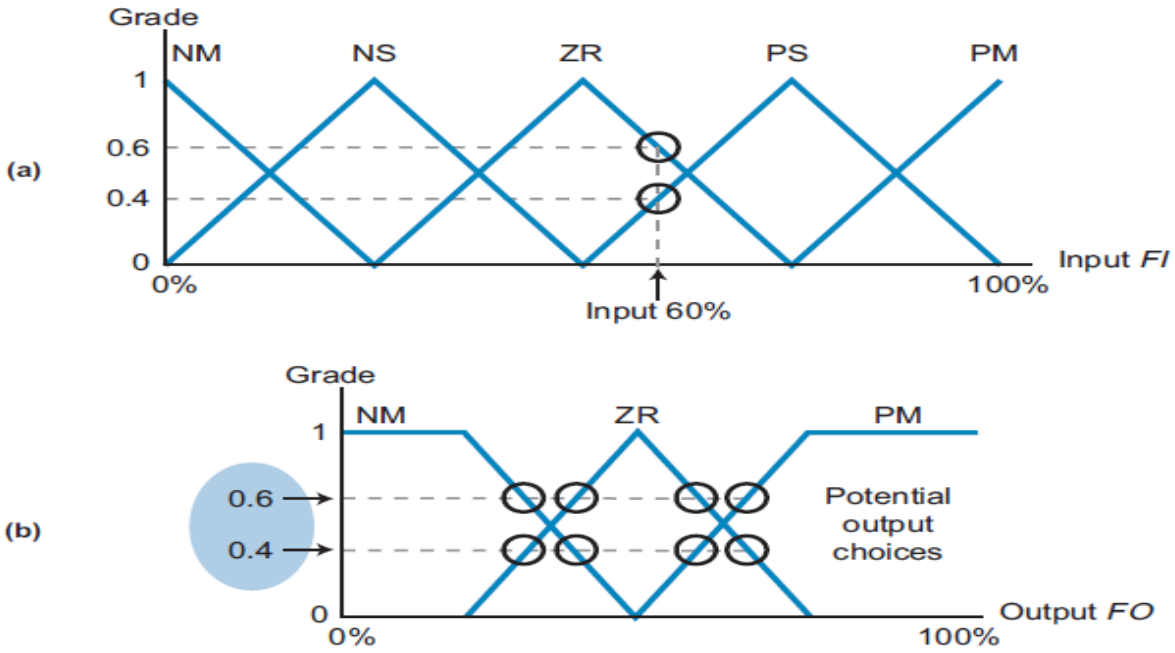


Figure 2.16: (a) Fuzzy input grades and (b) the resulting output grades [24]

The inference mechanism provides the mechanism for referring to the rule base such that the appropriate rules are fired. The two most commonly used inference procedures in FLC are Mamdani's Max-Min and Max-Algebraic Product (or Max-Dot) composition. The inference or firing with this fuzzy relation is performed via the operations between the fuzzified crisp input and the fuzzy relation representing the meaning of the overall set of rules. As a result of the composition, one obtains the fuzzy set describing the fuzzy value of the overall control output. In this thesis a Mamdani's Max-min composition inference method is used [24] [25].

Max-Min composition:

Consider a simple system where each rule comprises two antecedents and one consequent. A fuzzy system with two non-interactive inputs x1 and x2 (antecedents) and a single output y (consequent) are described by a collection of n linguistic IF-THEN rules [24] [25].

$$IF\ X_1\ is\ A_1{}^{(k)} and\ X_2\ is\ A_2{}^{(k)}\ THEN\ Y(k) is\ B^{(k)}, k = 1,2,3 \dots n\ , \quad (2.21)$$

Where

$A_1{}^{(k)}$ and $A_2{}^{(k)}$ are fuzzy sets representing the k^{th} antecedent pairs and $B^{(k)}$ are the fuzzy sets representing the k^{th} consequent.

Based on the Mamdani's max-min composition method of inference, and for a set of disjunctive rules, the aggregated output for the n rules will be given by [24] [25] [26]:

$$\mu_B{}^{(k)} = MaxMin\left[\left(\mu_{A1}{}^{(k)}\ input(i)\right).\left(\mu_{A2}{}^{(k)}\ input(j)\right)\right] \quad (2.22)$$

Where, i and j are input fuzzy set variables and y is output fuzzy set variable. The equation in (2.22) has a simple graphical interpretation, as seen in Figure 2.17.

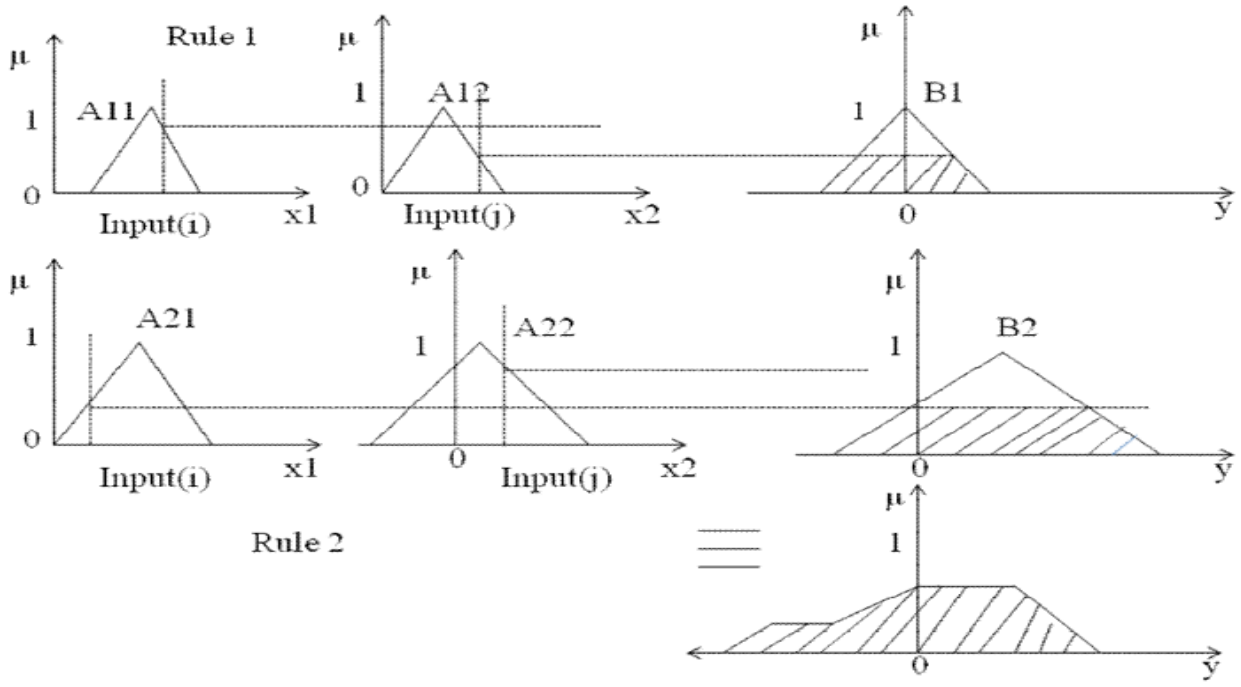


Figure 2.17: Fuzzy inference using Mamdani's max-min compositional operation [27]

The fuzzy IF-THEN rule in Figure 2.17 contains two rules. Both rules "IF x1 is A11 and x2 is A12 THEN y is B1" and "IF x1 is A21 and x2 is A22 THEN y is B2" are intersection fuzzy set operation and take the minimum membership values of the two inputs. Then the outputs of the two rules aggregated using the union fuzzy set operation that takes the maximum membership values of each fuzzy rule outputs. For this specific example equation (2.22) can be simplified as

$$\mu B(y) = Max\ [Min(\mu A11(input(i)), \mu A12(input(j)), Min\ (\mu A21(input(i)), \mu A22(input(j)))]. \quad (2.23)$$

Defuzzification Components

The final output value from the fuzzy controller depends on the defuzzification method used to compute the outcome values corresponding to each label. The defuzzification process examines all of the rule outcomes after they have been logically added and then computes a value that will be the final output of the fuzzy controller. The Fuzzy controller then sends this value to the output module. Thus, during defuzzification, the controller converts the fuzzy output into a real-life data value [24] [25] .There are many defuzzification methods, but all are based on mathematical algorithms. The two most common defuzzification methods are

1. Maximum Value Method: The maximum value method bases the final output value on the rule output with the highest membership function grade. This method is mainly used with discrete output membership functions.

2. Center of Gravity Method: The center of gravity method, also referred to as "calculating the centroid," mathematically obtains the center of mass of the triggered output membership functions. The center of gravity method is the most commonly used defuzzification method because it provides an accurate result based on the weighted values of several output membership functions. The center of gravity method applies to non-continuous, or discrete, output membership functions, as well as continuous ones.

2.14 Related Works

Various control strategies and methodologies are available for position control of PEA such as, a charge controller for linear operation of a piezoelectric stack actuator [4], adaptive PI-based sliding mode control for nano-positioning of piezoelectric actuators [5], sliding mode-based robust control for piezoelectric actuators with inverse dynamics estimation [6], discrete sliding mode control of piezo actuator in nano-scale range [7], nano-positioning fuzzy control for piezoelectric actuators [8] and adaptive PI control of piezoelectric systems using Takagi-Sugeno FL [9]. These approaches improve the control performance of the motor from different aspects. Nevertheless, all of the above controller techniques depend on the exact mathematical model of the drive system, which is difficult to achieve practically except the fuzzy logic-based controllers.

In [4], a charge controller for linear operation of a piezoelectric stack actuator has been developed. This paper examines the position control problem of piezoelectric stack actuators and presents a method for overcoming the hysteresis nonlinearity between the applied voltage and the actuator displacement. An inverting charge control circuit is implemented to linearize the stack actuator movement by taking advantage of the linear relationship between charge and displacement. The dc feedback causes the charge controller to behave as a voltage source when operating under quasi-static conditions. As a result, the actuator hysteresis is not eliminated for quasi-static excitations. In addition to this it didn't consider the hysteresis model and creep effect of actuator, but its objective is to reduce the hysteresis.

In [5]**,** adaptive PI-based sliding mode control for nano-positioning of piezoelectric actuators have been developed. This paper proposes an adaptive proportion-integral (PI)-based sliding mode control design (APISMC) used for nano-positioning of piezoelectric actuators (PEAs). Uncertainties of PEAs can be addressed by sliding mode control (SMC) since SMC is promising for positioning and tracking control. To further improve the response speed, suppress chattering, and reduce the steady-state error, the adaptive PI-based SMC is employed to replace the discontinuous control. Actually, the adaptive PI-based SMC offers a fast convergence of the sliding surface. Further, another advantage of the proposed controller lies in that its implementation only requires the online tuning PI parameters without acquiring the knowledge of bounds on system uncertainties. However, in conventional SMC design, the uncertainties must be bounded a priori. This typically yields to over conservative controllers, which may introduce two drawbacks: Poor tracking performance and undesirable oscillations in the control signal.

In [6], sliding mode-based robust control for piezoelectric actuators with inverse dynamics estimation have been developed. This paper presents an improved control approach to be used for piezoelectric actuators. The proposed approach is based on sliding mode control with estimation perturbation (SMCPE) techniques. Also, a proportional–integral–derivative (PID)-type sliding surface is proposed for position tracking. The proposed approach has been studied and implemented in a commercial actuator. A model for the system is introduced, which includes the Bouc–Wen (BW) model to represent the hysteresis.

In [7], discrete sliding mode control of piezo actuator in nano-scale range have been developed. In this paper discrete SMC of piezo actuator is demonstrated in order to achieve a very high accuracy in nano-scale with the desired dynamics. Despite the fast dynamics of the piezo actuator

the problem of chattering is eliminated with the SMC control structure. The piezo actuator suffers from hysteresis loop which is the inherent property and it gives rise to the dominant non-linearity in the system. The proposed SMC control structure has been proved to deliver chattering free motion along with the compensation of the non-linearity present due to hysteresis in the system. To further enhance the accuracy of the closed loop system and to be invariant to changes in the plant parameters a robust disturbance observer is designed on SMC framework by taking into consideration the lumped nominal plant parameters.

Even though, sliding mode control is a powerful control method that can produce a very robust closed-loop system under plant uncertainties and external disturbances, it suffers from many disadvantages. In ideal sliding mode control, the switching of control occurs at infinitely high frequency to force the trajectories of a dynamic system to slide along the restricted sliding mode subspace. In practice, it is not possible to change the control infinitely fast because of the time delay for control computations and physical limitations of switching devices. As a result, the sliding mode control action can lead to high frequency oscillations called chattering which may excite unmodeled dynamics, energy loss, and system instability and sometimes it may lead to plant damage. Another disadvantage of sliding mode control is that sliding mode controllers fail to deal with unmatched uncertainties. Another main disadvantage of the conventional sliding mode control scheme is that the performance of the controller heavily depends on the sliding surface. If the sliding surface of sliding mode controller is not designed properly, it may lead to unacceptable performance. The selection of optimum sliding surface is tedious and a complicated task.

In [8], nano-positioning fuzzy control for piezoelectric actuators have been developed. This paper aims to design a fuzzy controller to manipulate piezoelectric (PZT) actuators for nano-positioning applications. A Bouc-Wen model is adopted to represent the dynamics and hysteresis behavior in a piezo-actuated positioning stage. A simulation work is carried out for fuzzy control development and the results are compared to that obtained using PI controller based on observer. The results affirmed the potential of the developed fuzzy control algorithm whereas the tracking error is reduced to a sub-nanometer precision.

In [9] , adaptive PI control of piezoelectric systems using Takagi-Sugeno FL have been developed**.** This paper presents the nano-positioning control of a piezoelectric platform. A Bouc-Wen model is established to describe the nonlinear hysteretic effect of piezoelectric systems. Three kinds of compensators, PI controller, PI-like FLC and adaptive PI-FLC controller, are designed for the

piezoelectric systems. The adaptive PI controller is tuned on-line by means of Takagi-Sugeno fuzzy logic. Computer simulation demonstrates that the adaptive PI-FLC controller possesses the best robustness against external disturbance. As a limitation in this work, instead of linearizing the hysteresis or using inverse hysteresis as feed forward in order to get appropriate (linearized) system model and it uses conventional PI controller.

From the above review different literatures are reviewed about PEAs properties, manufactures and different displacement controller mechanisms. In this paper self-tuning FPID controller for displacement control of PEAs with linearized hysteresis is modeled and simulated.

CHAPTER THREE
MATERIALS AND METHODS

This chapter deals with the materials and the methods used in accomplishing the thesis. The materials used are digital computer and MATLAB/SIMULINK software. Modeling, designing and analyzing are the methods used. The following sections present each of these in detail.

3.1 Modeling of Stack PEA

The first step in the analysis and design of the control system is mathematical modeling of the different components. The transfer function method is widely used in designing control systems. After proper assumptions and approximations are made to linearize the mathematical equations describing the PEA components, transfer functions are obtained. Thus, using these transfer functions, the stack PEA is modeled for position control.

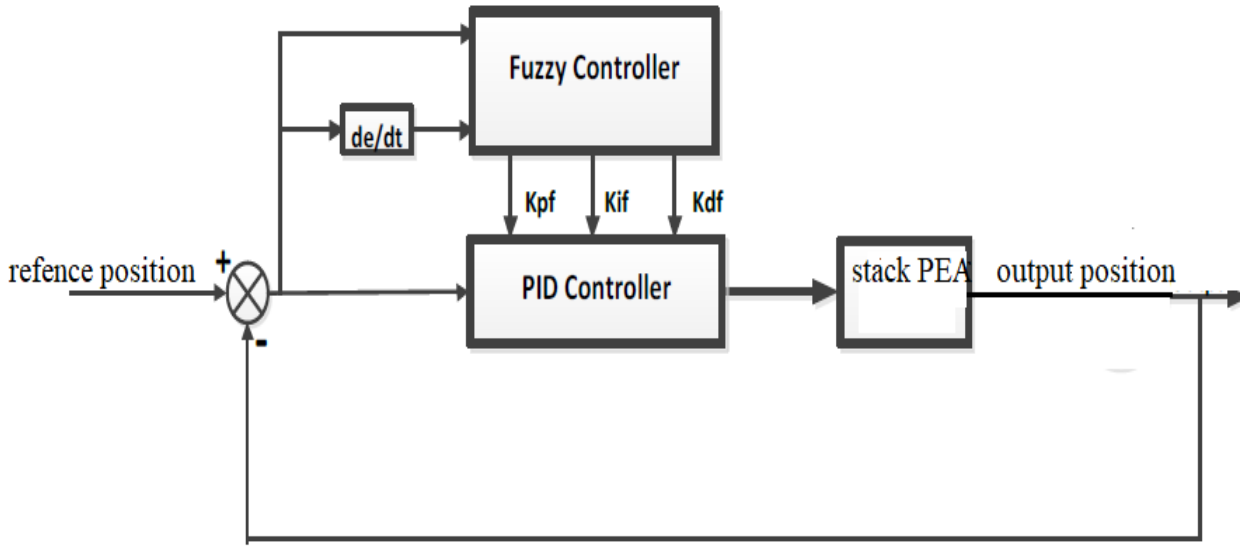


Figure 3.1: General block diagram of FPID based position control for stack PEA

3.1.1 Electromechanical Model of Stack PEA

The most widely spread PEA configuration is the stacked one, of which a schematic representation is given in Figure 3.2. Such a PEA stack consists of the series connection of a number of piezo wafers with an electrode between every two wafers. Clearly the wafers are in series mechanically and in parallel electrically. The latter is done in order to strengthen the effect of the individual wafers. With different sub-models representing hysteresis, creep, and vibration dynamics of PEAs

defined, macroscopic PEA models are constructed by connecting such sub-models according to certain model structures. There are two categories of model structures for macroscopic PEA models. In the first category, the behavior of a PEA, when subject to a voltage input and an external loading force, is decoupled into several effects such as rate-independent hysteresis, vibration dynamics, and creep based on physical laws. Such effects are then represented by individual sub-models and such sub-models are connected in various manners to form a comprehensive model of the PEA. The most well-known model structure of PEAs belonging to this category is the electromechanical model proposed in [11] . *H* represents the hysteresis effect and u_{in} is the voltage due to this effect.

The piezoelectric effect is represented by T_{em}, which is an electromechanical transducer with transformer ratio T_{em}. The capacitance C_e represents the sum of the capacitances of the individual PZT wafers, which are electrically in parallel. The total current flowing through the circuit is q. Furthermore, q may be seen as the total charge in the PZT actuator. The charge q_p is the transduced charge from the mechanical side. The voltage u_p is due to the piezo effect. The total voltage over the PZT actuator is u_{in}, F_p is the transduced force from the electrical side, F_{ext} is the externally applied force, and the resulting elongation of the PZT actuator is denoted by *x*. The mechanical relation between F_p and *x* is denoted by *M*. Note that we have equal electrical and mechanical energy at the ports of interaction, i.e.

$$u_p q_p = F_p x \tag{3.1}$$

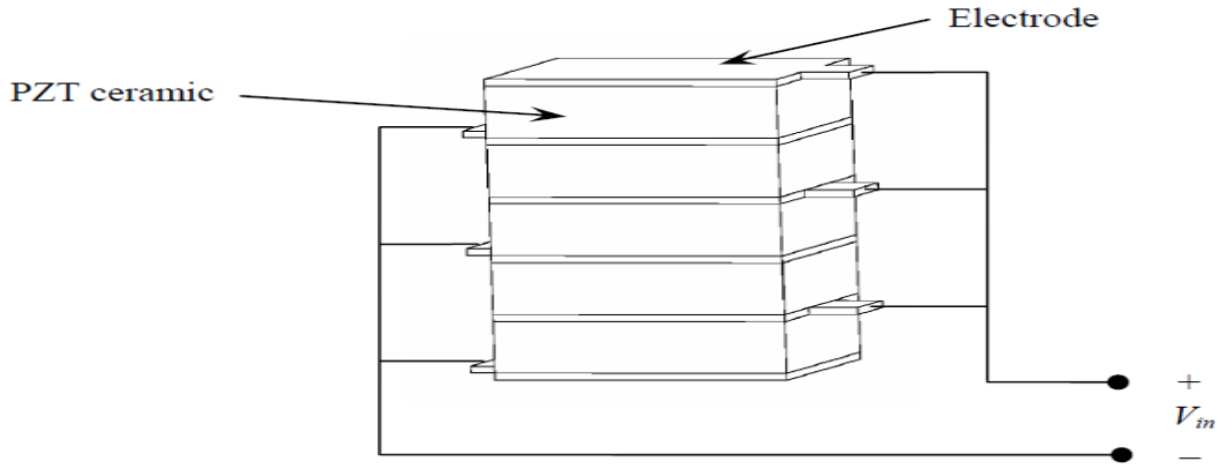


Figure 3.2: Illustration of a PZT stack actuator [7]

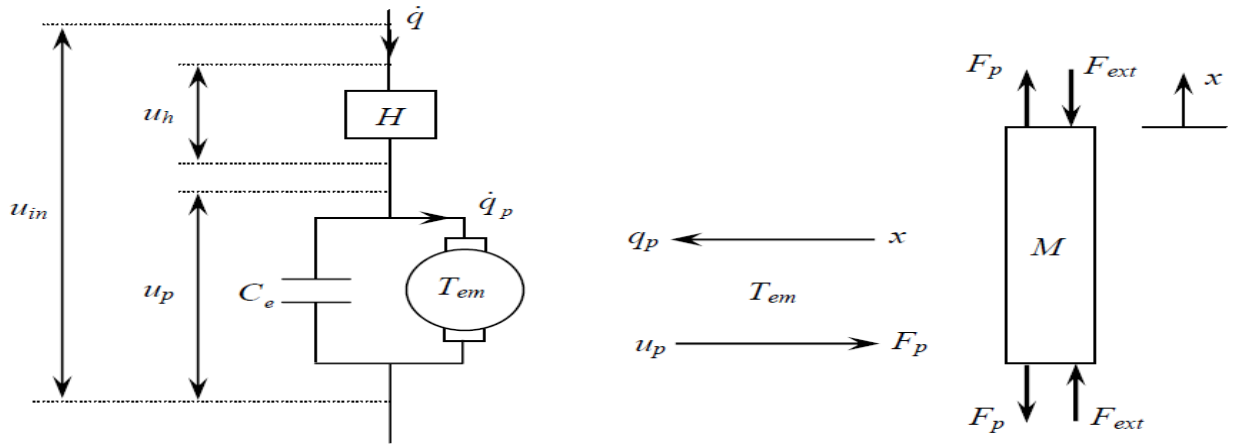


Figure 3.3: Electromechanical model [7]

The piezoelectric ceramic has elasticity modulus ε, viscosity η, and mass density ρ. Furthermore, the geometrical properties of the PZT actuator are length L and cross-sectional area A. Mass M, stiffness K, and damping coefficient C can be calculated from the material and geometrical properties as follows [7] [11]:

$$M = \rho AL \tag{3.2}$$

$$K = \frac{\varepsilon A}{L} \tag{3.3}$$

$$C = \frac{\eta A}{L} \tag{3.4}$$

The complete electromechanical Equations are defined by (3.5) to (3.10) [7] [11].

$$u_p = u_{in} - u_h \tag{3.5}$$

$$u_h = H_{(q)} \tag{3.6}$$

$$q = C_e u_p + q_p \tag{3.7}$$

$$q_p = T_{em} x \tag{3.8}$$

$$F_p = T_{em} u_p \tag{3.9}$$

$$M\ddot{x} + C\dot{x} + Kx = F_p - F_{ext} \tag{3.10}$$

3.1.2 Hysteresis Modeling of Stack PEA

Piezoelectric materials can undergo reversible phase transitions as a result of voltage and pressure. Due to these special material properties, piezoelectric materials have become increasingly popular in sensors and actuators. PEAs have been employed in precision positioning systems for their large force generation, high stiffness, high resolution and fast response. However, they commonly exhibit strong hysteresis behaviors, which greatly degrade the overall positioning accuracy. According to whether the rate of the input is considered or not, hysteresis behaviors can be divided into rate-dependent and rate-independent hysteresis behaviors. The corresponding hysteresis models can be classified into rate-dependent and rate-independent hysteresis models.

Over the past few decades, great efforts have been devoted to developing hysteresis models such as: Duhem model [28], Maxwell-Slip model [29],the Prandtl–Ishlinskii model, Preisach model, Polynomial-based hysteresis model, and Bouc–Wen model [30] [31] .For modeling of rate-independent hysteresis, it mainly focuses on the nonlinear relationship between the amplitude of input voltage and output displacement at low input frequency or rate. However, for modeling of rate-dependent hysteresis, it needs an analysis of the nonlinear relationship between the rate of input voltage and output displacement at high input frequency or rate. Comparisons of rate-dependent and rate-independent hysteresis models reveal that the rate-independent model is just a special kind of rate-dependent model when the rate of input is low enough. Therefore, it is more difficult to develop the rate-dependent model relatively. Overall, most related literatures focused on developing rate-independent hysteresis models and few literatures paid attention to modeling of rate-dependent hysteresis. Due to its differential equations and ability to capture an analytical form, the Bouc–Wen model has been widely applied in hysteresis modeling and compensation for PEAs [31].

3.1.2.1 Bouc-Wen Hysteresis Model

The model is starting on the force versus displacement graph below.

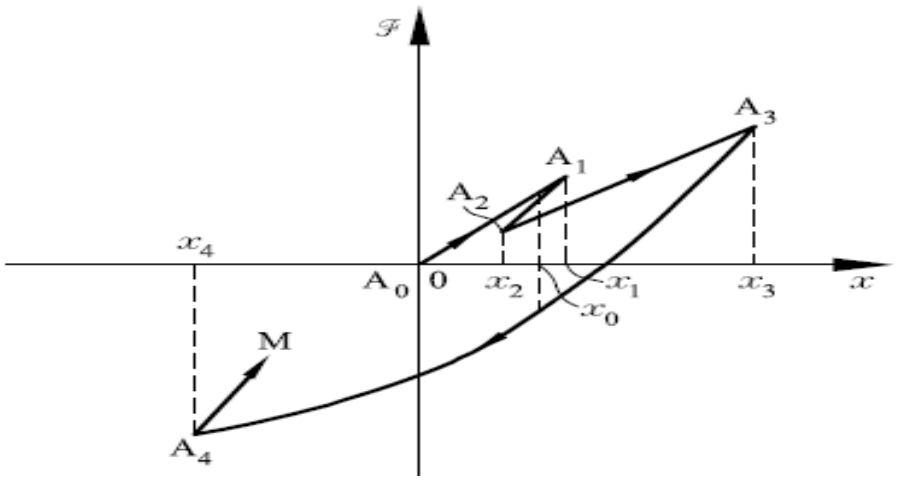


Figure 3.4: Force versus displacement for a hysteresis functional [32]

The hysteresis phenomenon was proposed. Consider Figure 3.4 where F is a force and x a displacement. Four values of F correspond to the single point $x = x_o$, which means that F is not a function. If we consider that x is a function of time, then the value of the force at the instant time t will depend not only on the value of the displacement x at the time t, but also on the past values of x. The following simplifying assumption is made.

Assumption: The graph of Figure 3.4 remains the same for all increasing function $x(\cdot)$ between 0 and x_1, for all decreasing function $x(\cdot)$ between the values x_1 and x_2, etc. Assumption is what, in the current literature, is called the rate-independent to precise the form of the functional F [32],

$$\frac{dF}{dt} = g(x, F, sign\left(\frac{dx}{dt}\right))\frac{dx}{dt} \tag{3.11}$$

Consider the equation

$$\frac{d^2x}{dt^2} + F\ (t) = p\ (t) \tag{3.12}$$

for some given input p(t) and initial conditions $\frac{dx}{dt}(t_o)$, x(t_o) and$F(t_o)$ at the initial time instant t_o. Equations (3.11) and (3.12) describe completely a hysteretic oscillator. It is difficult to give explicitly the solution of (3.11) due to the nonlinearity of the function g. For this reason, the author proposes the use of a variant of the Stieltjes integral to define the functional F [32];

$$\mathrm{F}(\mathrm{t}) = \mu^2 \mathrm{x}(\mathrm{t}) + \int_{\beta}^{t} F(V^t s)dx(s) \tag{3.13}$$

where $\beta \in (-\infty, +\infty)$ is the time instant after which the displacement and force are defined. The term V_s^t is the total variation of x in the time interval $[s, t]$. The function F is chosen in such a way that it satisfies some mathematical properties compatible with the hysteresis property [32].

$$F(u) = \sum_{i=1}^{N} A_i e^{-\gamma_i u} \tag{3.14}$$

Equations (3.12) – (3.14) can then be written in the form [32]

$$\frac{d^2x}{dt^2} + \mu^2 \mathrm{x} + \sum_{i=1}^{N} \mathrm{Z}_i = \mathrm{p}(\mathrm{t}) \tag{3.15}$$

$$\frac{d\mathrm{Z}_i}{dt} + \gamma_i \left|\frac{dx}{dt}\right| \mathrm{Z}_i - A_i \frac{dx}{dy} = 0, \quad \mathrm{i} = 1, \ldots\ldots, \mathrm{N} \tag{3.16}$$

Equations (3.15)– (3.16) are what is now known as the Bouc model. To describe restoring forces with hysteresis in the following form:

$$\dot{z}(t) = -\gamma|\dot{x}(t)|z(t)^{n^{\cdot}} - \beta\dot{x}(t)|z^n| + A\dot{x}(t) \qquad for\ n\ odd \tag{3.17}$$

$$\dot{z}(t) = -\gamma|\dot{x}(t)|z(t)^{n-1}|z(t)| - \beta\dot{x}(t)z(t)^n + A\dot{x}(t) \quad for\ n\ even \tag{3.18}$$

Equations (3.17)– (3.18) constitute the earliest version of what is called now the Bouc-Wen model. Re- write Equation (3.17) and (3.18) by replacing "z" by "h" for simple understanding and express thus equations as a function of time.

$$\dot{h}(t) = A\dot{x}(t) - \beta\dot{x}(t)|h(t)^n| - \gamma|\dot{x}(t)|h(t)^n \qquad \text{for n odd} \tag{3.19}$$

$$\dot{h}(t) = A\dot{x}(t) - \beta\dot{x}(t)h(t)^n - \gamma\dot{x}(t)h(t)^{n-1}|h(t)| \qquad \text{for n even} \tag{3.20}$$

Since n is odd, Equation (3.19) should be taken as the hysteresis equation. Where $h(t)$ indicates the variable obtained from the hysteretic nonlinear dynamics (i.e. hysteresis displacement). A, n, $\beta\ and\ \gamma$ are parameters describing the hysteretic loop's magnitude and shape with n governing the smoothness of the transition from elastic to plastic response. For the elastic structure and material,

$n = 1$ is assigned. For this paper $n = 1$, since the piezoelectric actuators have elastic behavior. A is parameter controlling hysteresis amplitude and x (t) is piezoelectric displacement substitute $n = 1$ in Equation (3.19) and it becomes [32] [33] [34] [35] [36]:

$$\dot{h}(t) = A\dot{x}(t) - \beta\dot{x}(t)|h(t)| - \gamma|\dot{x}(t)|h(t) \tag{3.21}$$

$$T_{em} = Kd \tag{3.22}$$

Where d is effective piezoelectric coefficient.

$$Fu_h = Kh(t) \tag{3.23}$$

Substitute the expression of T_{em} in Equation (3.22) into Equation (3.9), the expression of u_h in Equation (3.23) into Equation (3.5) and there for Equation (3.9) can be re write as:

$$F_p = K(du_{in} - h(t)) \tag{3.24}$$

There for Equation (3.10) can be re write as [7] [11]:

$$\mathrm{M}\ddot{x} + C\dot{x} + Kx = \mathrm{K}(\mathrm{d}u_{in} - \mathrm{h(t)}) - F_{ext} \tag{3.25}$$

$$F_{ext} = Kx_o \tag{3.26}$$

For the linearized hysteresis model Equation (3.25) can be re write as:

$$\mathrm{M}\ddot{x} + C\dot{x} + Kx = \mathrm{K}(\mathrm{d}u_{in} - \mathrm{z(t)}) - F_{ext} \tag{3.27}$$

Where $x_o$the initial displacement at u_{in} is zero. Equation (3.27) is the mathematical model of linearized stack PEA including hysteresis effect.

3.1.3 Gaussian Stochastic Linearization

The hysteretic behavior of materials, structural elements or vibration isolators is treated in a unified manner by a single strongly nonlinear differential equation. There are three most common linearization techniques. These are Fokker Planck equation, the perturbation technique and stochastic linearization approaches. Among these techniques stochastic linearization approach is one of the most efficient technique for approximating non-linear models within the system operating domain is the linearization method, both for deterministic and stochastic inputs [37].

The linearization method is presented and applied for a nonlinear system with hysteretic characteristic shown in Figure 3.5.

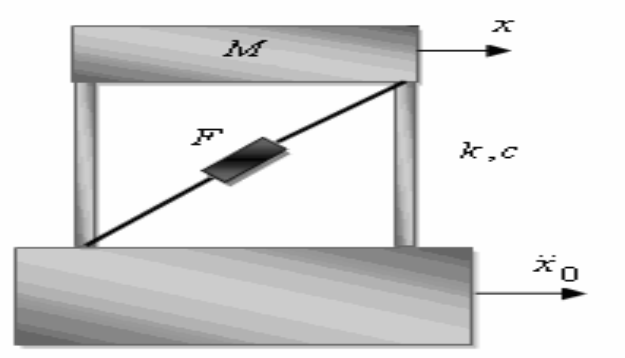


Figure 3.5: Schematic of mechanical system [37]

For the system given by Figure 3.6 the equation of motion for Gaussian stationary white noise process is given by [37];

$$M\ddot{x} + C\dot{x} + Kx + F(x,\dot{x}) = -M\ddot{x}_o \tag{3.28}$$

Where $F(x,\dot{x})$ is the symmetric restoring force developed by the bracing hysteretic device within the operating range $-x_m \le x(t) \le x_m$,$-F_m \le F(x) \le F_m$. $\ddot{x}_o$ is a Gaussian stationary white noise process. Assume the following expressions:

$$\left.\begin{aligned} \xi(t) = x(t)/x_m, \quad z(t) = F(x_m\xi)/Mx_m, \\ \xi_m = max|\xi(t)|, \quad z_m = max|z(t)| = F_m/Mx_m \end{aligned}\right\} \tag{3.29}$$

A generic plot of the symmetric hysteresis loop $z(\xi)$ is looks like in Figure 3.6. The output $\xi(t)$ and input $\eta(t)$ will be given the same name as its physical counterparts $x(t)$ and $\ddot{x}_o(t)$.

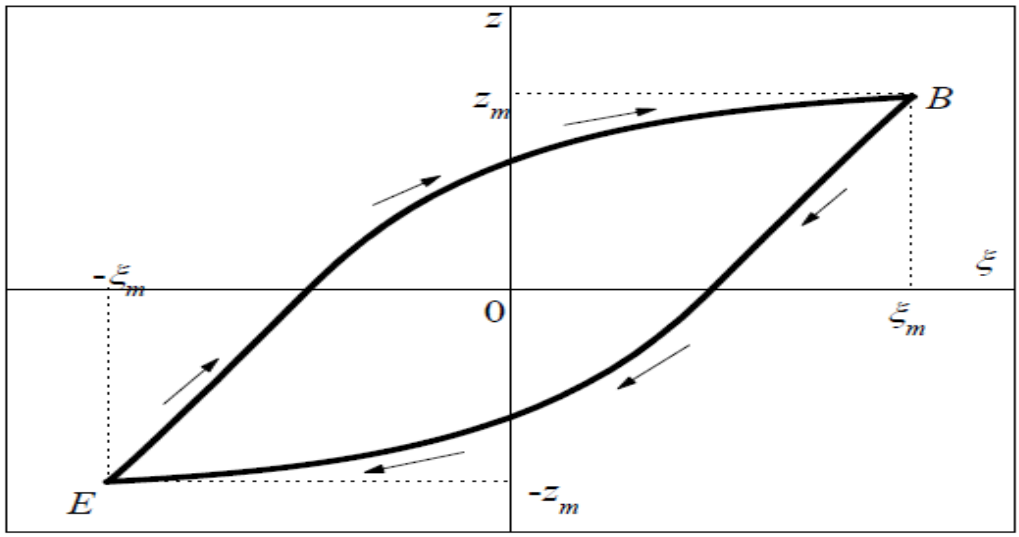


Figure 3.6: Generic experimental hysteretic loop [37]

Equation (3.28) can be written as [37]:

$$\left.\begin{aligned} \ddot{\xi} + 2\omega\zeta\dot{\xi} + \omega^2\xi + \mathrm{z} = \eta\,(\mathrm{t}) \\ \omega = \sqrt{\frac{K}{M}}, \zeta = \frac{C}{2\sqrt{KM}}\ ,\ \ \eta\,(\mathrm{t}) = -\frac{\ddot{x_o}}{x_m} \end{aligned}\right\} \tag{3.30}$$

Where $E[\eta(t')\eta(t'+t)] = 2\pi S_0\delta(t), S_\eta(\omega) = S_0$.

The nonlinear hysteresis displacement expression in Equation (3.21) can be rewrite as in the form of Equation (3.31) [37]:

$$\dot{z(t)} = a\mathrm{z} + \mathrm{b}\dot{\xi} + \mathrm{c}\xi \tag{3.31}$$

with $a < 0$, a, b and c are coefficients which are calculated by minimizing the expected value of the square error becomes [37]:

$$\mathcal{E}^2 = \dot{[}h(t) - \left(a\mathrm{z} + \mathrm{b}\dot{\xi} + \mathrm{c}\xi\right)]^2 \tag{3.32}$$

Linear equivalent system is given as [37]:

$$\left.\begin{aligned} \ddot{\xi} + 2\omega\zeta\dot{\xi} + \omega^2\xi + z = \eta(\mathrm{t}) \\ \dot{z}(t) = az + b\dot{\xi} + c\xi \end{aligned}\right\} \tag{3.33}$$

By solving Fokker-Planck equation the second order statistical moments of stabilized solution of stochastic system in Equation (3.33) can be determined. Using the notations [37]:

$$\xi = [\xi, \dot{\xi}, z\,]^T, \xi_{1=\xi}, \xi_2 = \dot{\xi}, \xi_3 = z, dw(t) = \eta(t)dt, \tag{3.34}$$

Where $dw(t) = w(t+dt) - w(t)$ is the infinitesimal Wiener increment, the system (3.33) is equivalent with [37]:

$$\left.\begin{aligned} \frac{d\xi_3}{dt} = \mathrm{c}\xi_1 + \mathrm{b}\xi_2 + a\xi_3 \\ \frac{d\xi_2}{dt} = -\omega^2\xi_1 - 2\omega\zeta\xi_2 - \xi_3 + \eta(\mathrm{t}) \\ \frac{d\xi_3}{dt} = \mathrm{c}\xi_1 + \mathrm{b}\xi_2 + a\xi_3 \end{aligned}\right\} \tag{3.35}$$

In matrix form it can be given by [37]:

$$\frac{d\xi(t)}{dt} = \begin{bmatrix} 0 & 1 & 0 \\ -\omega^2 & -2\omega\zeta & -1 \\ c & b & a \end{bmatrix} \begin{bmatrix} \xi_1 \\ \xi_2 \\ \xi_3 \end{bmatrix} + \begin{bmatrix} 0 \\ 1 \\ 0 \end{bmatrix} \eta(t) \tag{3.36}$$

The linear stochastic differential equation is given by [37]:

$$d\xi(t) = A\xi(t)dt + Gdw(t) \tag{3.37}$$

Where,

$$A = \begin{bmatrix} 0 & 1 & 0 \\ -\omega^2 & -2\omega\zeta & -1 \\ c & b & a \end{bmatrix} G = \begin{bmatrix} 0 \\ 1 \\ 0 \end{bmatrix} \tag{3.38}$$

From Planck equation [37]:

$$AC_\xi + C_\xi A^T + 2\pi G S_0 G^T = 0 \tag{3.39}$$

Where C_ξ is the solution of Equation (3.39) and represents the steady-state instantaneous covariance matrix which have the form [37]:

$$C\xi = \begin{bmatrix} C_{11} & C_{12} & C_{13} \\ C_{21} & C_{22} & C_{23} \\ C_{31} & C_{32} & C_{33} \end{bmatrix} \; C_{12}, C_{21} = 0 \tag{3.40}$$

Equation (3.39) yields [37]:

$$\left.\begin{aligned} \sigma_\xi^2 = C_{11} &= \frac{\pi S_0}{\Delta}(\omega^2 a - 2\omega\zeta a^2 + a^3 - c\,), \\ \sigma_{\dot{\xi}}^2 = C_{22} &= \frac{\pi S_0}{\Delta}[\omega^4 a - 2\omega^3\zeta a^2 + \omega^2(a^3 + ab - c) + 2\omega\zeta ac - c(a^2 + b)] \\ \sigma_z^2 = C_{33} &= \frac{\pi S_0}{\Delta}(\omega^2 ab^2 - 2\omega\zeta c^2 + ac^2 - b^2 c) \end{aligned}\right\} \tag{3.41}$$

And

$$\left.\begin{aligned} \sigma_{\xi z} = C_{13} &= \frac{\pi S_0}{\Delta}[\omega^2 ab + 2\omega\zeta ac - c(a^2 + b)] \\ \sigma_{\dot{\xi} z} = C_{23} &= \frac{\pi S_0}{\Delta}[-\omega^2 a(ab + c) + c^2 + abc] \\ \rho_{\xi z} = \frac{\sigma_{\xi z}}{\sigma_{x\sigma_z}}, \rho_{\dot{\xi} z} &= \frac{\sigma_{\dot{\xi} z}}{\sigma_{\dot{\xi}}\sigma_z} \end{aligned}\right\} \tag{3.42}$$

With $\Delta = 2\omega^5\zeta a - 4\omega^4\zeta^2 a^2 + 2\omega^3\zeta(a^3 + ab - c) + \omega^2 a(4\zeta^2 c - ab - c) - 2\omega\zeta c(a^2 + b) + abc \neq 0,$ (3.43)

From joint Gaussian behavior of the state vector $\xi = [\xi, \dot{\xi}, z\ ]^T$, the values of the coefficients can be determined using Equation (3.44) [37] [38].

$$\left.\begin{array}{c} a = E[\frac{\partial h}{\partial z}] = -\beta F_3 - \gamma F_4 \\ a = E[\frac{\partial h}{\partial z}] = -\beta F_3 - \gamma F_4 \\ c = 0 \end{array}\right\} \quad (3.44)$$

Where the functions $F_i, i = 1, 2, 3, 4$ are given by Equation (3.45) [37] [38]:

$$\left.\begin{array}{c} F_1 = \frac{\sigma_z^n}{\pi}\Gamma\left(\frac{n+2}{2}\right)2^{n/2} I_s \\ F_2 = \frac{\sigma_z^n}{\sqrt{\pi}}\Gamma\left(\frac{n+1}{2}\right)2^{n/2} \\ F_3 = \frac{n\sigma_{\dot{\xi}}\sigma_z^{n-1}}{\pi}\left(\frac{n+2}{2}\right)2^{n/2}\left[2\left(1-\rho_{\dot{\xi}z}^2\right)^{\frac{n+1}{2}} + \rho_{\dot{\xi}z} I_S\right] \\ F_4 = \frac{n\rho_{\dot{\xi}z}\sigma_{\dot{\xi}\sigma_z^{n-1}}}{\sqrt{\pi}}\Gamma\left(\frac{n+1}{2}\right)2^{n/2} \end{array}\right\} \quad (3.45)$$

With

$$I_s = 2\int_l^{\frac{\pi}{2}} sin^n\theta \mathrm{d}\theta, \mathrm{l} = \tan^{-1}\left(\frac{\sqrt{1-\rho_{\dot{\xi}z}^2}}{\rho_{\dot{\xi}z}}\right) \quad (3.46)$$

For $n = 1$, using (3.41) and (3.42), the relations (3.45) become [37] [38]:

$$\left.\begin{array}{c} F_1 = \sqrt{2S_0}\frac{b}{\sqrt{\Delta_1\Delta_2}}, F_2 = \sqrt{2S_0}\frac{b}{\sqrt{\Delta_1}} \\ F_3 = \sqrt{2\pi S_0}\frac{\Delta_2 - 2}{\sqrt{\Delta_1\Delta_2}}, F_4 = -\frac{\sqrt{2S_0}}{\sqrt{\Delta_1}} \end{array}\right\} \quad (3.47)$$

Where $$\left.\begin{array}{c}\Delta_1 = 2\omega^3\zeta - 4\omega^2\zeta^2 a + 2\omega\zeta a^2 + 2\omega\zeta b - ab \\ \Delta_2 = \omega^2 - 2\omega\zeta a + a^2 + \mathrm{b}\end{array}\right\} \quad (3.48)$$

With $\Delta_1 > 0$ and $\Delta_2 > 0$

Therefore, the system (3.44) becomes [37] [38]:

$$\left.\begin{array}{c} a\sqrt{\Delta_1} + \beta\sqrt{2S_0}\sqrt{\Delta_2} - \gamma\sqrt{2S_0}a = 0 \\ \mathrm{A}\sqrt{\Delta_1\Delta_2} + \beta a\mathrm{b}\sqrt{2S_0} - \gamma\mathrm{b}\sqrt{2S_0}\sqrt{\Delta_2} - \mathrm{b}\sqrt{\Delta_1\Delta_2} = 0 \\ c = 0\end{array}\right\} \quad (3.49)$$

Where S_0 is the amplitude of power spectral density. The coefficients *a*, *b*, *c*, are calculated from relation (3.49) using MATLAB fsolver and the values of the coefficients are -0.0032, 1.0000 and 0.0000 respectively and substitute the coefficients into Equation (3.31) gives:

$$\dot{z}(\mathrm{t}) = -0.0032\mathrm{z} + 1.0000\dot{\xi} \quad (3.50)$$

The maximum displacement of the PEA x_m is 1.667μm, ξ(t) becomes approximately 0.6*10^4*x(t) from Equation (3.29). Substitute Equation (3.50) into Equation (3.27) and substitute the parameters from Appendix D and using the expression of Appendix E the transfer function becomes as follows:

$$\mathrm{G(s)} = \frac{5 \times 10^4(s + 0.0032)}{s^3 + 1000s^2 + 3 \times 10^{14}s + 1.6 \times 10^6} \quad (3.51)$$

3.2 Design and Analysis of Stack PEA Control System

There are different types of controllers used for position control of stack PEA among those in the following section we discussed on PID and FPID controllers.

3.2.1 Design and Analysis of PID

Despite a lot of research and the huge number of different solutions proposed, most industrial control systems are still based on conventional PID regulators. Different sources estimate the share taken by PID controllers at between 90 and 99%. Some of the reasons for this situation may be given as follows [39].

a) PID controllers are robust and simple to design.

b) There exists a clear relationship between PID and system response parameters. As a PID controller has only three parameters, plant operators have a deep knowledge about the influence of these parameters and the specified response characteristics on each other.
c) Many PID tuning techniques have been elaborated during recent decades, which facilitates the operator's task.
d) Because of its flexibility, PID control could benefit from the advances in technology.

PID controller can be understood as a controller that takes the present, the past, and the future of the error into consideration. Tuning a control loop is the adjustment of its control parameters (proportional band/gain, integral gain/reset, derivative gain/rate) to the optimum values for the desired control response. Stability (bounded oscillation) is a basic requirement, but beyond that, different systems have different behavior, different applications have different requirements, and requirements may conflict one with another.

3.2.1.1 Loop Tuning Mechanism

Tuning a control loop is the adjustment of its control parameters (proportional band/gain, integral gain/reset, derivative gain/rate) to the optimum values for the desired control response. Stability (no unbounded oscillation) is a basic requirement, but beyond that, different systems have different behavior, different applications have different requirements, and requirements may conflict with one another [18] [21] [22]. PID tuning is a difficult problem, even though there are only three parameters and in principle is simple to describe, because it must satisfy complex criteria within the limitations of PID control. There are accordingly various methods for loop tuning [18] [20]. The most employed PID design technique used in the industry is the Ziegler–Nichols method, which avoids the need for a model of the plant to be controlled and relies solely on the step response of the plant. It is desirable to have no overshoot at all in PEA for high precision application; therefore, the Ziegler–Nichols method cannot be used to tune PID controllers for these systems. Another restriction of Ziegler–Nichols is that it is only suitable for systems with monotonic step response (S-shape response) [20]. In this paper manual tuning using Mat lab's "SISO TOOL".

At undergraduate level, controller design for single-input- single-output (SISO) systems would normally involve the earlier analysis tools in Control; in particular root locus, or frequency response plots (most popularly, the Bode plot). As controller design is normally an iterative process, it will require re-drawing of those analysis plots, which can be tedious and time-

consuming. For undergraduates who would have just learnt Bode plots and root locus very recently, this can be particularly frustrating and discouraging, and could therefore impede their learning. 'SISOTOOL' is a graphical user interface (GUI) in MATLAB developed by the Math works to assist in the process of designing controllers for SISO systems [40].

SISOTOOL in the Design Process

The first step in controller design is to choose the architecture of the controller, whether it is to be in the feed forward or feedback loop. SISOTOOL allows the user to specify the controller configuration. After the architecture has been decided, the user needs to specify the structure of the controller, whether to use a lead, lag, PI, PD, PID controller, or even any other controllers whose number of poles and zeros do not match those mentioned. Following that, the poles and zeros need to be added to the design plots. SISOTOOL will instantaneously show how the design plots change as the poles/zeros are added in. SISOTOOL provides the option of inserting and adjusting the poles and zeros either graphically or numerically; each mode having its own advantages. Inserting them numerically is advantageous when precise values are wanted (for example a pole at the origin for a controller with Integral term). By inserting them (and moving them) graphically the user can perform adjustments very quickly to see which controller configuration will be able to let the root locus approximately pass through the desired poles. Following the determination of the controller structure, the numerical values of the controller need to be calculated. The root locus and Bode plot are updated instantaneously each time there is a change in poles/zeros or even the gain. In addition to the real-time update feature, SISOTOOL also aids design by allowing users to set design constraints on their design plots. For the root locus plot, the user can specify the maximum allowable overshoot and settling time, which are real physical parameters. Then SISOTOOL will show which region on the root locus the dominant poles must be in so that the specifications can be specified. For the frequency response plots, users can specify the minimum required phase and gain margins, and SISOTOOL will show the visible bounds on the design plot [41].

For manual tuning in online system one of the methods is first setting all gains to zero. Increase the K_p value until the constant oscillation of the output is obtained and then K_p should be set to approximately half of that value for a quarter amplitude decay type response. After that increase to minimize the K_i term offset in a particular time for the process considering that too much can

be a cause of instability. Finally, increase K_d if required, until the system becomes acceptably quick to reach the set point and decrease the oscillation. However, too much K_d will lead to overshoot in the system. A quick PID controller loop normally has a little overshoot to achieve the desired value very fast; but in some systems cannot receive overshoot. In these systems a K_p should be set remarkably less than half of the K_p setting which provoked oscillation, to make over-damped in the closed-loop system [18] [21] [22].

Table 3.1: Effects of independent P, I and D tuning on closed-loop response

Parameter	Rise Time	Overshoot	Settling Time	Steady-State Error	Stability
Increasing K_p	Decrease	Increase	Small Increase	Decrease	Degrade
Increasing K_i	Small Decrease	Increase	Increase	Large Decrease	Degrade
Increasing K_d	Small Decrease	Decrease	Decrease	Minor Change	Improve

The values of those parameters K_p, K_i and K_d are obtained as, 8.85×10^7,8.72×10^{13} and 1.45×10^3 respectively. Thus, the controller transfer function is given by

$$G_c(s) = 8.85 \times 10^7 + \frac{8.72 \times 10^{13}}{s} + 1.45 \times 10^3 s \tag{3.50}$$

3.2.2 Simulink Model for PID Controller

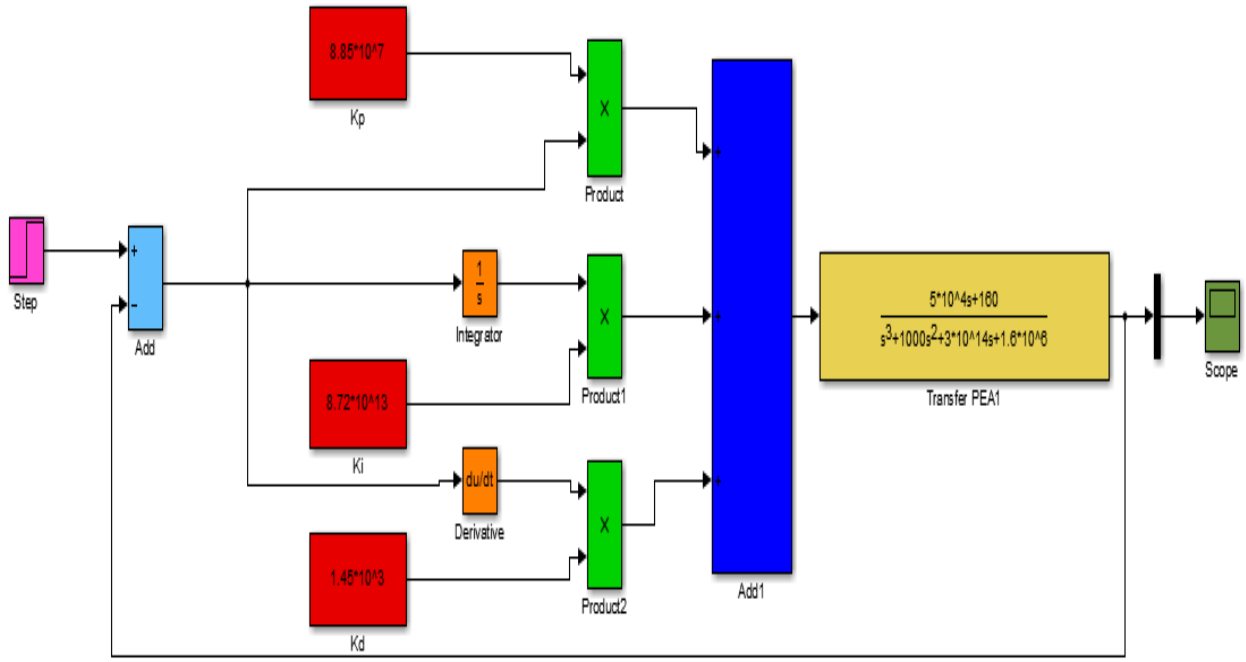


Figure 3.7: Simulink model of PID controller

3.2.3 Modeling and Analysis of FPID Controller

A FPID controller takes the conventional PID controller parameter values as the basis which uses the fuzzy reasoning and variable universe of discourse to regulate the PID parameters. The characteristics of a fuzzy system such as robustness and adaptability can be successfully incorporated into the controlling method for better tuning of PID parameters. The term self-tuning refers to the characteristics of the controller to tune its controlling parameters on-line automatically to have the most suitable values of those parameters which result in optimization of the process output. Fuzzy self-tuning PID controller works on the control rules designed based on theoretical and experience analysis. Therefore, it can tune the parameters K_p, K_i and K_d by adjusting the other controlling parameters and factors on-line. This, in result makes the precision of overall control higher and hence gives a better performance than the conventional PID controller.

Several assumptions are implicit in a fuzzy control system design. Six basic assumptions are commonly made whenever a fuzzy rule-based control policy is selected [27].

I. The plant is observable and controllable: state, input, and output variables are usually available for observation and measurement or computation.
II. There exists a body of knowledge comprised of a set of linguistic rules, engineering common sense, intuition, or a set of input–output measurements data from which rules can be extracted.
III. A solution exists.
IV. The control engineer is looking for a good enough ‘‘solution, not necessarily the optimum one.
V. The controller will be designed within an acceptable range of precision.
VI. The problems of stability and optimality are not addressed explicitly; such issues are still open problems in fuzzy controller design.

The FLC consists basically of four parts: fuzzification interface, knowledge base, inference engine, and a defuzzification interface [42].

- ✓ A **fuzzification** unit which maps measured inputs of crisp value into fuzzy linguistic values to be used by a fuzzy reasoning mechanism.
- ✓ A **knowledge base** (**KB**) which is the collection of expert control knowledge required to achieve the control objective. It contains knowledge about all the input and output fuzzy partitions. It includes the membership functions defining the input variables to the fuzzy rule base.
- ✓ **A fuzzy reasoning mechanism (inference engine)** that performs various fuzzy logic operations to infer the control action for the given fuzzy inputs. It contains rules in an antecedent-consequent form that sets the foundation for approximate (imprecise) reasoning.
- ✓ **A defuzzification** unit which converts the inferred fuzzy control action into the required crisp control values to be entered into the system process.

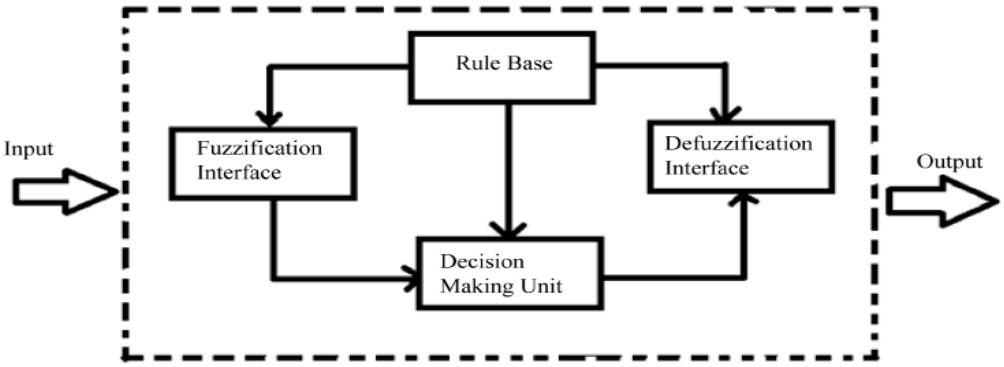


Figure 3.8: Fuzzy logic process [43]

Design Process of FLC [27]:

- ✓ Identify controller Inputs and Outputs as the Fuzzy variables.
- ✓ Break up Inputs and Outputs into several Fuzzy Sets and label them according to the problem to be solved.
- ✓ Assign or determine a membership function (MF) for each fuzzy set.
- ✓ Fuzzify the inputs.
- ✓ Develop the fuzzy IF-THEN rules to solve the problem.
- ✓ Choose Inference Mechanism engine procedure.
- ✓ Aggregate the fuzzy outputs of each rule.
- ✓ Choose a defuzzification method.
- ✓ Tune the adjustable parameters.

3.2.3.1 Fuzzy Inference System

The typical fuzzy inference system (FIS) inputs are the signals of error "e" and rate of change of error "ce" in displacement. The FIS output is the control action inferred from the fuzzy rules. The configuration of FIS for the system fuzzy controller is given in the Figure 3.9. Set the deviation "e" basic domain $\{e_l, e_h\} = \{-1, 1\}$, change of error ce basic domain $\{ce_l, ce_h\}$= {-1, 1}, ΔK_{pf} basic domain {250,350}, ΔK_{df} basic domain {5, 10} and ΔK_{if} basic domain {100,200}.

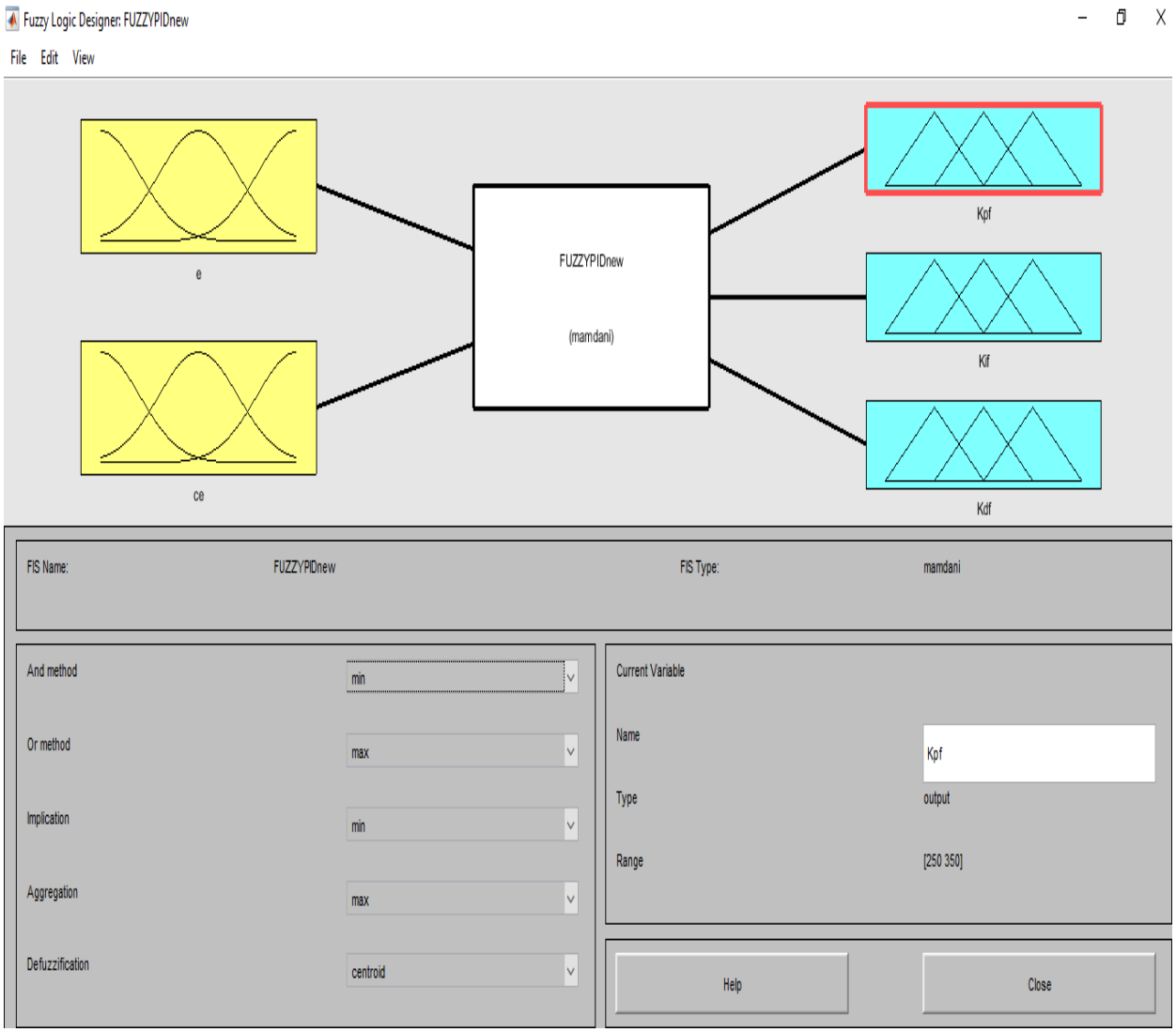
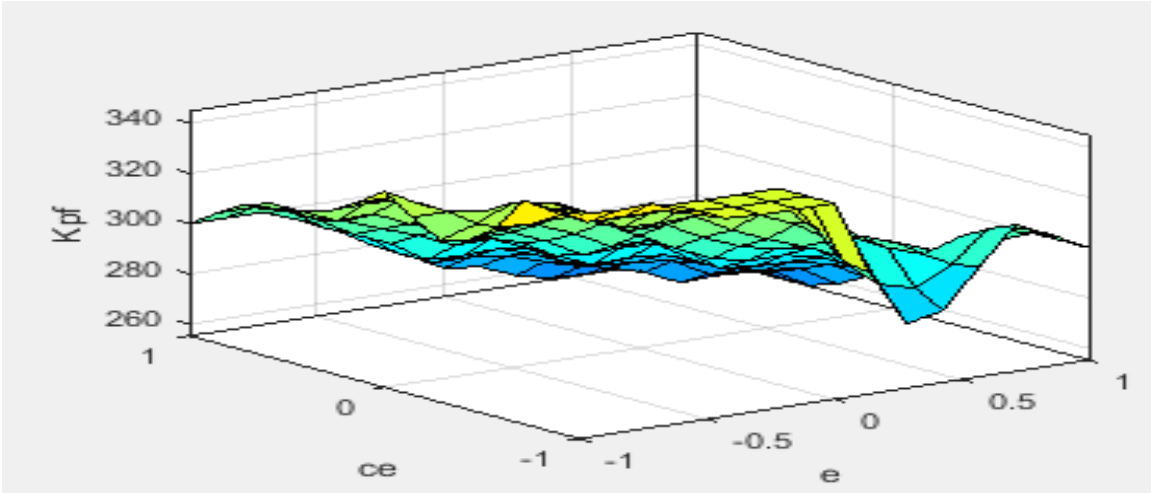
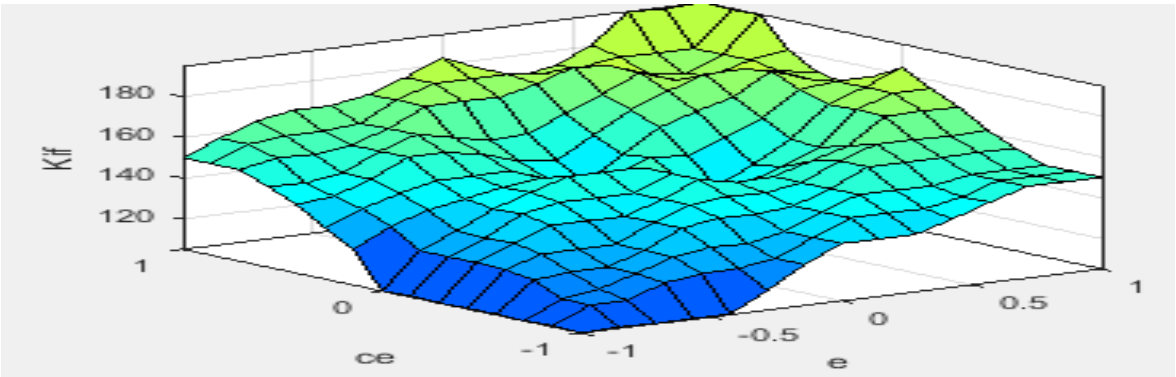


Figure 3.9: Fuzzy Inference System of the proposed system

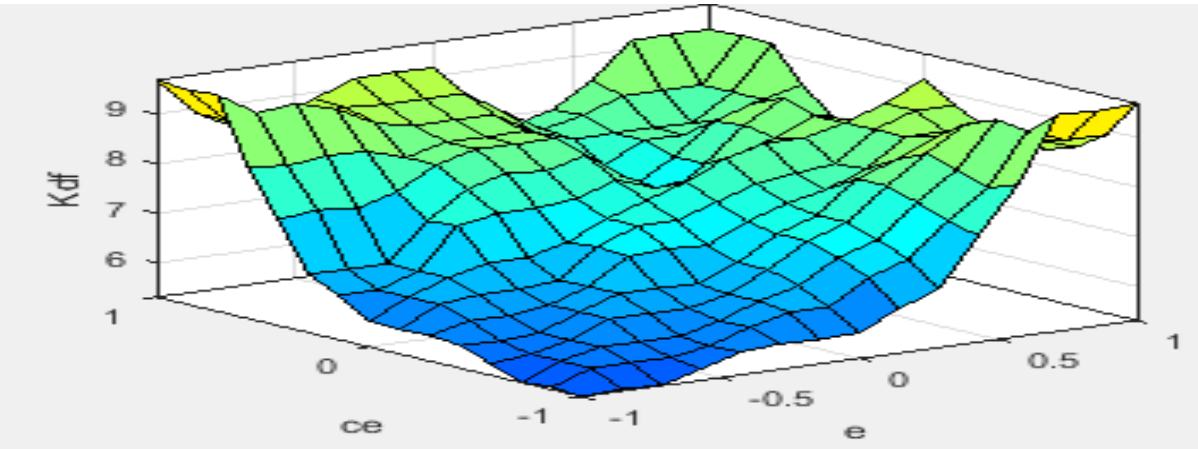
Figure 3.10 (a), (b) and (c) shows the surface viewer of K_{pf}, K_{if} and K_df with e and ce respectively and Figure shows rule viewer of fuzzy interface system.



(a) Kpf surface viewer



(b) Kif surface viewer



(c) Kdf surface viewer

Figure 3.10: Surface viewers of Kpf, Kif and Kdf

3.2.3.2 Fuzzier Design

Figure 3.11 is a graph of the position error and change in position error fuzzy membership functions. It assigns a crisp value's degree of membership to seven fuzzy linguistic values $NB, NM, NS, Z, PS, PM\ and\ PB$. The fuzzy input membership functions used for error in position and rate of change of error in position are triangular type. The universe of discourse of each membership function is shown in Table 3.2 with degree of membership.

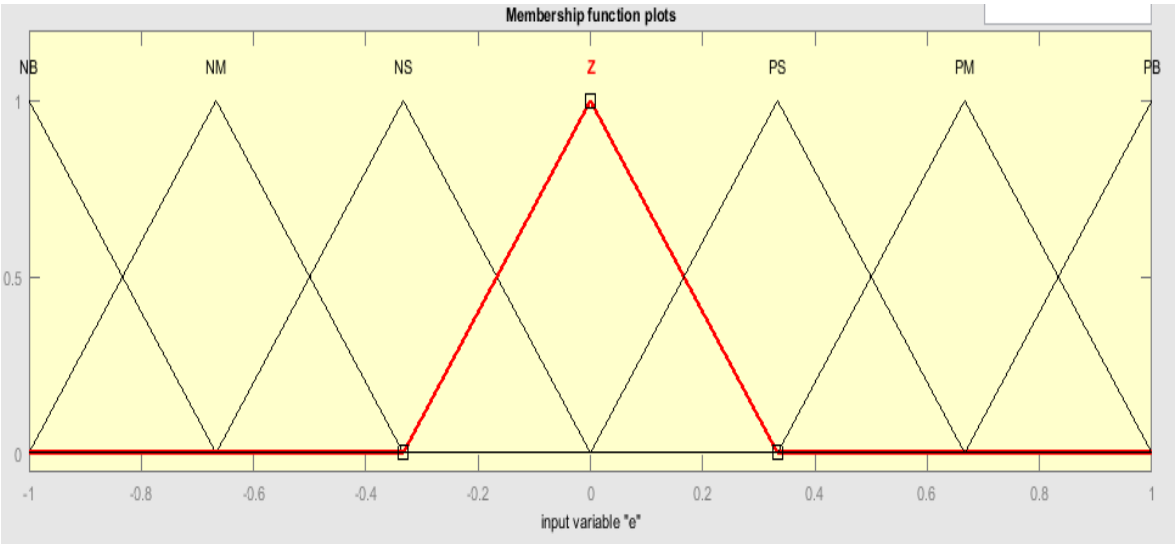


Figure 3.11: Membership function for position error and rate of position error (e,ce)

Table 3.2: Membership function universe of discourse of error and change of error in position

Interval of e and ce	Degree of membership						
	NB	NM	NS	Z	PS	PM	PB
-1 to -0.6667	1 to 0	0 to 1	0	0	0	0	0
-1 to -0.3333	0	1 to 0	0 to 1	0	0	0	0
-0.3333 to 0	0	0	1 to 0	0 to 1	0	0	0
0 to 0.3333	0	0	0	1 to 0	0 to 1	0	0
0.3333 to 0.6667	0	0	0	0	1 to 0	0 to 1	0
0.6667 to 1	0	0	0	0	0	1 to 0	0 to 1

3.2.3.3 Rule Base Construction

Here in this thesis the rules based is derived on the typical step response of the process shown in Figure 3.12. At the beginning, around a1, a big control signal is needed in order to achieve a fast rise time. To produce a big control signal, we need a large proportional gain K_p, a small derivative gain K_d, and a large integral gain K_i. Consequently, the rule around a_1 is:

IF e (t) is PB (Positive Big) and ce (t) is Zero, THEN K_{pf} is Big,K_{if} is Big, K_{df} is small.

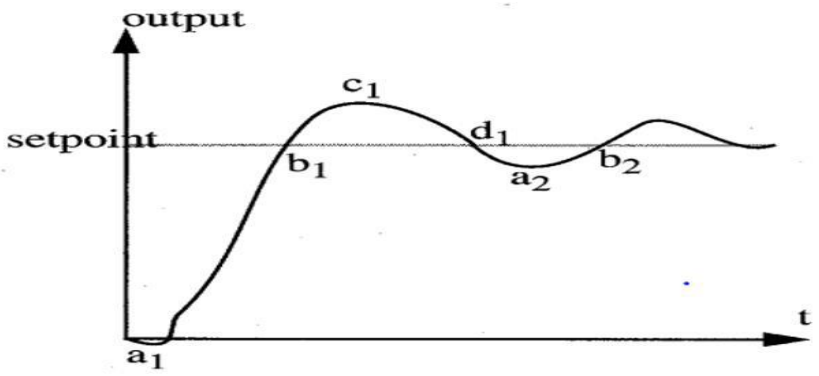


Figure 3.12: Typical step response of the system [44]

Around point b_1 in Figure 3.12, the control single has to be small to avoid a large overshoot. So, we need a small proportional gain, a small integral gain and a large derivative gain. Thus, the following rule is taken:

IF e(t) is Z and ce(t) is NB (Negative Big), THEN K_{pf} is small,K_{if} is Small, K_{df} is Big.

The control signal actions around points around c_1 and d_1 are like those around points a_1 and b_1 respectively. Based on this concept three set of rules for K_{pf}, K_{if} and K_{df} has been determined and each set consists of 49 rules. These three set of rules are shown in Table 3.3- 3.5 respectively and the universe of discourse of each membership functions are shown in Table 3.6-3.8 with degree of membership respectively.

Table 3.3: Rule table for Kpf

ce	e						
	NB	NM	NS	Z	PS	PM	PB
NB	PVB	PVB	PB	PM	PMS	PMB	PM
NM	PVB	PB	PM	PM	PMB	PM	PM
NS	PB	PM	PMB	PMB	PM	PS	PS
Z	PM	PMB	PMB	PM	PS	PS	PMS
PS	PMB	PMB	PM	PS	PS	PMS	PVS
PM	PMB	PM	PS	PS	PMS	PVS	PVS
PB	PM	PM	PS	PMS	PVS	PVS	PVS

Table 3.4: Rule table for Kif

ce	e						
	NB	NM	NS	Z	PS	PM	PB
NB	PVS	PVS	PVS	PS	PS	PM	PM
NM	PVS	PMS	PS	PS	PM	PM	PM
NS	PVS	PS	PS	PM	PM	PMB	PMB
Z	PS	PS	PM	PM	PS	PMB	PB
PS	PS	PM	PM	PS	PMB	PB	PMB
PM	PM	PM	PMB	PMB	PB	PMB	PVB
PB	PM	PMB	PMB	PB	PMB	PVB	PVB

Table 3.5: Rule table for Kdf

ce	e						
	NB	NM	NS	Z	PS	PM	PB
NB	PVS	PVS	PMS	PMS	PS	PVB	PVB
NM	PVS	PMS	PMS	PS	PM	PVB	PMB
NS	PMS	PMS	PS	PS	PM	PMB	PMB
Z	PMS	PS	PS	PM	PMB	PMB	PB
PS	PS	PS	PMB	PMB	PS	PB	PM
PM	PVB	PVB	PMB	PMB	PB	PM	PB
PB	PVB	PMB	PB	PB	PM	PB	PB

3.2.3.4 Defuzzification Design

Centroid de-fuzzification method is used in this paper to convert from the inference mechanism into the crisp values applied to the actual system. The output defuzzification membership functions for Kpf, Kif and Kdf are shown in Figures 3.13-3.15 respectively.

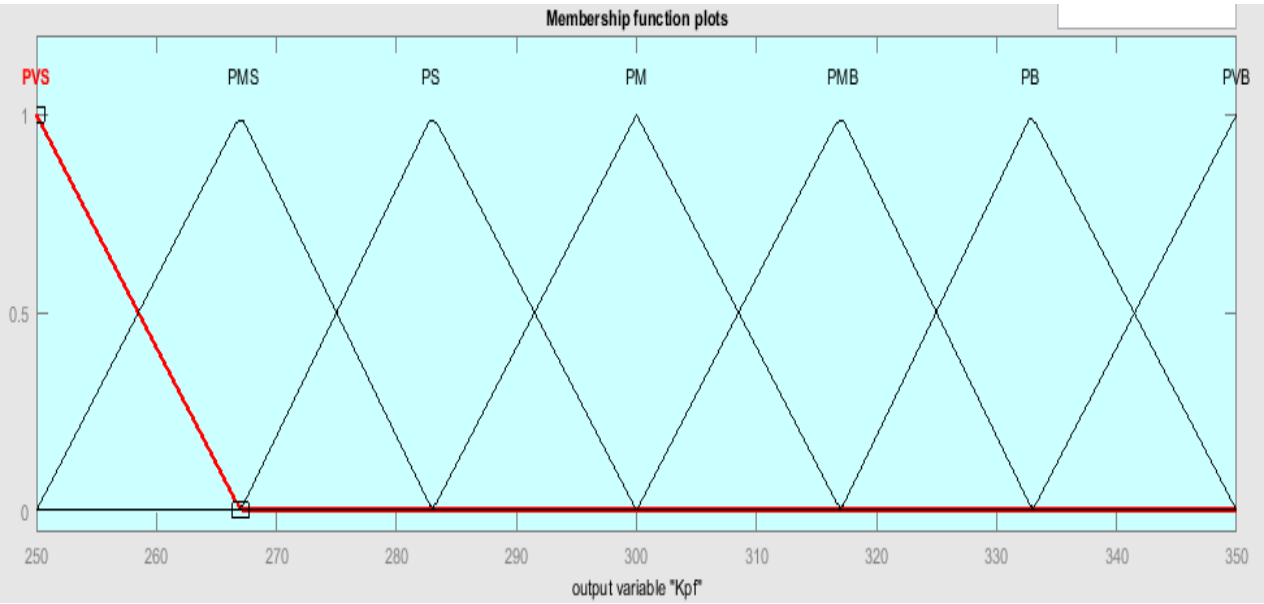


Figure 3.13: Membership function fuzzy output for proportional gain Kpf

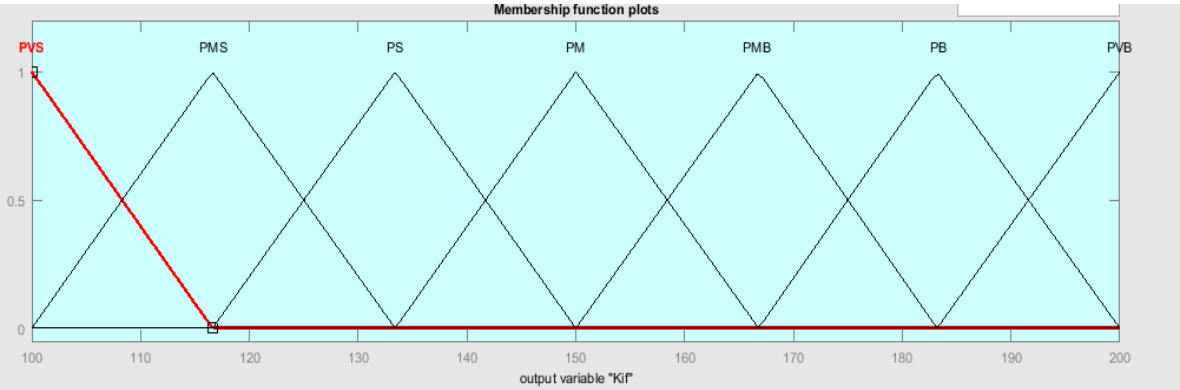


Figure 3.14: Membership function fuzzy output for proportional gain Kif

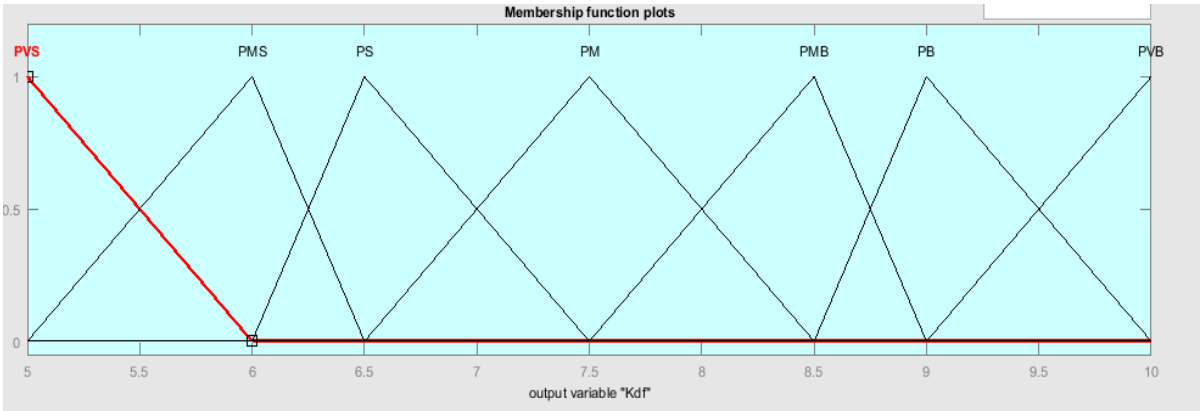


Figure 3.15: Membership function fuzzy output for proportional gain Kdf

Table 3.6: Membership function universe of discourse for Kpf

Interval of Kpf	Degree of membership						
	PVS	PMS	PS	PM	PMB	PB	PVB
250 to 267	1 to 0	0 to 1	0	0	0	0	0
267 to 283	0	1 to 0	0 to 1	0	0	0	0
283 to 300	0	0	1 to 0	0 to 1	0	0	0
300 to 317	0	0	0	1 to 0	0 to 1	0	0
317 to 333	0	0	0	0	1 to 0	0 to 1	0
333 to 350	0	0	0	0	0	1 to 0	0 to 1

Table 3.7: Membership function universe of discourse for Kif

Interval of Kif	Degree of membership						
	PVS	PMS	PS	PM	PMB	PB	PVB
100 to 116.6	1 to 0	0 to 1	0	0	0	0	0
116.6 to 133.4	0	1 to 0	0 to 1	0	0	0	0
133.4 to 150	0	0	1 to 0	0 to 1	0	0	0
150 to 168.8	0	0	0	1 to 0	0 to 1	0	0
168.8 to 183.2	0	0	0	0	1 to 0	0 to 1	0
183.2 to 200	0	0	0	0	0	1 to 0	0 to 1

Table 3.8: Membership function universe of discourse for Kdf

Interval of Kdf	Degree of membership						
	PVS	PMS	PS	PM	PMB	PB	PVB
5 to 6	1 to 0	0 to 1	0	0	0	0	0
6 to 6.5	0	1 to 0	0 to 1	0	0	0	0
6.5 to 7.5	0	0	1 to 0	0 to 1	0	0	0
7.5 to 8.5	0	0	0	1 to 0	0 to 1	0	0
8.5 to 9	0	0	0	0	1 to 0	0 to 1	0
9 to 10	0	0	0	0	0	1 to 0	0 to 1

It is assumed that K_p , K_i and K_d are in prescribed ranges $[K_{p\,min}\ K_{p\,max}]$, $[K_{i\,min}\ K_{i\,max}]$ and $[K_{d\,min}\ K_{d\,max}]$ respectively. For convenience they are normalized by the following linear transformation [45].

$$K_p{}' = \frac{kp - K_{p\,min}}{K_{p\,max} - K_{p\,min}} \tag{3.51}$$

$$K_i{}' = \frac{ki - K_{i\,min}}{K_{i\ max} - K_{i\ min}} \tag{3.52}$$

$$K_d{}' = \frac{kd - K_{d\,min}}{K_{d\ max} - K_{d\ min}} \tag{3.53}$$

Where, $K_p{}'$, $K_i{}'$ and $K_d{}'$ are the initial PID parameters, and kp, ki and kd are the adjusted PID parameters. The ranges of kp, ki amd kd are determined from the initial PID parameters as

$[8.8 \times 10^7 \ \ 8.9 \times 10^7]$, $[8.7 \times 10^{13} \ \ 8.8 \times 10^{13}]$ and $[1.4 \times 10^3 \ \ 1.5 \times 10^3]$ respectively.

3.2.4 Simulink Model of Overall System

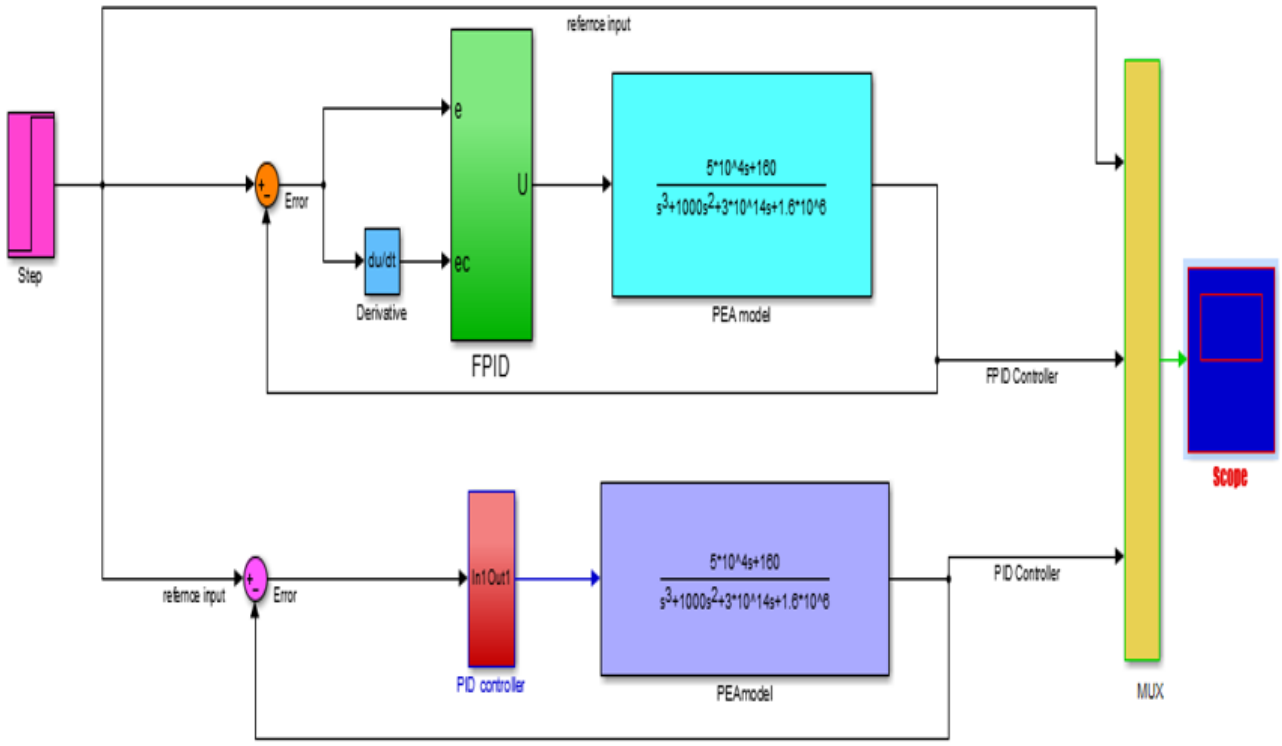


Figure 3.16: Over all simulink model of FPID and PID controller

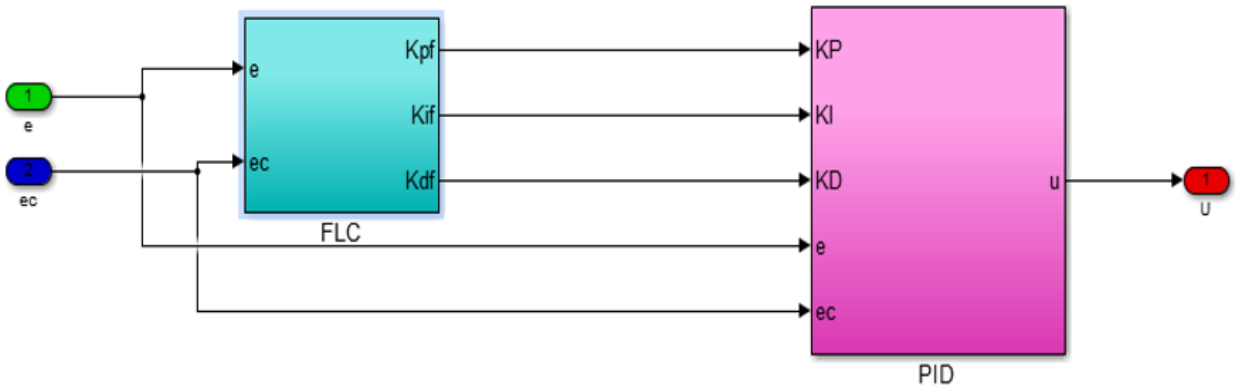


Figure 3.17: Model components under FPID block

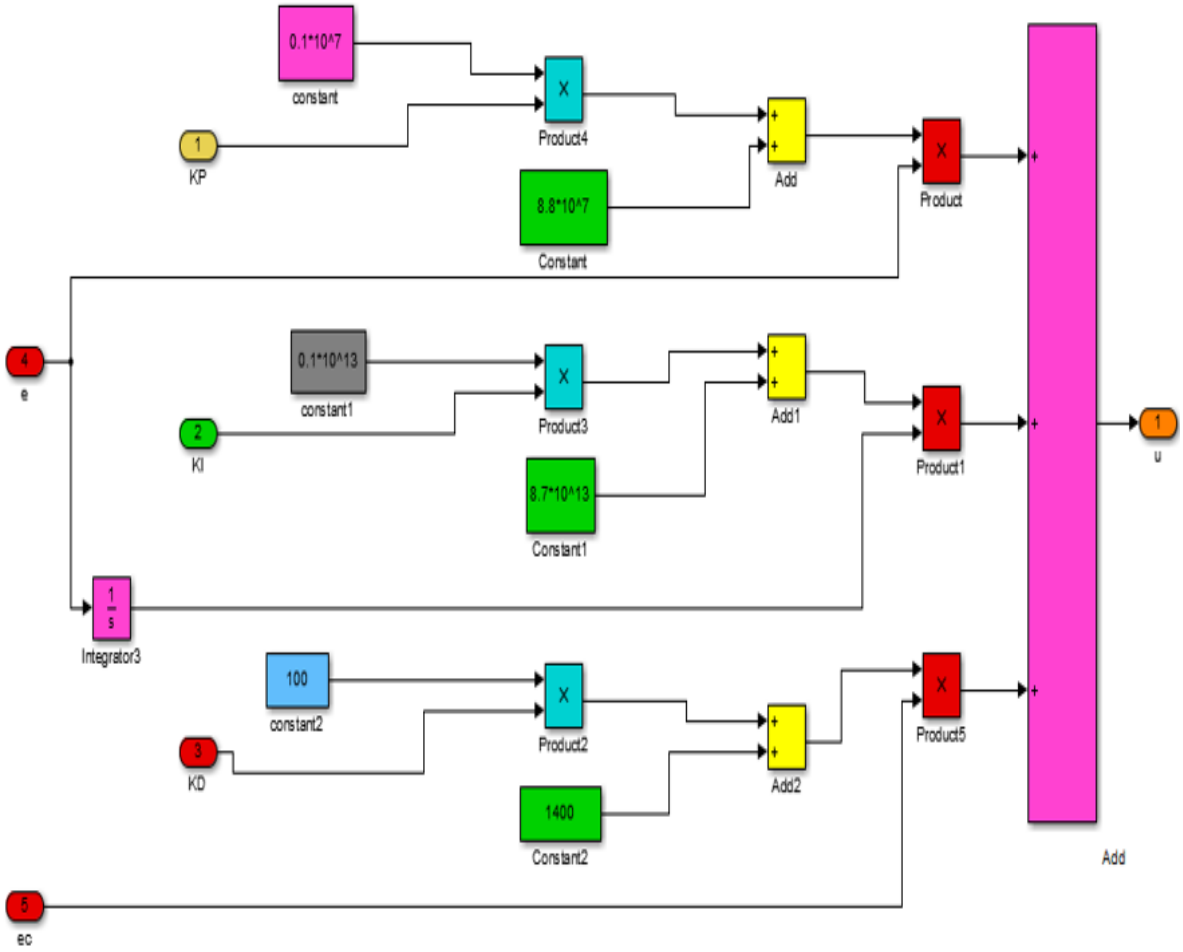


Figure 3.18: PID controller block model components under FPID block

CHAPTER FOUR

SIMULATION RESULTS AND DISCUSSIONS

This chapter deals with the results and discussions of MATLAB simulations. It is deals with simulation results of the closed loop control of the system using self-tuning FPID and PID with MATLAB/SIMULINK in different conditions. Then, the simulation studies the system in dynamic and transient performance using MATLAB/Simulink 2015a environment and the results are discussed. The Simulink model shown in Figure 3.16 is used to carry out simulation studies and analyze the performance of the controllers under different operating conditions.

4.1 Comparison of PID and FPID Controller Mechanisms

Figure 4.1 shows the displacement (position) response of the system for unity step input and Figure 4.2 shows the response of the system with 1.667μm input (reference) for PID controller and FPID controller respectively. In both cases the system is stable and as it is observed from the simulation result of Figure 4.2 FPID controller achieves better transient response than that of PID controller. The response of Figure 4.2 is described in Table 4.1.

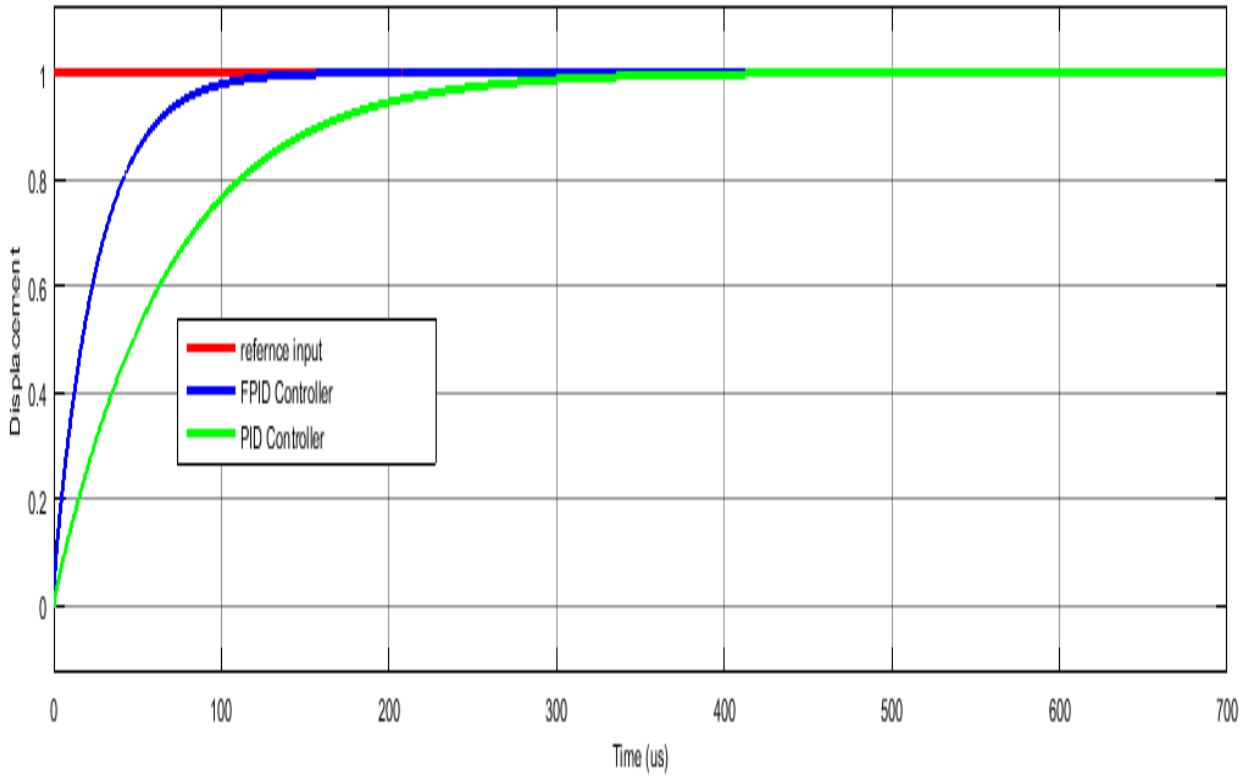


Figure 4.1: Unity step response of the system

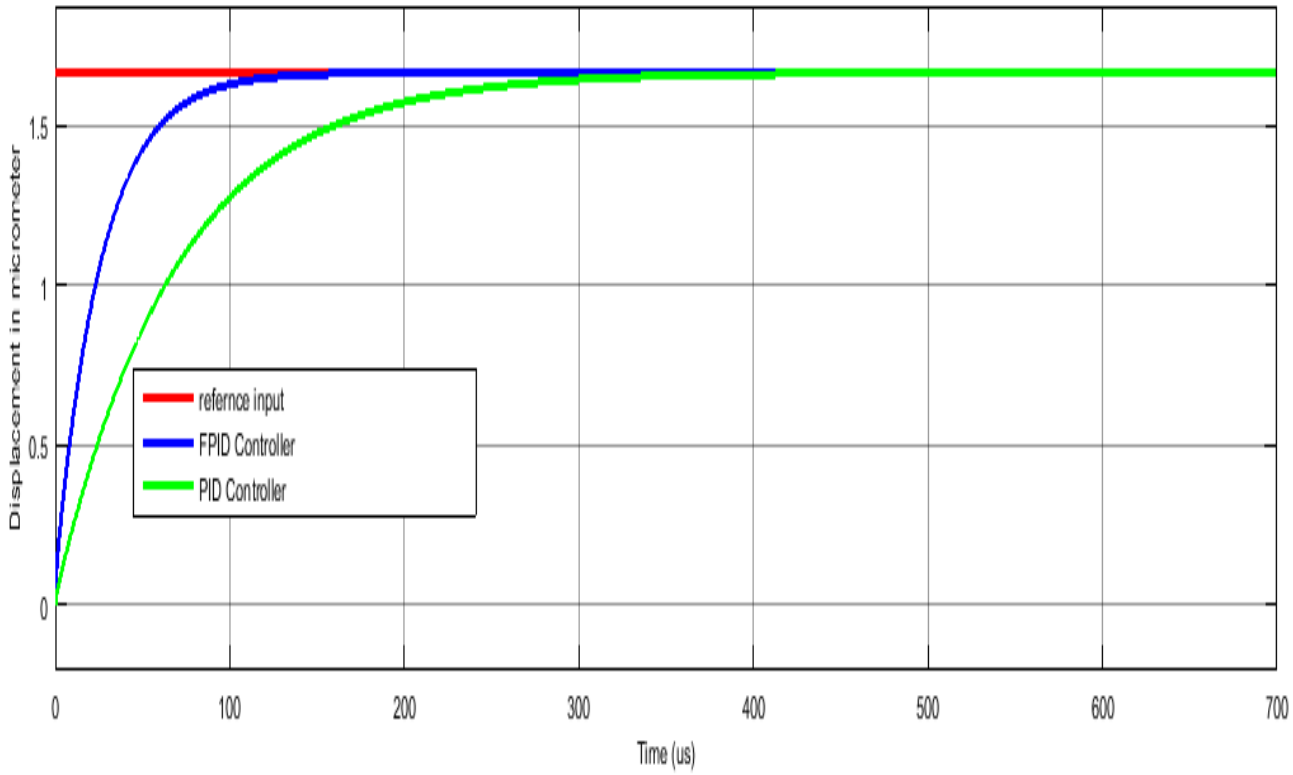


Figure 4.2: Simulation results of FPID and PID controller

Table 4.1: The comparison of PID and FPID controller

Controller	Transient response		
	Rise time (μs)	Settling time (μs)	Steady state error (%)
PID	152.260	475.692	0.01
FPID	57.062	165.113	0

4.1.1 Comparison of PID and FPID Controller in Parameter Variations

In order to test the robustness, stability and effectiveness of the proposed FPID controller, different operating conditions are checked by parameter variation like stiffness, damping factor mass and Dc gain. Figure 4.3 shows the simulation results of PID and FPID controller for 50% decrease damping factor and Figure 4.4 shows the results of the controllers for 75% increase damping factor. As shown in Figures 4.3, Figures 4.4, table 4.2 and Table 4.3 the responses of FPID controller achieve better transient response than PID controller.

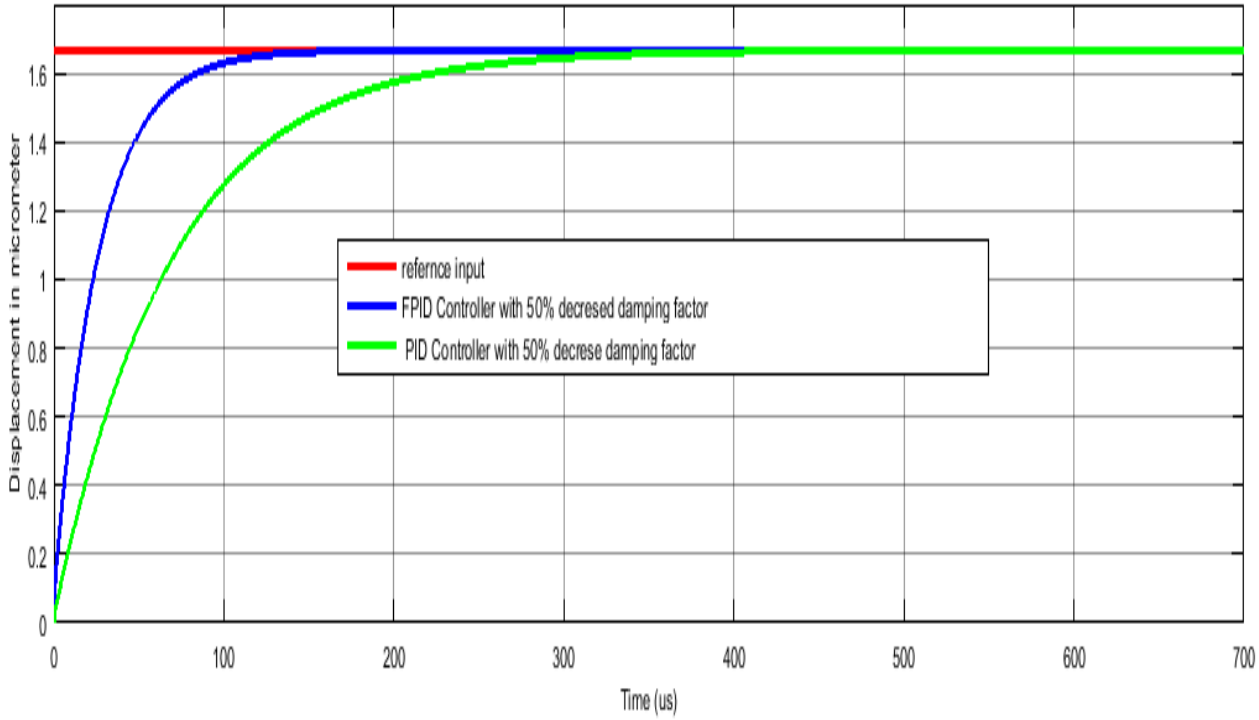


Figure 4.3: Simulation results of FPID and PID controllers with 50% decrease damping factor

Table 4.2: The comparison of PID and FPID controller with 50% decrease damping factor

Controller	Transient response		
	Rise time (μs)	Settling time (μs)	Steady state error (%)
PID with 50% decrease damping factor	151.601	475.403	0.01
FPID with 50% decrease damping factor	56.685	186.248	0

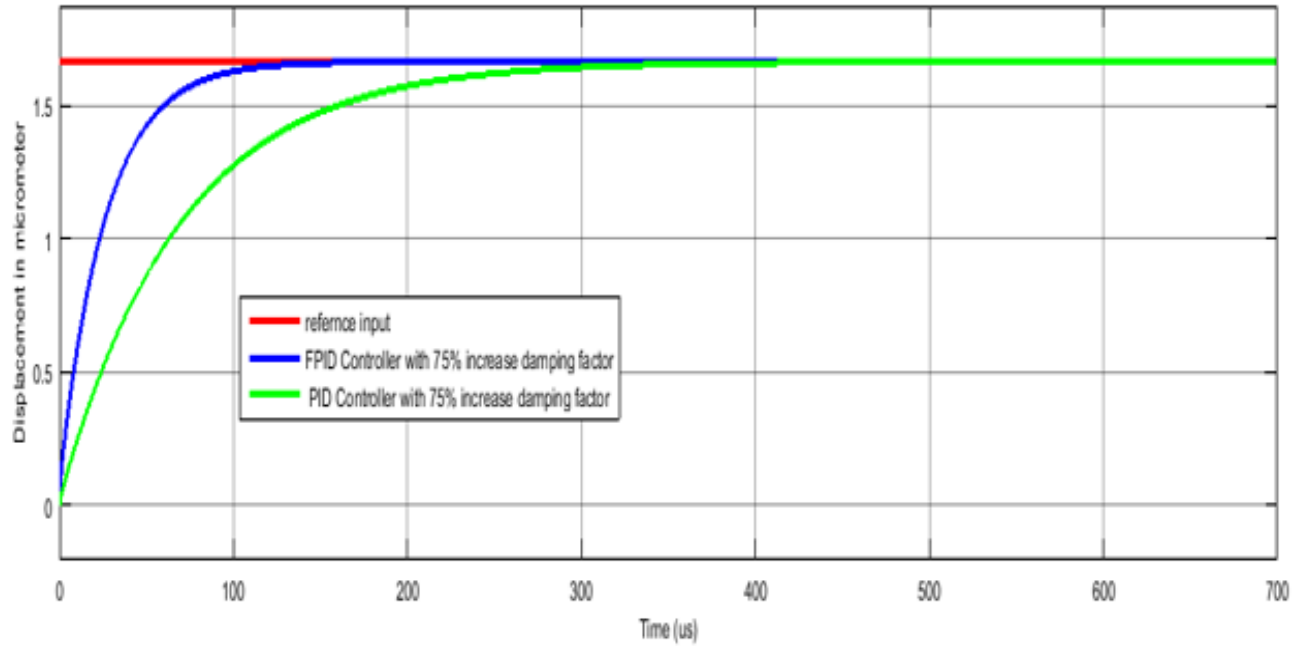


Figure 4.4: Simulation results of FPID and PID controllers with 75% increase damping factor

Table 4.3: The comparison of PID and FPID controller with 75% increase damping factor

Controller	Transient response		
	Rise time (μs)	Settling time (μs)	Steady state error (%)
PID with 75% increase damping factor	154.013	485.964	0.01
FPID with 75% increase damping factor	58.168	182.106	0

Figure 4.5 shows the simulation results of PID and FPID controller for 50% decrease mass and Figure 4.6 shows the results of the controllers for 75% increase mass. As shown in Figures 4.5, Figures 4.6, Table 4.4 and Table 4.5 the responses of FPID controller achieve better transient response than PID controller.

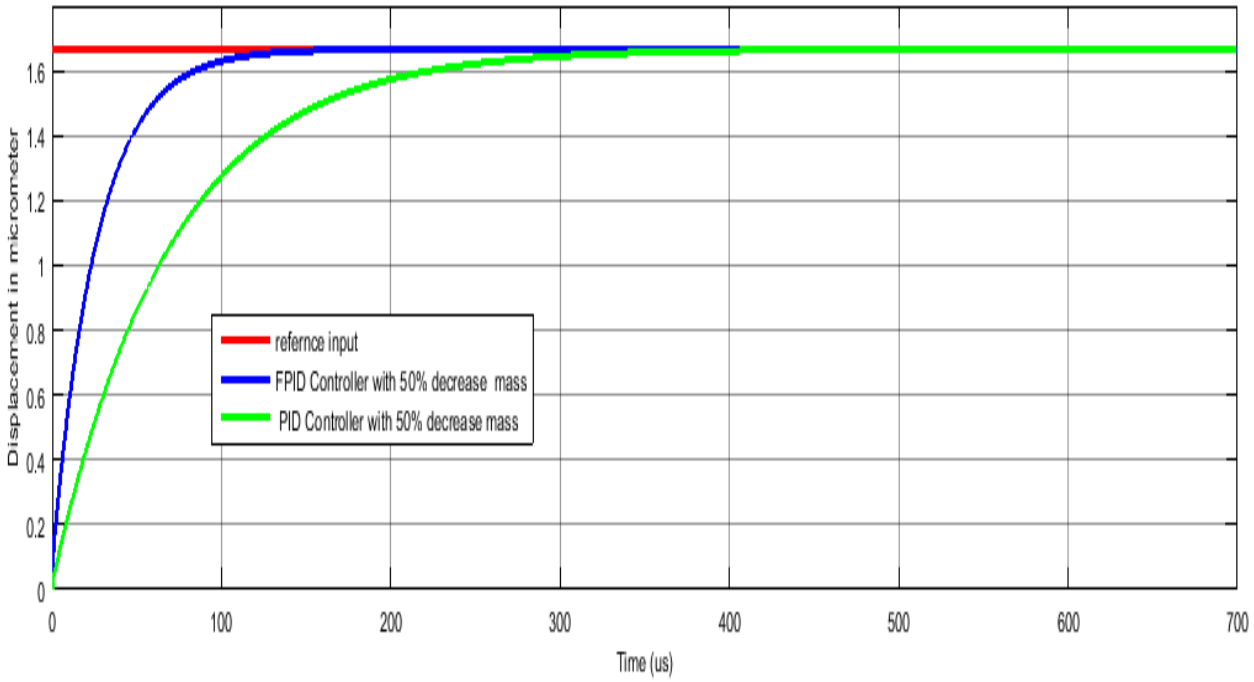


Figure 4.5: Simulation results of PID and FPID controller with 50% decrease mass

Table 4.4: The comparison of PID and FPID controller with 50% decrease mass

Controller	Transient response		
	Rise time (μs)	Settling time (μs)	Steady state error (%)
PID with 50% decrease mass	152.607	446.209	0.01
FPID with 50% decrease mass	57.062	169.526	0

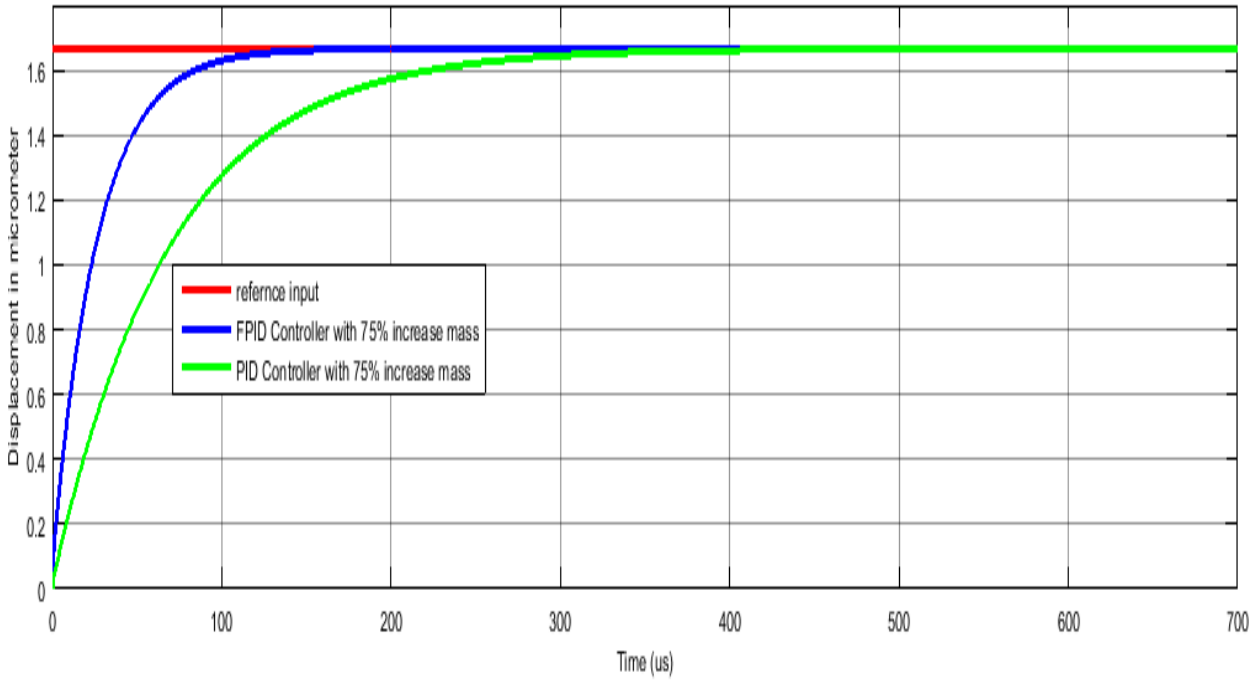


Figure 4.6: Simulation results of FPID and PID controllers with 75% increase mass

Table 4.5: The comparison of PID and FPID controller with 75% increase mass

Controller	Transient response		
	Rise time (μs)	Settling time (μs)	Steady state error (%)
PID with 75% increased mass	155.482	487.287	0.01
FPID with 75% increased mass	59.546	186.248	0

Figure 4.7 shows the simulation results of PID and FPID controller for 50% decrease stiffness and Figure 4.8 shows the results of the controllers for 75% increase mass. As shown in Figure 4.7, Table 4.6, Figure 4.8 and Table 4.7 the responses of FPID controller achieve better transient response than PID controller.

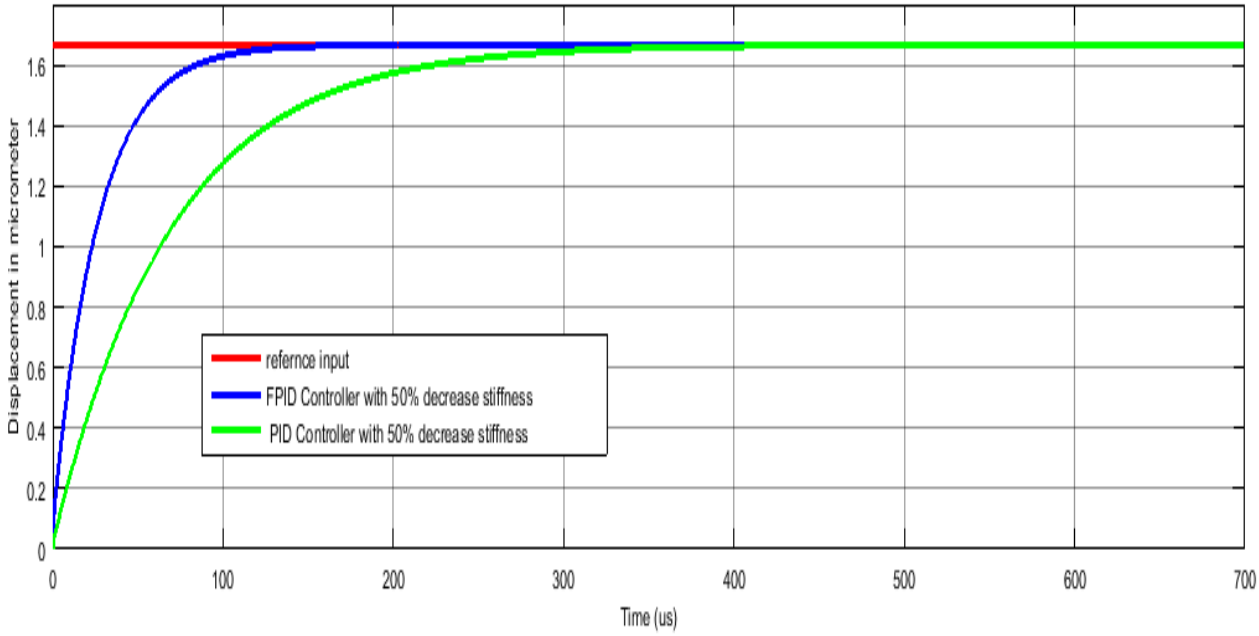


Figure 4.7: Simulation results of PID and FPID controller for 50% decrease stiffness

Table 4.6: The comparison of PID and FPID controller with 50% decrease stiffness

Controller	Transient response		
	Rise time (μs)	Settling time (μs)	Steady state error (%)
PID with 50% decreased stiffness	152.000	446.209	0.01
FPID with 50% decreased stiffness	56.667	185.000	0

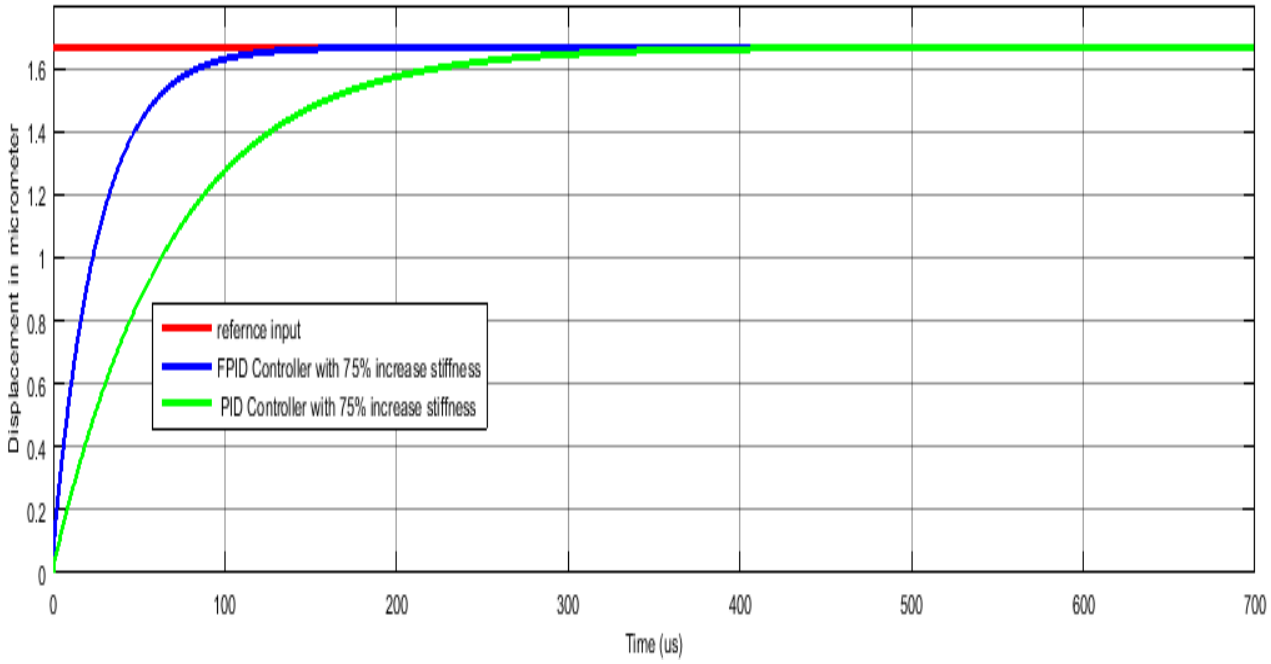


Figure 4.8: Simulation results of PID and FPID controller with 75% increase stiffness

Table 4.7: The comparison of PID and FPID controller with 75% increase stiffness

Controller	Transient response		
	Rise time (μs)	Settling time (μs)	Steady state error (%)
PID with 75% increase stiffness	156.000	476.066	0.01
FPID with 75% increase stiffness	58.000	185.000	0

Figures 4.9, 4.10 and 4.11 show the simulation results of PID and FPID controller with $\pm 15\%$ Dc gain, response of the system with $\pm 25\%$ Dc gain and response of PID and FPID controller for 50% increased Dc gain respectively. Their transient responses for Dc gain variations are described in Table 4.8, Table 4.9 and Table 4.10 respectively.

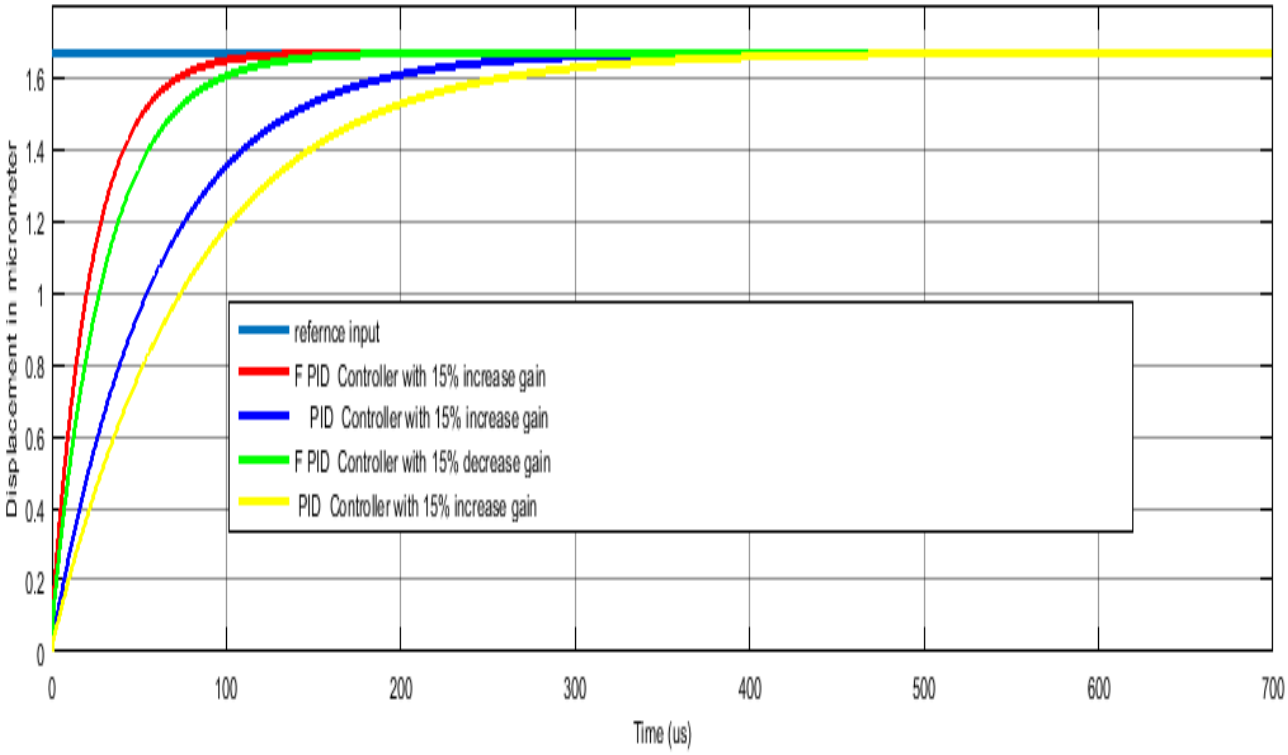


Figure 4.9: Simulation results of PID and FPID controller with ±15% Dc gain

Table 4.8: The comparison of PID and FPID controller with ±15% Dc gain

Controller	Transient response		
	Rise time (μs)	Settling time (μs)	Steady state error (%)
PID with 15% increase gain	133.333	355.667	0.01
FPID with 15% increase gain	52.667	161.015	0
PID with 15% decrease gain	181.333	569.667	0.02
FPID with 15% decrease gain	68.667	216.333	0

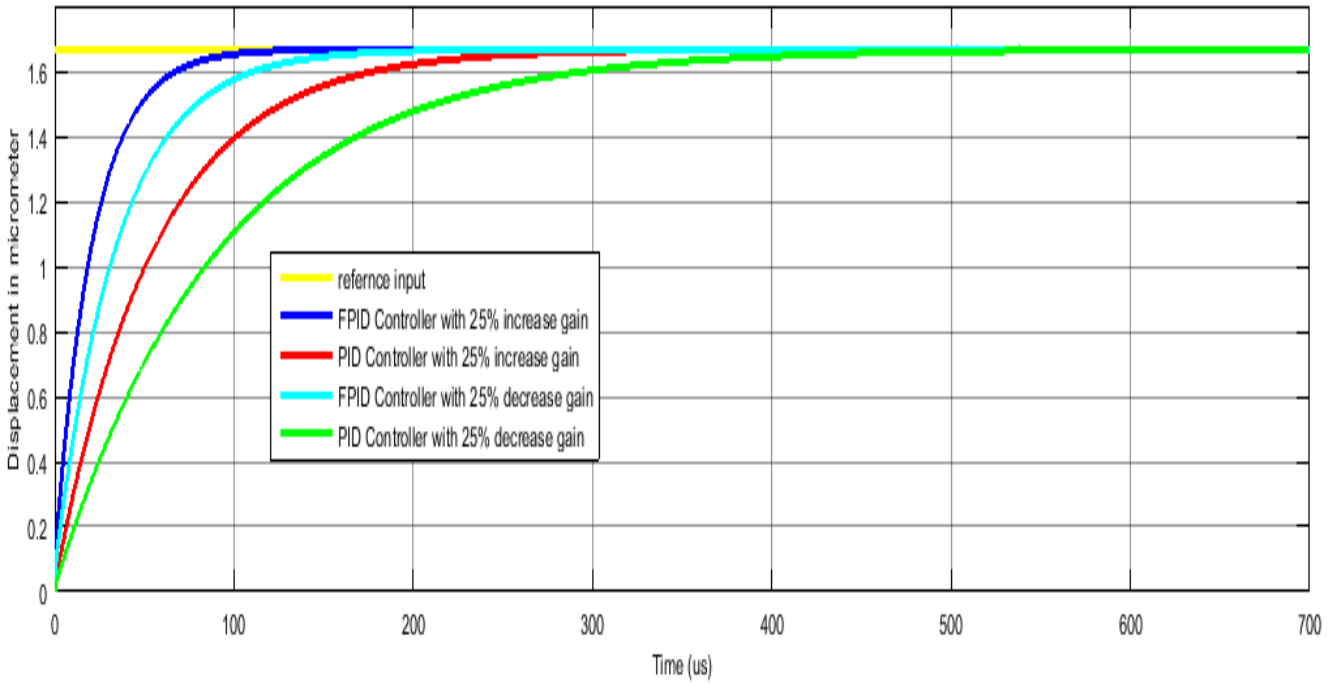


Figure 4.10: Simulation results of PID and FPID controller with ±25% Dc gain

Table 4.9: The comparison of PID and FPID controller with ±25% Dc gain

Controller	Transient response		
	Rise time (μs)	Settling time (μs)	Steady state error (%)
PID with 25% increase gain	122.667	215.972	0
FPID with 25% increase gain	46.667	149.000	0
PID with 25% decrease gain	205.333	517.867	0.09
FPID with 25% decrease gain	75.333	244.333	0.02

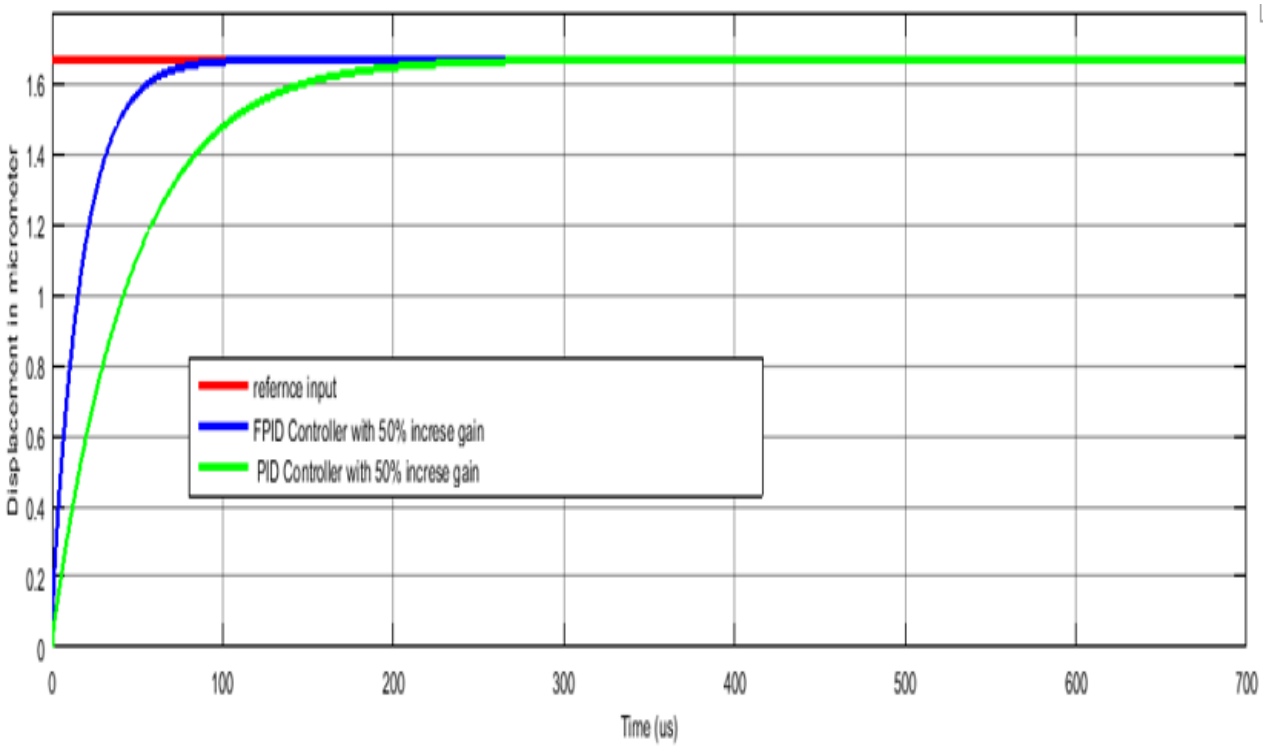


Figure 4.11: Simulation results of PID and FPID controller with 50% increase Dc gain

Table 4.10: The comparison of PID and FPID controller with 50% increase Dc gain

Controller	Transient response		
	Rise time (μs)	Settling time (μs)	Steady state error (%)
PID with 50% increase gain	103.333	323.204	0.01
FPID with 50% increase gain	38.000	125.000	0

The previous tables and figures show that the responses of FPID controller achieve better transient response than PID controller for different variations of Dc gain.

4.1.2 Comparison of PID and FPID Controllers in Disturbance Rejection and Delay Time

The capability of the controllers in disturbance rejection is checked by adding step disturbance signal from signal builder after settling time that has magnitude of one as shown in Figure 4.12

and Figure 4.13 shows that FPID controller has better disturbance rejection than conventional PID controller. The comparison of PID and FPID controller response with time delay is as shown in Figure 4.14. And it shows that FPID controller has better response than PID controller.

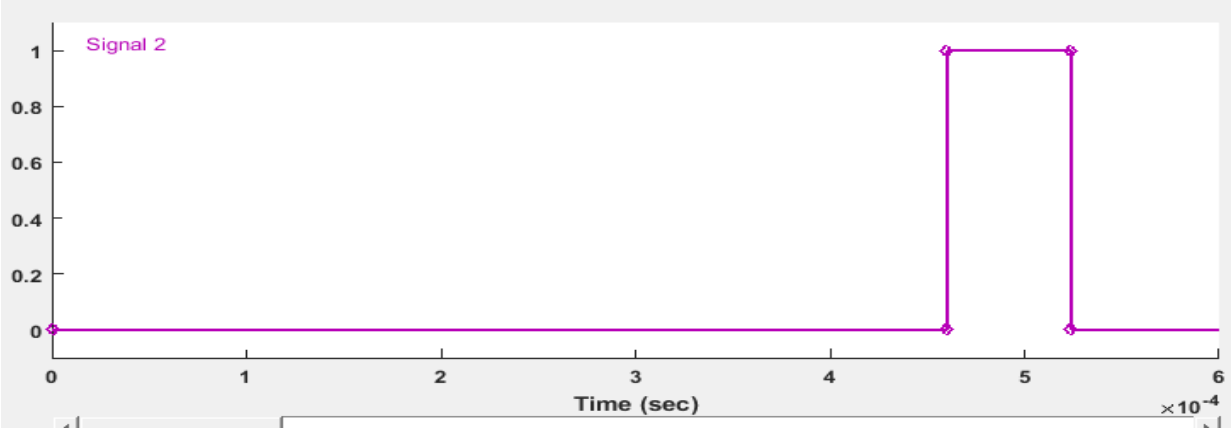


Figure 4.12: Disturbance signal added to the system after settling time

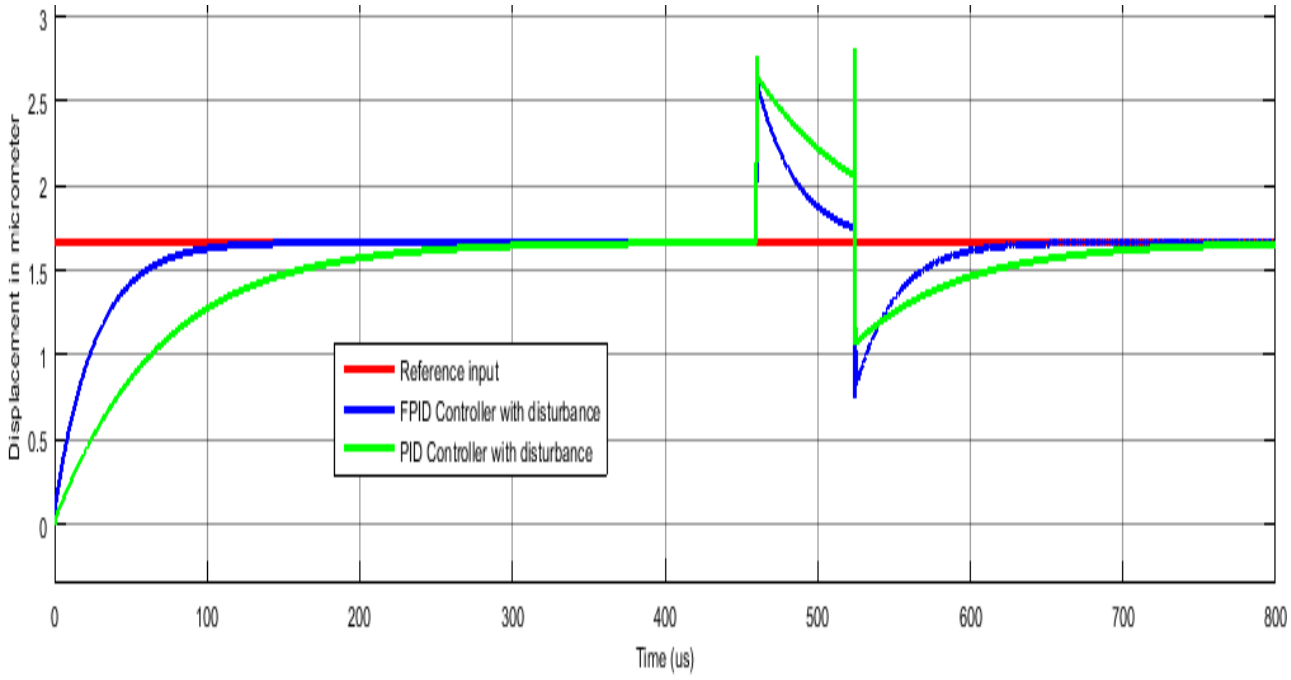


Figure 4.13: The simulation result of disturbance rejections of PID and FPID controller

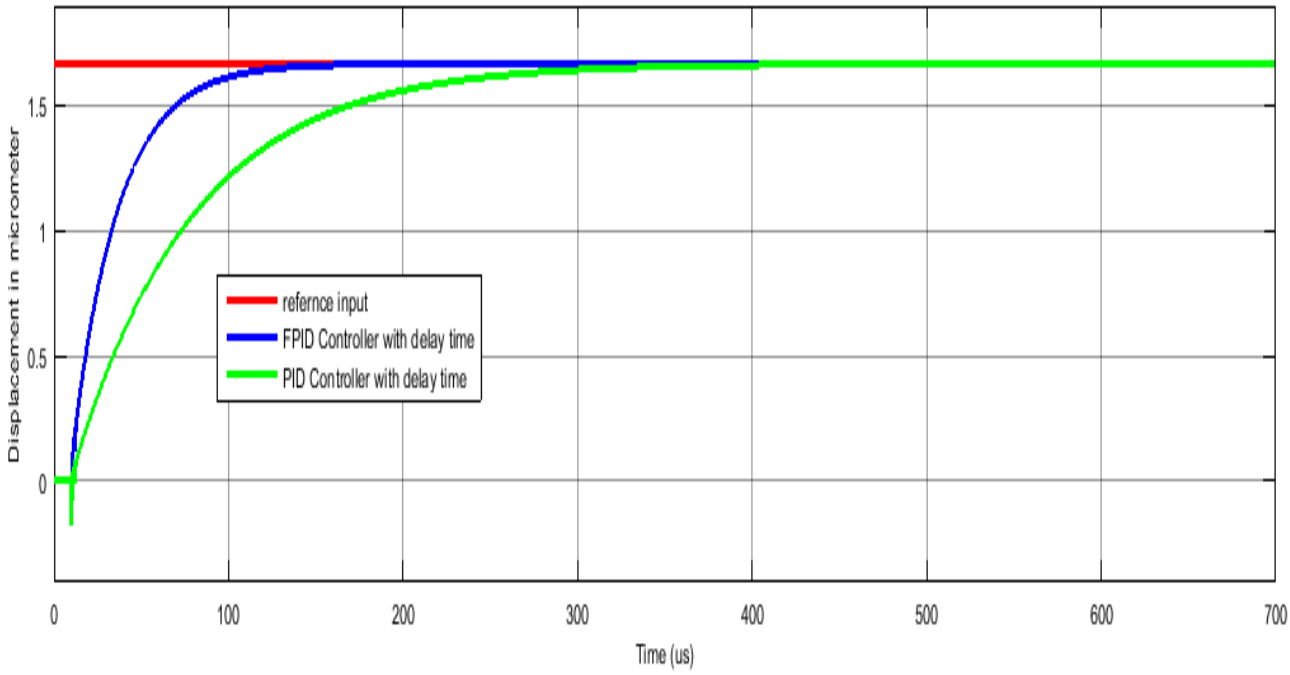


Figure 4.14: Response of the stack PEA with time delay

Generally, the simulation results show that the proposed controller works efficiently for different conditions like parameter variation, disturbance rejection and delay time. Thus, the FPID controller has already performed well in transient as well as steady states.

CHAPTER FIVE

CONCLUSIONS AND RECOMMENDATIONS

5.1 Conclusions

In this thesis, self-tuning FPID based position control of stack piezoelectric actuator for high precision applications using MATLAB is presented. PEA is a nonlinear and time-varying complex system. After proper assumptions and approximations are made to model and linearize the mathematical equations describing the stack actuator, transfer functions are obtained in frequency domain. Bouc-Wen hysteresis modeling is used in thesis paper in order to design the hysteresis of the stack PEA and Gaussian stochastic linearization is used to linearize it. The results of PID position controller are not satisfactory to the higher degree of accuracy condition. Even it introduces steady state error to the system, fuzzy control not only has the prominent advantage in complex, time-varying and nonlinear system control but also don't need the mathematical model of controlled object.

FLC is proposed to tune the parameters of PID controller for stack PEA, which has the advantages of PID control and fuzzy control. The performance of the proposed self-tuning FPID and PID controller is tested through simulation studies using MATLAB/SIMULINK. It is observed from the simulation results that the average overshoot is zero, rising time 57.062 microseconds, the settling time is 165.113 microseconds and steady state error is zero with the proposed self-tuning FPID controller. While overshoot is zero, rising time is 152.260 microseconds, settling time is 475.692 microseconds and steady state error is 0.01% with traditional PID controller.

The proposed self-tuning FPID controller is able to maintain the position of the stack PEA despite the parameter variation like stiffness, damping factor, mass and Dc gain. Furthermore, the capability of disturbance rejection of FPID controller is cheeked by giving step signal after settling time and it founded better than traditional PID.

5.2 Recommendations

For fuzzy interface system the rule base and scale factor can be optimized with genetic algorithm for further improvements in the performance of position control of PEA.

In this paper FPID controller is developed, but with PID self-tuning fuzzy neural controller the system response can be improved better. Moreover, the hardware of self-tuning FPID controller/ fuzzy supervisor PID controller can be developed for position control of PEA.

REFERENCES

[1] Tan Kok Kiong , Lee Tong Heng , Huang Sunan, Precision Motion Control Design and Implementation, 2nd ed., Singapore: Springer, 2007.

[2] R. Ramanujam, "Modeling Control of Piezoelectric Actuators," Purdue University Mechanical Engineering Department, West Lafayette, 2001.

[3] Priyanka Singh et al., "Design of Tuning Methods of PID Controller Using Fuzzy Logic," *International Journal of Emerging trends in Engineering and Development*, vol. 5, no. 3, pp. 239-248, September 2013.

[4] King A. Yi and Robert J. Veillette, "A Charge Controller for Linear Operation of a Piezoelectric Stack Actuator," *IEEE Transactions on Control Systems Technology*, vol. 13, no. 4, pp. 517-526, July 2005.

[5] Jin Li and Liu Yang, "Adaptive PI-Based Sliding Mode Control for Nanopositioning of Piezoelectric Actuators," *Hindawi Publishing Corporation,* vol. 1, pp. 1-10, 2014.

[6] Ander Chouza,Oscar Barambones,Isidro Calvo and Javier Velasco, "Sliding Mode-Based Robust Control for Piezoelectric Actuators with Inverse Dynamics Estimation," *MDPI*, pp. 1-19, 2019.

[7] Shahzad Khan, Meltem Elitas and Asif Sabanovic, "Discrete Sliding Mode Control of Piezo Actuator in Nano-Scale Range," Sabanci University Department of Mechatronics Engineering , Istanbul Turkey, 2003.

[8] Basem M. Badr and Wahied. G. Ali, "Nanopositioning Fuzzy Control for Piezoelectric Actuators," *International Journal of Engineering & Technology IJET-IJENS,* vol. 10, no. 01, pp. 1-5, 2010.

[9] Gwo-Ruey Yu, Wen-Bin Lin and Shih-Wei Liu, "Adaptive PI Control of Piezoelectric Systems Using Takagi-Sugeno Fuzzy Logic," National Ilan University Electrical Engineering Department, Yilan,Taiwan, 2004.

[10] Ismail H. Altas and Adel M. Sharaf, "A Generalized Direct Approach for Designing Fuzzy Logic Controllers in MATLAB/SIMULINK GUI Environment," *International*

Journal of Information Technology and Intelligent Computing,Int.j.IT&IC, vol. 1, no. 4, pp. 1-28.

[11] Jingyang Peng, "Modeling and Control of Piezoelectric Actuators," University of Saskatchewan, Saskatoon, August 2012.

[12] Ziqiang Chi and Qingsong Xu, "Recent Advances in the Control of Piezoelectric Actuators," *International Journal of Advanced Robotic Systems,* vol. 11, no. 182, 2014.

[13] Jain and Dr. Sheilza, "Settling Time Improvement of Piezoelectric Actuated Nanopositioning System Using Fuzzy Logic Based PID Controller," *International Journal of in Multidisciplinary and Academic Research (SSIJMAR),* vol. 4, no. 3, June 2015.

[14] M. Yoichi, "Applications of Piezoelectric Actuator," *Nec Technical Journal,* vol. 1, no. 5, pp. 82-86, 2006.

[15] Quanlu Zhao,Juntao Zhao and Xiangfeng Tan, "Classification, preparation process and its equipment and applications of piezoelectric ceramic," *Materials Physics and Chemistry,* pp. 20-27, 2018.

[16] P. Insturment, "PI motion and Positioning," 05 January 2012. [Online]. Available: http://www.piezo.ws/piezoelectric_actuator_tutorial/Piezo_Design_part3.php. [Accessed 10 May 2017].

[17] K. Johan, "PID Control," in *Control System Design*, 2002, pp. 216-251.

[18] Diwakar T. Korsane, Vivek Yadav and Kiran H. Raut, "PID Tuning Rules for First Order plus Time Delay System," *International Journal of Innovative Research In Electrical, Electronics, Instrumentation and Control Engineering,* vol. 2, no. 1, January 2014.

[19] K. J. Astrom and T. Haglund, PID Controllers: Theory, Design and Tuning, United State of America: Instrument Society of America, 1995.

[20] J. C. Basilio and S. R. Matos, "Design of PI and PID Controllers with Transient Performance Specification," *IEEE Transactions on Education,* vol. 45, no. 4, pp. 364-370, November 2002.

[21] Babak Rooholahi* and P. Lokender Reddy, "Concept and Application of PID Control and Implementation of Continuous PID Controller in Siemens PLCs," *Indian Journal of Science and Technology*, vol. 8, no. 35, pp. 1-9, December 2015.

[22] Wikipedia, the free encyclopedia, "PID controller," [Online]. Available: https://en.wikipedia.org/wiki/PID. [Accessed 15 August 2017].

[23] Ikpe Aniekan E*, Owunna Ikechukwu and Satope Paul, "Comparative Analysis of a PID Controller using Ziegler-Nichols and Auto Turning Method," *International Academic Journal of Science and Engineering*, vol. 3, no. 10, pp. 1-16., 2016.

[24] L. A. Bryan and E. A. Bryan, Programmable Controllers Theory and Implemetation, Atlanta: Industrial Text & Video Company, 1997.

[25] Walter Banks and Gordon Hayward, Fuzzy Logic in Embedded Microcomputers and Control Systems, Canada: Byte Craft Limited, 1993.

[26] L. Zadeh, "Information and Control," in *Fuzzy Sets*, vol. 8, 1965, pp. 338-353.

[27] M. Legesse, "Speed Control of Vector Controlled PMSM Drive using Fuzzy Logic-PI Controller," Addis Ababa Institute of Technology (AAiT), Addis Ababa, August 2001.

[28] Jin Hyoung Oh and Dennis S. Bernstein, "Semilinear Duhem Model for Rate-Independent and Rate-Dependent Hysteresis," *IEEE Transactions on Automatic Control*, vol. 50, no. 5, pp. 631-645, May 2005.

[29] Tri Vo-Minh,Tegoeh Tjahjowidodo, Herman Ramon and Hendrik Van Brussel, "A New Approach to Modeling Hysteresis in a Pneumatic Artificial Muscle Using The Maxwell-Slip Model," *IEEE/ASME Transactions on Mechanics*, vol. 16, no. 1, pp. 177-186, February 2011.

[30] Guo-Ying Gu, Li-Min Zhu, Chun-Yi Su,Han Ding, and Sergej Fatikow, "Modeling and Control of Piezo-Actuated Nanopositioning Stages: A Survey," *IEEE Transactions on Automation Science and Engineering*, vol. 13, no. 1, pp. 313-327, 2016.

[31] Jinqiang Gan and Xianmin Zhang, "Nonlinear Hysteresis Modeling of Piezoelectric Actuators Using a Generalized Bouc–Wen Model," *Micromachines*, vol. 10, no. 118, pp. 1-12, March 2019.

[32] Mohammed Ismail ,Fayçal Ikhouane and José Rodellar, "The Hysteresis Bouc-Wen Model, a Survey," *Arch Comput Methods Eng*, vol. 16, pp. 161-188, 2009.

[33] Prof. Dr. Eleni Chatzi, Dr. K. Agathos and Dr. G. Abbiati, "Modeling of Hysteresis," in *Method of Finite Elements II*, Zürich, Institute of Structural Engineering (IBK) Department of Civil, Environmental, and Geomatic Engineering (DBAUG), 2017.

[34] Fay¸cal Ikhouane . Jorge E. Hurtado ·Jos´e Rodellar, "Variation of the hysteresis loop with the Bouc–Wen model parameters," *Nonlinear Dyn (2007)*, vol. 48, no. 4, p. 361–380, 2006.

[35] A. M. Mustafah, "Proposed Framework of Building Nonlinear Models:A Study using the Bouc-Wen Hysteretic Model," The University of Sheffield ,Faculty of Engineering, Department of Mechanical Engineering, Sheffield, 30 September 2016.

[36] Xudong Zhu and Xilin Lua, "Parametric Identification of Bouc-Wen Model and Its Application in Mild Steel Damper Modeling," *Procedia Engineering* , vol. 14 , p. 318–324, 2011.

[37] Ovidiu Solomon, Ana Maria Mitu and Marius Giuclea, "Stochastic Linearization of Systems with Hysteretic Characteristics," *Rom. J. Techn. Sci. − Appl. Mechanics,* vol. 59, no. 3, p. 231−242, 2014.

[38] Jorge E. Hurtado and Alex H. Barbat, "Equivalent linearization of the Bouc–Wen hysteretic model," *Engineering Structures*, vol. 22, no. 2000, pp. 1121-1131, 1999.

[39] L. Reznik, "PID plus fuzzy controller structures as a design base for industrial applications," School of Communications and Informatics Victoria University of Technology, Victoria.

[40] Chee Pin Tan, Kok Soo Teoh and Lim Jen Nee Jones, "A review of Matlab's SISOTOOL; features and contributions to Control education," in *Proceedings of the 17th World Congress the International Federation of Automatic Control*, Seoul, 2018.

[41] Zuwwar Khan Jadoon, et al., "A Comparative Analysis of PID, Lead, Lag, Lead-Lag, and Cascaded Lead Controllers for a Drug Infusion System," *Journal of Healthcare Engineering,* vol. 2014, p. 13, 2017.

[42] Fayçal Chabni, Rachid Taleb, Abderrahmen Benbouali and Mohammed Amin Bouthiba, "The Application of Fuzzy Control in Water Tank Level Using Arduino," *International Journal of Advanced Computer Science and Applications,* vol. 7, no. 4, pp. 261-265, 2016.

[43] Shahid, H., Murawwat, S., Ahmed, I., Naseer, S., Fiaz, R., Afzaal, A. and Rafiq, S., "Design of a Fuzzy Logic Based Controller for Fluid Level Application," *World Journal of Engineering and Technology,* vol. 4, pp. 469-476, 2016.

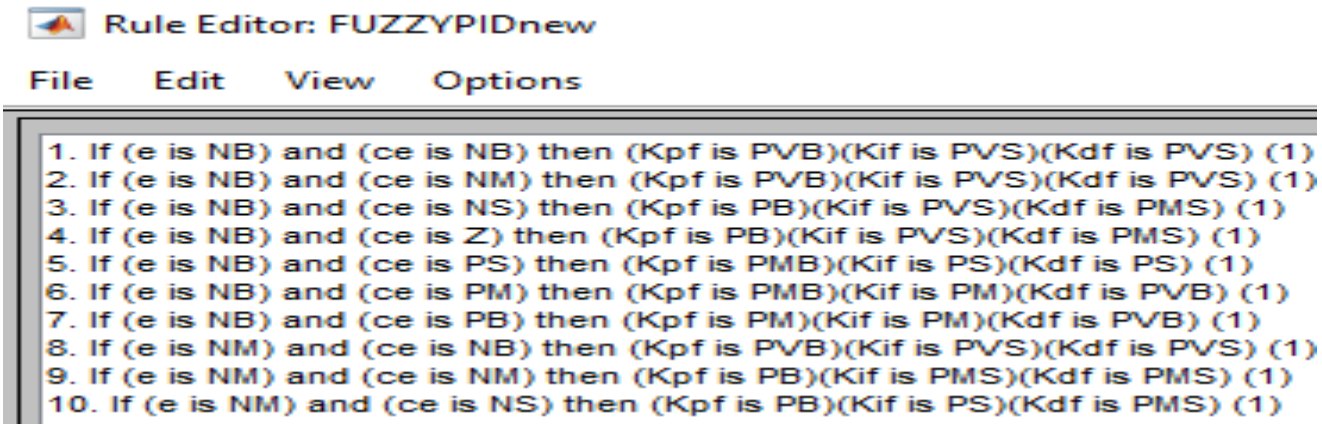
[44] H. Teshager, "Design and Simulation of Speed Control of PMSM with Fuzzy Logic Self-Tuning PID," Addis Ababa Institute of Technology (AAIT), Addis Ababa, Ethiopia, 2017.

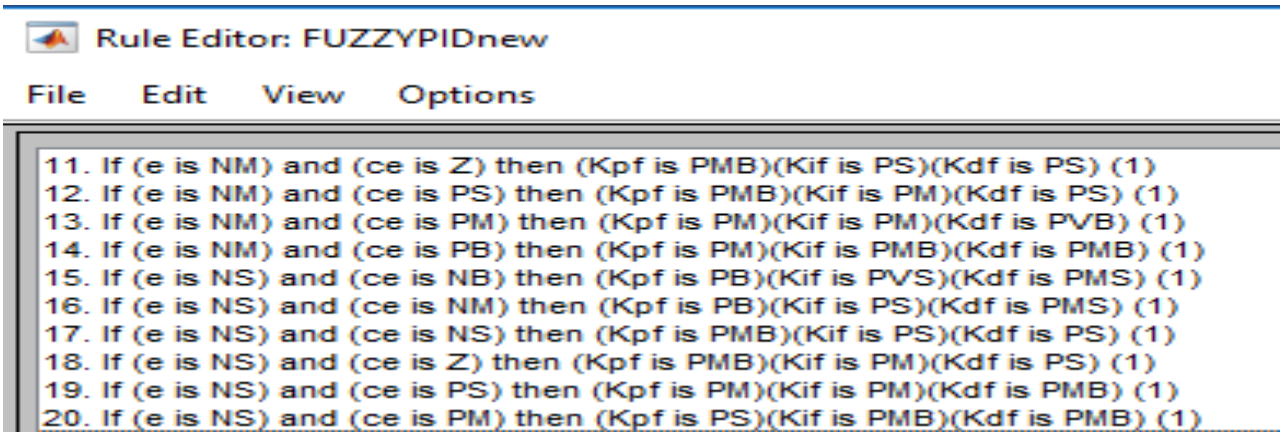
[45] Zulfatman and M. F. Rahmat, "Application of Self-Tuning Fuzzy PID Controller on Industrial Hydraulic Actuator Using System Identification Approach," *International Journal on Smart Sensing and Intelligent Systems,* vol. 2, no. 2, pp. 246-257, JUNE 2009.

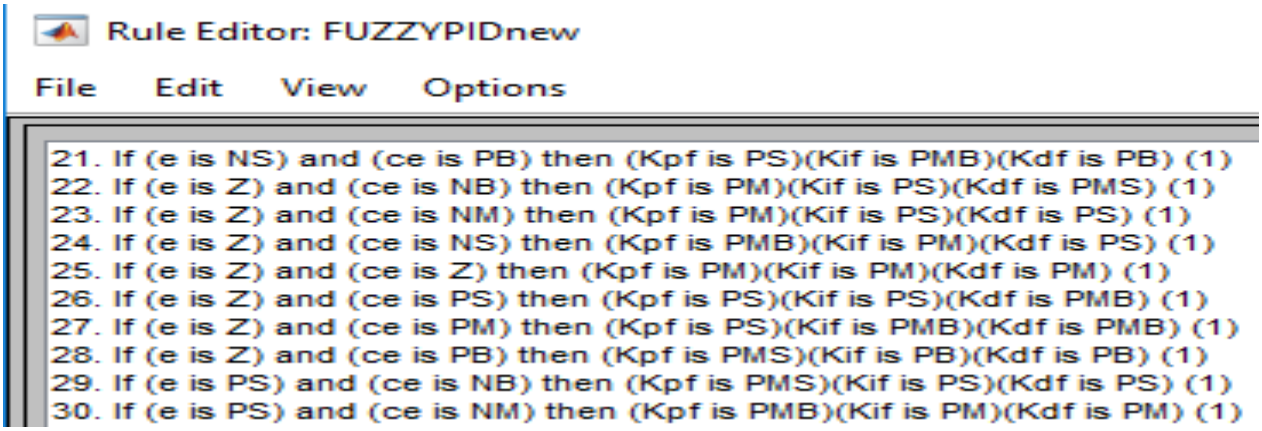
APPENDIXES

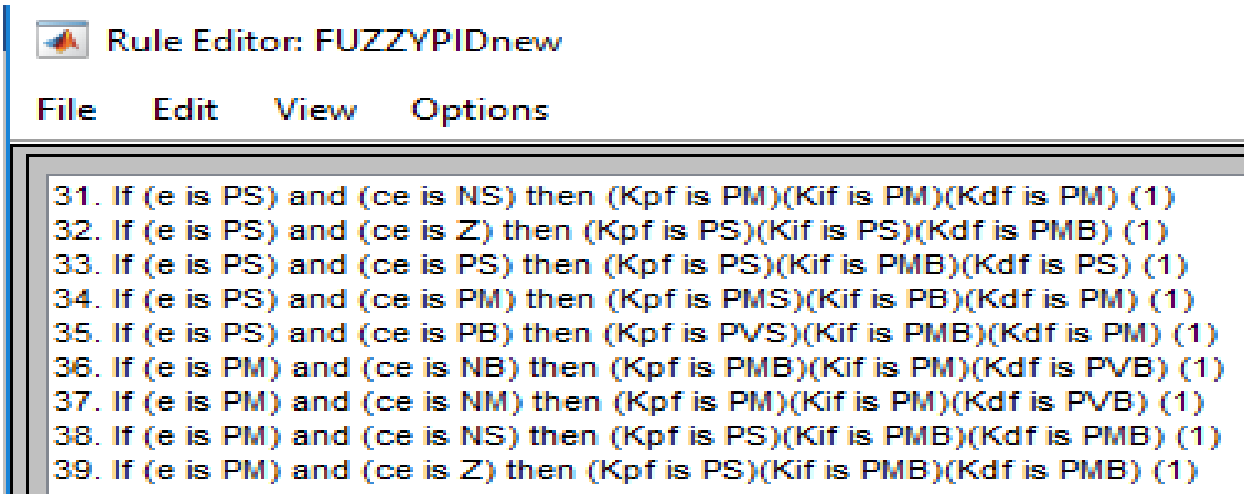
Appendix A

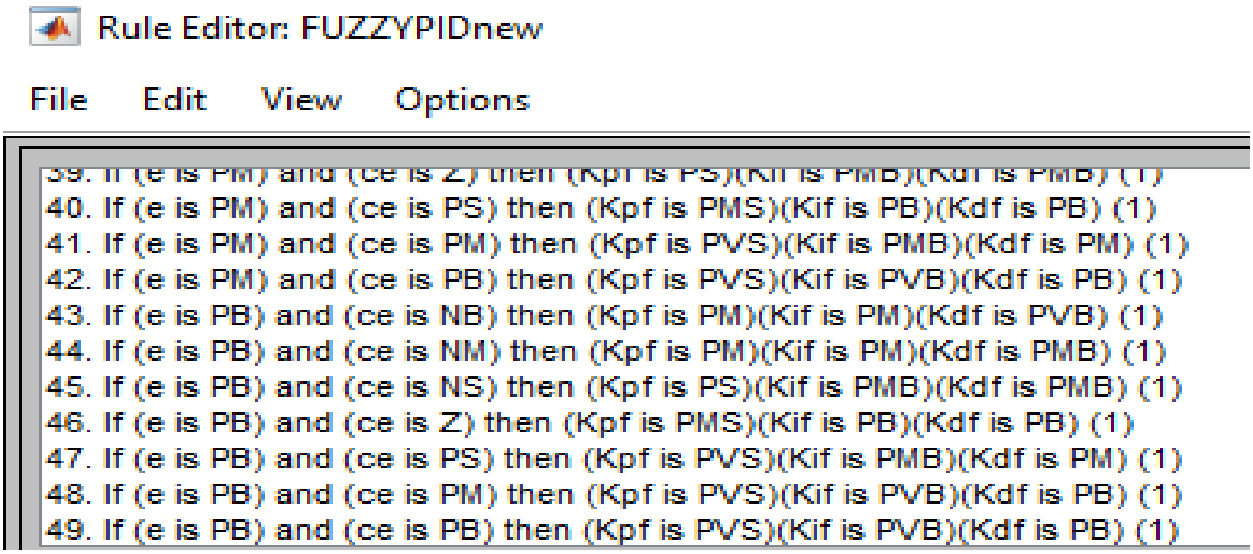
FLC 49 rules





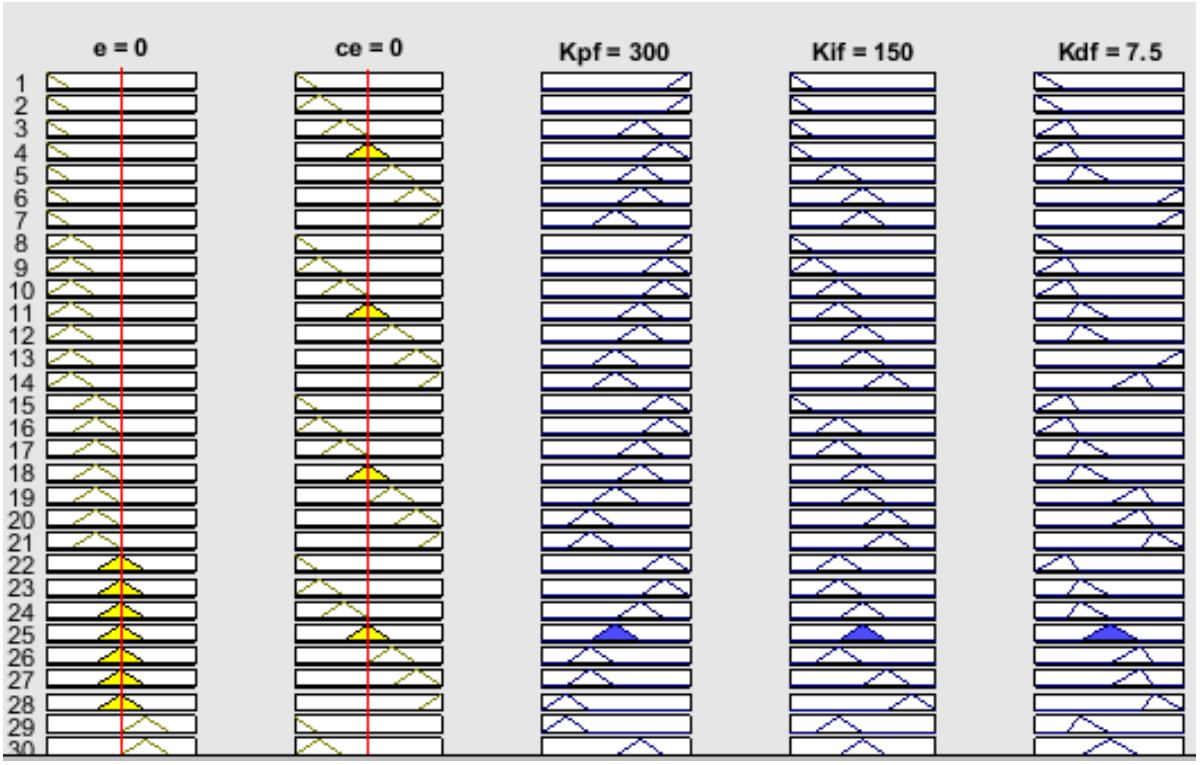



Rule Editor: FUZZYPIDnew
File Edit View Options
31. If (e is PS) and (ce is NS) then (Kpf is PM)(Kif is PM)(Kdf is PM) (1)
32. If (e is PS) and (ce is Z) then (Kpf is PS)(Kif is PS)(Kdf is PMB) (1)
33. If (e is PS) and (ce is PS) then (Kpf is PS)(Kif is PMB)(Kdf is PS) (1)
34. If (e is PS) and (ce is PM) then (Kpf is PMS)(Kif is PB)(Kdf is PM) (1)
35. If (e is PS) and (ce is PB) then (Kpf is PVS)(Kif is PMB)(Kdf is PM) (1)
36. If (e is PM) and (ce is NB) then (Kpf is PMB)(Kif is PM)(Kdf is PVB) (1)
37. If (e is PM) and (ce is NM) then (Kpf is PM)(Kif is PM)(Kdf is PVB) (1)
38. If (e is PM) and (ce is NS) then (Kpf is PS)(Kif is PMB)(Kdf is PMB) (1)
39. If (e is PM) and (ce is Z) then (Kpf is PS)(Kif is PMB)(Kdf is PMB) (1)


Rule Editor: FUZZYPIDnew
File Edit View Options
40. If (e is PM) and (ce is PS) then (Kpf is PMS)(Kif is PB)(Kdf is PB) (1)
41. If (e is PM) and (ce is PM) then (Kpf is PVS)(Kif is PMB)(Kdf is PM) (1)
42. If (e is PM) and (ce is PB) then (Kpf is PVS)(Kif is PVB)(Kdf is PB) (1)
43. If (e is PB) and (ce is NB) then (Kpf is PM)(Kif is PM)(Kdf is PVB) (1)
44. If (e is PB) and (ce is NM) then (Kpf is PM)(Kif is PM)(Kdf is PMB) (1)
45. If (e is PB) and (ce is NS) then (Kpf is PS)(Kif is PMB)(Kdf is PMB) (1)
46. If (e is PB) and (ce is Z) then (Kpf is PMS)(Kif is PB)(Kdf is PB) (1)
47. If (e is PB) and (ce is PS) then (Kpf is PVS)(Kif is PMB)(Kdf is PM) (1)
48. If (e is PB) and (ce is PM) then (Kpf is PVS)(Kif is PVB)(Kdf is PB) (1)
49. If (e is PB) and (ce is PB) then (Kpf is PVS)(Kif is PVB)(Kdf is PB) (1)

Appendix B

Partial rule views of the FIS



Appendix C

// solving linearized form of hysteresis variables “a” and “b” using Matlab

```
syms x1;

 syms x2;

z=2.459*10^11-9.679*10^5*x1+983.84*x1^2+983.84*x2-x1*x2 ;

y=5*10^8-938.84*x1+x1^2+x2;

>> m=simplify(x1*sqrt(z)+0.05*sqrt(2)*sqrt(y)-0.01*sqrt(2)*x1)

n=simplify(sqrt(z*y)+0.05*x1*x2-0.01*x2*sqrt(2)*sqrt(y)-x2*sqrt(z*y))
```

```
m =x1*((24596*x2)/25 - 967900*x1 - x1*x2 + (24596*x1^2)/25 + 245900000000)^(1/2) -
(2^(1/2)*x1)/100 + (2^(1/2)*(x1^2 - (23471*x1)/25 + x2 + 500000000)^(1/2))/20

n =((x1^2 - (23471*x1)/25 + x2 + 500000000)*((24596*x2)/25 - 967900*x1 - x1*x2 +
(24596*x1^2)/25 + 245900000000))^(1/2) - x2*((x1^2 - (23471*x1)/25 + x2 +
500000000)*((24596*x2)/25 - 967900*x1 - x1*x2 + (24596*x1^2)/25 + 245900000000))^(1/2)
+ (x1*x2)/20 - (2^(1/2)*x2*(x1^2 - (23471*x1)/25 + x2 + 500000000)^(1/2))/100

>> f=@(x)[x(1)*((24596*x(2))/25 - 967900*x(1) - x(1)*x(2) + (24596*x(1)^2)/25 +
245900000000)^(1/2) - (2^(1/2)*x(1))/100 + (2^(1/2)*(x(1)^2 - (23471*x(1))/25 + x(2) +
500000000)^(1/2))/20

 ;((x(1)^2 - (23471*x(1))/25 + x(2) + 500000000)*((24596*x(2))/25 - 967900*x(1) - x(1)*x(2) +
(24596*x(1)^2)/25 + 245900000000))^(1/2) - x(2)*((x(1)^2 - (23471*x(1))/25 + x(2) +
500000000)*((24596*x(2))/25 - 967900*x(1) - x(1)*x(2) + (24596*x(1)^2)/25 +
245900000000))^(1/2) + (x(1)*x(2))/20 - (2^(1/2)*x(2)*(x(1)^2 - (23471*x(1))/25 + x(2) +
500000000)^(1/2))/100 ];

>> x=[-5;5];

x=fsolve(f,x)

Equation solved, fsolve stalled.

fsolve stopped because the relative size of the current step is less than the

default value of the step size tolerance squared and the vector of function values

is near zero as measured by the default value of the function tolerance.

<stopping criteria details>

x =

 -0.0032

    1.000
```

Appendix D

Values of Parameters for simulation and design

Parameter	Identified value
M	0.2 Kg
C	200 Ns/m
K	10^8 N/m
β	0.05
A	1
γ	0.01
D	0.0001 m/V
S_0	1
m_{eff}	0.064 Kg
x_m	1.667μm

Appendix E

// derivation of the system transfer function

Laplace transform of Equation (3.50) can be write as:

$$sz(s) = -0.0032z(s) + 6 \times 10^5 sx(s)$$

Express $z(s)$ interms of $x(s)$ and the above equation becomes:

$$z(s) = \frac{6 \times 10^5 sx(s)}{s + 0.0032}$$

and the laplace transform of Equation (3.27) becomes:

$$Ms^2x(s) + Csx(s) + Kx(s) = K[duin(s) - z(s)]$$

Substitute the expression of $z(s)$ in to the above equation and re arranging it gives:

$$Ms^2x(s) + Csx(s) + Kx(s) + \frac{K \times 6 \times 10^5}{s + 0.0032} = \text{Kduin(s)}$$

The transfer function is given by:

$$\frac{x(s)}{uin(s)} = \frac{\text{Kd(s} + 0.0032)}{Ms^3 + (C + 0.0032M)s^2 + (K + K \times 6 \times 10^5 + C \times 0.0032)s + 0.0032 \times K}$$

Therefore by using the parameters given by appendix D the above expression approximately becomes:

$$\text{G(s)} = \frac{x(s)}{uin(s)} = \frac{5 \times 10^4(s + 0.0032)}{s^3 + 1000s^2 + 3 \times 10^{14}s + 1.6 \times 10^6}$$